Identification and Retraining of Sensorimotor Deficits to Reduce Intention Tremor in Multiple Sclerosis

Megan Heenan
Marquette University

IDENTIFICATION AND RETRAINING OF SENSORIMOTOR DEFICITS TO REDUCE INTENTION TREMOR IN MULTIPLE SCLEROSIS

by

Megan Heenan

A Dissertation submitted to the Faculty of the Graduate School,
Marquette University,
in Partial Fulfillment of the Requirements for
the Degree of Doctor of Philosophy

Milwaukee, Wisconsin

May 2015

ABSTRACT
IDENTIFICATION AND RETRAINING OF SENSORIMOTOR DEFICITS TO
REDUCE INTENTION TREMOR IN MULTIPLE SCLEROSIS

Megan Heenan

Marquette University, 2015

Multiple sclerosis (MS) affects approximately 1 in 1000 Americans and is a significant cause of disability in the United States. One significant contributor to disability in MS is intention tremor, which manifests as an oscillation about the endpoint of a goal-directed movement. A major challenge of treating intention tremor is that the underlying causes of tremor in MS are unknown. In this study, we describe a systems-level computational model and an experimental technique that parameterizes subject-specific deficits in sensory feedback control during goal-directed movements. We used this approach to characterize sensorimotor control and examine how sensory and motor processes are differentially impacted by age and MS. The specific aims of this study were to: 1) characterize age-related changes in sensorimotor control during goal-directed movements; 2) characterize deficits in sensorimotor control in individuals with multiple sclerosis; and 3) determine whether sensorimotor control deficits can be modified and intention tremor reduced using robot-assisted therapy. We show that age-related changes in movement control can be ascribed to increases in sensory noise, leading to slower and less accurate movements. In persons with MS, changes in movement control associated with intention tremor can be attributed to increases in visual response delay that are unaccounted for by predictive neuromotor control mechanisms. Finally, we show that training of goal-directed movements using carefully selected feedback delays can enable subjects to adapt to their increased visual delay, thereby reducing system instability and tremor. The results demonstrate that systems identification techniques provide an informative framework for investigating how neuromotor disease affects motor control and for developing individually targeted rehabilitation strategies to reduce motor disability.

ACKNOWLEDGMENTS

Megan Heenan

TABLE OF CONTENTS

LIST OF TABLES

LIST OF FIGURES

CHAPTER 1: INTRODUCTION AND BACKGROUND

1.1   INTRODUCTION

The objective of this research is to use systems identification – a process of mathematical and statistical modeling – to examine how sensorimotor control of voluntary movement can be altered by aging or disease. One challenge of examining the mechanisms that guide goal-directed movements is the complex interaction between sensory, motor, and movement planning processes. Systems identification and modeling allow us to describe the complexity of highly redundant systems – such as sensorimotor control – with quantifiable parameters. Model-based approaches to understanding movement control have been widely used for decades to describe motor phenomena, guide human-machine interaction, and investigate the sources of deficits in motor disability [1-34].

This dissertation aims to extend the understanding of motor deficits by using a systems-level model to characterize changes in sensorimotor control during aging and in persons with multiple sclerosis (PwMS) and to develop and analyze a rehabilitative protocol for subjects with MS and intention tremor. The following sections provide an overview of sensorimotor control in the context of goal-directed movement that forms the basis of the model developed here. Current understanding of motor control during pursuit and compensatory tracking and how they are differentially affected by aging and progression of MS with intention tremor will be reviewed. Finally, current rehabilitative strategies for MS will be outlined and the advantages of individualized rehabilitation techniques will be discussed.

1.2   PHYSIOLOGICAL BASIS OF VOLUNTARY MOTOR CONTROL

Control of voluntary movement is a complex process that forms the basis of our ability to interact with the environment. Deficits in control can result in disabilities that significantly affect quality of life. Understanding how movements are controlled, and how they can be impacted by disease, is therefore critical to understanding how healthy and impaired individuals perform daily tasks; it is also the first step in understanding and reducing motor disability.

Limb movement is planned and executed - in the cortex - primarily by the contralateral hemisphere, however, imaging studies have demonstrated that ipsilateral brain activity related to specialization of hemispheres is also present, especially during complex movements [35]. In general, the (contralateral) hemisphere that controls the dominant arm is also active during open-loop movements of the (ipsilateral) non-dominant arm, while the (contralateral) hemisphere that controls the non-dominant arm is active during closed-loop movements which stabilize the dominant arm against external perturbations [36-42]. These two components of movements, controlled separately, may correspond to a two-stage movement process during reach: an initial "trajectory" phase, and a secondary "endpoint acquisition" phase [43, 44]. This lateralization of neural control based on the phase of movement can result in differential impairments of hand and arm movement due to cortical damage and disease [41, 42, 45].

Once movement begins, information regarding the state of the limb is unavailable until after sensory information is transmitted and processed, resulting in a reliance on past sensory information to guide future movements. Sensory delays result from signal conduction through the peripheral (PNS) and central nervous systems (CNS) combined

with delays associated with the processing of sensory inputs into estimates of movement outcome [20]. For proprioceptive feedback, conduction delays, which scale with the length of the path traveled through the PNS and spinal cord, form a large part of the total delay, resulting in delays that are approximately 100-150 ms in healthy adults [10]. For vision, conduction delays are much shorter, while processing delays are much longer due to the complexity of combining and interpreting visual signals. This extra processing time results in delays that are approximately 300-400 ms in healthy adults [46, 47].

The delays in sensory transmission and processing make on-line error reduction difficult due to long latencies between current position and sensory estimates of position. These delays can be compensated for by estimating current movement error and thereby allowing for correction of movement errors before delayed sensory feedback becomes available [19, 48, 49]. The cerebellum has been proposed to play a role in providing these forward estimates of sensory outcomes of movement. Population activity in the cerebellum has been shown to correlate with future sensory feedback, while damage to the cerebellum results in an inability to adapt to force fields [49]. In simulations, inaccuracies in the forward model produce similar movements to those seen in cerebellar ataxia, which provides a possible link between cerebellar activity and forward modeling [4, 33].

For these predictive models to be generated, sensory estimates of position are generally combined from multiple sensory modalities. According to one model, sensory estimates of position are weighted based on the amount of uncertainty in each estimate such that sensory estimates with less variability are given more weight [15, 20, 23, 50-52]. For example, if additional noise is present in visual estimates of position (i.e. "jitter"

in a visual feedback scenario), visual gain is decreased, while other relevant sensory inputs (proprioception, hearing) are up-weighted to optimize the accuracy of the combined sensory estimate [15, 20, 23, 50-52]. These weighted estimates are combined to produce a single, unified estimate of limb position. With additional information about the environment, Bayesian estimation – reweighting of sensory information based on previous information – acts to maximize the amount of sensory information available while decreasing the impact of errors in sensory processing [52].

Sensory weighting is also dependent on internal sources of uncertainty inherent to the nervous system. Sensory uncertainty, or noise, arises from several physiological mechanisms. Variability in firing rates of sensory neurons (i.e. photoreceptors in the retina) reduces accuracy in sensory perception [53, 54]. Information is lost during transmission [55] and during processing [54, 55] of sensory information due to variability in action potential spike timing. These sources of variability reflect noise inherent in the system and place limits on the accuracy of the sensory percept such that signals smaller than the noise cannot be reliably detected [53]. Inaccuracies in sensory estimates exist in all sensory modalities and, in the context of movement control, reflect the uncertainty in sensory estimates of limb kinematics [53]. In the sensorimotor control systems of healthy adults, the effects of sensory variability at the output of a movement are an order of magnitude smaller than the movement itself [53].

1.3   MODELING OF GOAL-DIRECTED MOVEMENTS

Modeling has been used to characterize motor control during balance [9-11, 13-15, 20, 21] and arm movements [2, 4, 19, 22, 25, 30, 31, 56, 57] including goal-directed

movements about the elbow and wrist. The primary purpose of these models has been to investigate the means by which posture and voluntary movements are controlled. Some of the earliest comprehensive models of motor control were designed to interpret human-controller interactions in order to improve pilot performance during flight [12, 29, 30]. More recent models have been used to examine the processes that guide the maintenance of human balance, an inherently unstable process [9-11, 16-18, 20, 21, 58-62]. Models characterizing sensorimotor control as a whole have also been applied to the understanding of tracking movements of the wrist [2, 22, 25] and arm [4, 56, 57, 63] to investigate the neuromotor control of voluntary, goal-directed movements.

The means by which the brain plans and executes goal-directed movements can be modeled in several ways. A simple and effective class of controllers used for error reduction in control systems modeling include the PD (proportional-derivative) or PID (proportional-integral-derivative) controller [1, 20, 22, 56, 57, 61]. PD controllers respond to several aspects of the error: proportional control reduces the *current* error while derivative control responds to the *change* in error, allowing for faster responses and damping of oscillatory responses. PD controllers can result in significant endpoint error, which can be reduced with the addition of integral control (PID controllers). Other types of controllers employ cost functions designed to generate trajectories that minimize jerk [64] or minimize metabolic cost [65]. Minimum-jerk and minimum-cost trajectories have been shown to closely resemble reaching movements in human subjects [64, 65]. Intermittent control, or control using discrete "taps" in order to reduce error, has been examined in the context of balance control; it has been found to be an effective method of reducing movement error in unstable systems. Although intermittent control is effective,

it is also non-linear, making parameters difficult to estimate experimentally [9, 10]. Artificial neural networks (ANNs), which are typically more complex, have also been used to generate stereotyped movements similar to natural movements [66]. Models of error reduction span a continuum trading off simplicity (PD/PID, minimum-jerk) for model accuracy (intermittent control, ANNs).

Delays in feedback during movement control can make systems inherently unstable and errors difficult to respond to [4, 19-22, 48, 49, 60, 61, 67, 68]. Intermittent controllers compensate for instability in continuous feedback systems by using small, discrete movements; this mode of control has been shown to closely replicate human movement during balancing tasks [9, 10]. The discretization of error compensation reduces oscillatory behavior without the need for predictive feedback [9, 10]. Another way to compensate for long delays is through the use of a Kalman filter to estimate the state of the system using an efferent copy of the motor command in combination with sensory information [60, 68]. In systems engineering, feedback delays can be compensated using a Smith Predictor, a predictive mode of control which contains additional feedback models of both the plant dynamics and predictions of delayed sensory feedback [19, 49]. Smith Predictors are particularly robust against long sensory delays, however, the neurological correlates of this type of forward model are unclear [60].

Recently, models of sensorimotor control have been used to investigate the causes of movement dysfunction in stroke [44], Huntington's disease [69, 70], cerebellar ataxia [33], vestibular deficits [71], and Parkinson's disease [1]. These studies have quantified motor deficits in terms of an underlying control architecture to identify where subclinical

deficits may be present, for example, in early stages of Huntington's disease [69, 70]. They can also help identify mechanistic causes of specific deficits that may be targeted for rehabilitation; a recent study of cerebellar ataxia found that subjects with ataxia may be unable to predict limb dynamics accurately [33]. Devices and therapies to modulate limb dynamics may, therefore, be able to reduce ataxia in individuals with cerebellar damage [5, 33].

1.4   AGING AND MOVEMENT CONTROL

Healthy older adults (> 60 years old) exhibit several changes in motor control. Older adults tend to move more slowly [72-76], and with decreased accuracy [77-80] compared with younger subjects. Older subjects also exhibit increased trajectory and endpoint variability, which may be associated with decreased accuracy [79, 81]. They also may have difficulty coordinating complex movements, particularly those that require coordination of multiple joints and/or integration of information from multiple sensory sources [74-77, 82]. Additionally, older subjects also rely more heavily on sensory feedback information during closed-loop movements [83, 84], but use sensory information less efficiently and take more time to process sensory inputs [80]. Older subjects also exhibit more difficulties in adjusting to late changes in target position [80] and perform more poorly at adapting to novel force fields [65].

Changes in muscle and the peripheral nervous system may contribute to alterations in motor control, including a reduction in the ability to generate large muscle forces [73, 85] and an increase in signal-dependent motor noise [81, 86]. Central nervous system deficits may also contribute. Loss of grey matter in the cerebellum may result in poor

formation of new internal models and degradation of existing models [87, 88]. The cortex also exhibits reduced volume in both white [88-91] and grey [90] matter in older adults, which could also alter movement profiles by affecting the integrity of sensory input, sensory integration, and movement planning [92]. In particular, reductions in the size of the corpus callosum, common in older adults, could potentially lead to difficulty in coordinating complex movements, especially those that rely on ipsilateral movement control [92]. Older subjects may also prioritize accuracy over speed [73, 81], leading to changes in endpoint acquisition strategies; these changes could also be used as a compensatory mechanism to address deterioration in sensory or motor systems as described above [81].

1.5   MULTIPLE SCLEROSIS AND MOVEMENT CONTROL

In persons with multiple sclerosis (PwMS), neuromotor dysfunction is due to a loss of myelin in the CNS which disrupts the transmission of information within and between brain areas. Arm movement and balance are particularly affected; tremor and ataxia may impact up to 75% of PwMS, while balance dysfunction affects nearly 80% of PwMS [93]. Arm movement can be particularly affected by intention tremor, a form of low-frequency (3-5Hz) tremor about the endpoint of a visually-guided, goal-directed movement. Intention tremor affects up to 15% of PwMS and is a particular cause of upper extremity disability [94]. Although there are several medical options available, most do not result in significant, long-term effects due to either increasing drug tolerance or to increasing symptom severity. Drug therapies – including isoniazid, propanolol, and carbamazepine – have been able to reduce intention tremor in select populations [95, 96].

Side effects can also be significant, including reduced liver function, fatigue, and weakness [95]. Surgical treatments, including DBS and thalamotomy, can mitigate some effects of tremor [95]. However, the treatments are invasive and entail relatively high-risk and, like medications, their effectiveness at reducing tremor also decreases over time [96]. Recently, rTMS has been shown to reduce tremor, although the treatment period can be long and the effects are typically short-lived [97, 98].

Physical therapy has been used successfully to reduce motor symptoms in other neurodegenerative illnesses, including Huntington's disease and Parkinson's disease [99], as well as for select motor symptoms in MS, including posture and balance deficits [100]. In particular, balance-based torso weighting has been shown to effect long-term improvements in mobility in persons with MS [100]. The goal of most exercise-based rehabilitation programs has been management, but not necessarily treatment, of motor symptoms. Because of this, exercise-based rehabilitation strategies have generally not been successful in achieving significant long-term improvements in motor performance [101]. Recent, more targeted studies by Feys et al. have shown that intention tremor in MS can be reduced through alteration of computer-generated visual feedback [102]. Delaying or time-averaging visual feedback information has been shown to reduce intention tremor during functional tasks [102-104], and the effect has been used successfully to assist with computer usage for people with intention tremor [102]. The effects do not persist once the altered feedback has been removed, suggesting that the procedure can be used to help manage the functional impact of intention tremor during select tasks, but does not improve motor performance generally.

Motor training using robotic devices to introduce proprioceptive and visual perturbations has been shown to reduce motor impairment in persons with MS [105-107]. Subjects with MS are able to correct movement trajectories in force fields, indicating that their ability to adapt is not completely lost due to neurological changes resulting from MS [105]. Moreover, the force field adaptations were shown to reduce tremor during and immediately post-task [106]. Error enhancement (an increase in visual error relative to position error) during visually guided tasks has also been shown to improve performance during and immediately following reaching tasks compared to training without error enhancement or training using error reduction (a decrease in visual error relative to position error) [107]. These short-term improvements in motor function suggest robot-assisted training therapies may provide a viable approach to reducing motor dysfunction in MS.

Intention tremor in MS also differentially impairs two types of movement; subjects with intention tremor perform nearly normal open-loop movements (movements which are made without sensory feedback). However, closed-loop control (movement control under sensory feedback) is impaired, and endpoint acquisition is severely impaired by the addition of tremor [45]. Despite this impairment, individuals with MS often select a closed-loop control strategy when an open-loop strategy may be more appropriate [108, 109]. By better understanding how open- and closed-loop movements are controlled, we can gain a better understanding of how control of movement is impacted by disease. A better understanding of the sensorimotor control mechanisms specifically impacted by MS may also maximize the impact of retraining on motor performance and functional outcomes in PwMS.

1.6 AIMS AND SIGNIFICANCE OF RESEARCH

The goal of the proposed work is to use a multi-input, single-output linear model of sensorimotor control to identify deficits in control that occur with aging and in PwMS. To achieve this goal, the research addresses three specific aims:

Aim 1: Develop and use our model to characterize deficits in sensorimotor control due to aging during goal-directed movements. Previous research has demonstrated that significant changes in motor control take place during aging. Here, we aim to systematically quantify these changes in motor control for three distinct types of goal-directed tasks: visual compensatory tracking, visual pursuit tracking, and proprioceptive compensatory tracking. Elbow joint kinematic data will be collected and subjects' motor performance in each task will be used together with systems identification techniques to characterize a model of sensorimotor control. Changes in model parameters with age will be examined using structural equation modeling to test causal models of motor deficits. We expect that this analysis will reveal directed relationships between age-related changes in sensorimotor control parameters that can be used to identify specific deficits in motor control that occur in healthy aging.

Aim 2: Use our model to characterize deficits in sensorimotor control in individuals with multiple sclerosis. Multiple sclerosis is a debilitating, degenerative disease whose symptoms can vary widely from person to person. Because individuals' impairments are so diverse, it can be difficult to ascribe a specific cause to symptoms. Here, we will characterize sensorimotor control in individuals with MS using the model and

experiments developed in Aim 1. Elbow joint kinematic data will be compared against age- and gender-matched control subjects to determine which aspects of sensorimotor control are altered in persons with MS and characterize their functional contribution to intention tremor. We expect that characterization of the sensory and motor sources of impairment present in individuals with MS will form the basis for the development of targeted rehabilitation strategies to improve movement control.

Aim 3: Determine whether sensorimotor control deficits identified in Aim 2 can be modified and intention tremor reduced using robot-assisted therapy. Current physical therapies for MS emphasize general strength training to alleviate the effects of fatigue and improve postural control. Here we test the hypothesis that functional outcomes may be improved by tailoring retraining strategies to subject's individual deficits in sensorimotor control. Persons with MS will perform an adaptation task tailored to their individual sensorimotor deficits to determine whether targeted rehabilitation can be used to induce changes in sensory and motor processes that are beneficial in reducing intention tremor. Clinical measurements will be performed to determine the short- and long-term functional impact of the adaptation. We expect that targeted rehabilitation techniques will be more successful in reducing intention tremor than general therapeutic strategies and will provide a direction for future research in assisting persons with MS in reducing intention tremor and improving functional performance.

CHAPTER 2: CHANGES IN SENSORIMOTOR CONTROL DURING HEALTHY AGING IN ADULTS[1]

[1]This work is intended for publication. Authorship: M. Heenan, R.A. Scheidt, S.A. Beardsley.

2.1   INTRODUCTION

Healthy adults exhibit changes in sensory and motor performance related to aging. During reaching movements, healthy older (> 60 years old) adults move more slowly than younger adults [72-76]. They also exhibit decreased movement accuracy [77-80], and increased variability in both trajectory planning and endpoint acquisition [79, 81, 82]. Older subjects also exhibit increased intermittency during movement [77, 110], with movements that require a larger number of corrective submovements to acquire a target [81]. Older subjects also have difficulty creating smooth, complex movements [77, 79], particularly those that require coordination of multiple joints and/or integration of information from multiple sensory sources [74-76, 82]. This may be related to changes in sensory processing, including decreased effectiveness of visual feedback [80, 84] and alterations in proprioceptive control of movement [77, 84].

Several mechanisms have been proposed to explain why sensorimotor control changes with age. One source of decreased velocity and increased intermittency during goal-directed movement may be a reduction in the ability to generate the large muscle forces required for fast, long distance movements [73, 85]. Signal-dependent motor noise – associated with muscle fiber recruitment - may also increase in response to muscle weakness and reductions in motor neurons, both of which occur more frequently in older adults [81, 86]. A moderate reduction in maximum muscle force has a larger impact on

fast or forceful movements than on shorter movements at a self-selected speed, which do not require large amounts of force [81, 86].

Deficits in central planning mechanisms have also been implicated in movement changes in older adults [74-76, 78]. Deficits have been attributed to slowed conduction times in the peripheral and central nervous systems [89-91], imprecision in internal models [77, 87, 88], loss of gray and white matter [89-91], and decreased effectiveness of working memory. Recent work has demonstrated that the cerebellum exhibits significant loss of connectivity with age which may result in difficulty in forming new predictive models of limb dynamics, and degradation of existing internal models [88].

Decreased reliability of sensory feedback could also potentially cause difficulties in generating movements that require significant reliance on sensory inputs to generate motor outputs [84]. Older subjects rely more heavily on sensory feedback information during closed-loop movements [83, 84], but use this information less efficiently and take more time to process sensory inputs [80]. They also exhibit more difficulties in adjusting to late changes in target position [80], suggesting that they require more time to process alterations in the movement plan. Older subjects also perform poorly at adapting to novel force fields, a task that requires subjects to rely heavily on sensory feedback errors for optimal performance [65].

Widespread, generalized cognitive slowing, linked to reductions in volume in both white [87, 89-91] and grey [90] matter, could also alter movement profiles by affecting the integrity of sensory input, sensory integration, and movement planning simultaneously [92]. Additional cognitive load caused by decreased cognitive capacity in older adults has been shown to lead to movement slowing [111]. In particular, reductions in corpus

callosum size, common in older adults, can lead to difficulty in coordinating complex movements, especially in tasks that rely on the ipsilateral hemisphere for movement planning and control [92].

Finally, older subjects may alter their movement goals (either to compensate for any of the factors listed above or due to practice), for example, to prioritize accuracy over speed [73, 81]. Previous research has speculated that older subjects are more "error-averse" than younger subjects, leading to changes in endpoint acquisition strategies. Such changes would present as altered movement planning processes [81]. Altered movement goals could also be used as a compensatory mechanism for deterioration in sensory or motor systems as described above [81].

We have previously used systems identification techniques to characterize changes in sensorimotor control during goal-directed movement [6], in subjects with multiple sclerosis [57], and during aging [56]. In the current study, we examine the changes in sensorimotor control that occur with age during single-joint tracking tasks to determine which aspects of sensorimotor control are directly impacted during normal, healthy aging. Further, we examine the plausibility of the hypotheses described above, including (1) whether all facets of sensorimotor control are directly altered by aging; (2) whether changes in strategy (controller), limb dynamics (plant), or sensory noise drive changes in motor strategy; (3) whether changes in sensorimotor control can be described by a combination of hypotheses – that sensory gains are altered as a result of changes in sensory noise, and that aging directly affects either the controller or plant; and finally, (4) whether aging directly affects only sensory noise, which, in turn, alters sensory gains, and the neural controller/plant.

2.2   METHODS

2.2.1   Participants

Twenty-five healthy volunteers (14 women) between 19 and 76 years old (mean: 40 ± 19 years) participated in the study. One subject was excluded from the final analysis because she was ambidextrous. Twenty-two of the twenty-four subjects were right handed, according to the Edinburgh Handedness Inventory. All subjects self-reported normal or corrected-to-normal vision. None reported any history of neurological, motor, or sensory deficits, or use of medications that would cause changes in motor control or attention. Written, informed consent was obtained from each subject in accordance with the Declaration of Helsinki and as approved by the Marquette University Institutional Review Board.

2.2.2.   Sensory Feedback Control Model

Sensory feedback control includes adaptive feedforward and feedback mechanisms. Based on the work of Peterka [20], and McRuer [12, 112], we have developed a closed-loop model of sensory feedback control during single-joint, goal-directed movement and have used it previously to describe sensorimotor responses to environmental perturbations and distortions of visual feedback (Figure 2-1) [6, 22]. In this study, we use the sensory feedback control model to examine how aging in healthy adults impacts feedback control. In the model, angular position error of the elbow joint (i.e. *performance error*) is calculated as the difference between desired position (θ_d) and

the weighted sum of visual and proprioceptive estimates of the actual arm position (θ_a)

[6, 13, 20, 22, 62]. Desired position is weighted by a gain, K_s. The weights of the visual

and proprioceptive paths are represented by K_v and K_p, respectively. Delays in visual and

proprioceptive processing are modeled separately (T_v and T_p, respectively) to account for

the overall response delay in each sensory path; these lumped-parameter terms combine

feedback delays due to signal conduction and sensory information processing. In the

forward path, actual performance error is compared to the predicted consequences of the

intended action (i.e. the output of a forward model) to yield an instantaneous prediction

error, which gives rise to a set of muscle activations through the action of a neural

feedback controller, which for simplicity we model using a Proportional-plus-Integral-

plus-Derivative (PID) controller, C(s):

$$C(s) = K_d s + K_{pr} + \frac{K_i}{s}. \tag{1}$$

This generic controller, which has previously been used to model movement

control [20], contains separate derivative (K_d) proportional (K_{pr}) and integral (K_i) gains to

allow the controller to minimize transient response errors as well as steady state errors.

The output of the controller is a scalar quantity representing the intended net muscle

activations, which in turn act through the musculoskeletal geometry (muscle attachment

points and moment arms) to give rise to a net torque applied to the physical plant (the

forearm / hand pivoting about the elbow). Note that we have simplified our model of the

physical plant by discounting muscle activation/contraction dynamics, which are assumed

to be dominated by the second-order passive dynamics of the arm. We do, however,

account for variations in muscle fiber recruitment [113] by reducing the precision of the

intended torque by a multiplicative motor noise (α).

The arm's dynamic response to the applied torque is estimated using a second-

order model of the plant, P(s),

$$P(s) = \frac{1}{Js^2 + Bs + K} \tag{2}$$

This model simulates the passive mechanical properties of the forearm and hand about

the elbow via separate inertia (J), viscosity (B), and stiffness (K) terms.
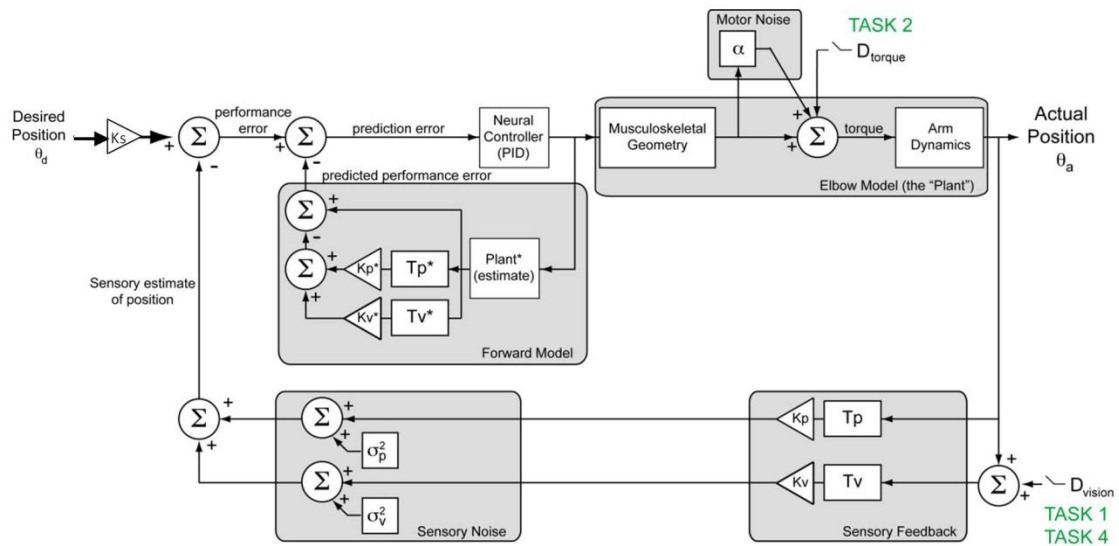
Figure 2-1: Multisensory feedback model of sensorimotor control [57].
Feedforward (action selection) pathways have been omitted for simplicity. The model consists of a feed-
forward motor control path and three nested feedback paths. The outermost feedback path accounts for
sensory (visual and proprioceptive) feedback. In the feedforward path, desired position (θ_d) is weighted
(K_s) and the sensory estimate of position is subtracted to generate a performance error. Neural processing
associated with the correction of state is modeled generically by a PID controller (neural controller)
containing separate proportional, integral, and derivative gains. Motor noise in the generation of torques is
modeled by a multiplicative noise (α). Corrective torque is converted to angular position of the arm using a
2nd order model characterizing the inertia, viscosity, and stiffness about the elbow. In each branch of the
outer-most feedback path, arm position is delayed (T) and weighted (K) to provide a combined sensory
estimate of arm position. The forward model provides predictive compensation of the arm dynamics and
delays via the inner feedback loops. D_{vision}/ D_{torque} denote external perturbations applied to the perceived
visual (Tasks 1 and 4) and/or proprioceptive (Task 2) feedback of arm position.

The sensory feedback control model also includes an internal feedback path (referred to here as a forward model), which provides predictions of movement kinematics and the sensory consequences of those actions based on efference copy of the intended motor actions and internal estimates of the sensory gains (K_v^*, K_p^*), system delays (T_v^*, T_p^*), and limb dynamics (Plant* - Eq. 2). One important effect of the forward model is to compensate for the long-latency feedback loops (>100ms) associated with sensory processing.

2.2.3. Experimental Setup

All subjects participated in a single, two-hour experimental session wherein they performed a series of visual and proprioceptive tracking tasks to characterize sensory feedback control about the elbow. Tasks and analysis are summarized in Table 2-1. Elbow angle and joint torque data collected during performance of six single-joint tracking tasks were used to obtain an individualized (best-fit) estimate of the sensory feedback control model depicted in Figure 2-1. Data collected from an additional single-joint tracking task was used for model validation. The order of task presentation was counterbalanced across subjects. In order to account for potential task-related variations in subjects' responses, all model parameters (aside from the physiological parameters: sensory delays and muscle noise) were estimated simultaneously from data collected during a single, high-frequency tracking task ("task 4", described below).

During single-joint tracking tasks, subjects held the handle of a 1-D robotic manipulandum with their right hand (Figure 2-2); the robot's axis of rotation was aligned

with that of the elbow joint when the subjects' arms were supported at an angle of approximately 90º of shoulder flexion and 90º of shoulder adduction. Details of the robot implementation and control can be found in [114]. Rotation of the manipulandum about the elbow (limited to ±40° relative to 90º of elbow flexion) was yoked to the horizontal position of a cursor (a red ring) displayed on a 19-inch computer monitor. The monitor was placed perpendicular to the line of sight at a distance of 60 cm, which resulted in a cursor diameter of 0.67^o. During the tasks, a stationary target (a black circle 0.33^o in diameter) was also displayed on the screen. Direct view of the arm was blocked using an opaque barrier such that the cursor provided the sole visual cue of arm position. Rigid supports were placed on either side of the subject's upper arm to minimize shoulder and/or upper arm movements.
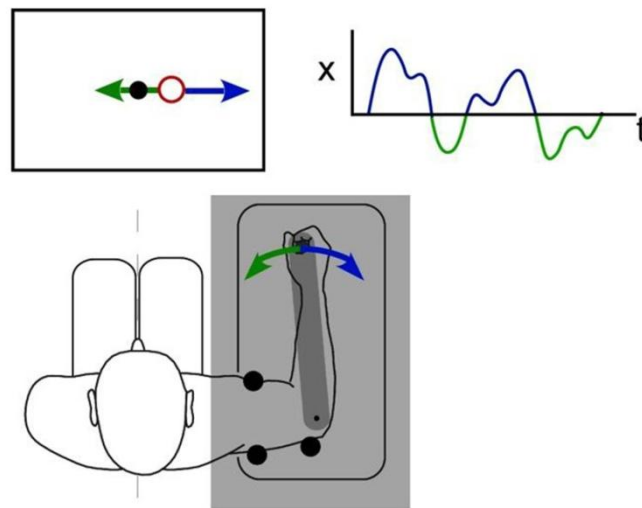
Figure 2-2: 1-D target tracking setup [57].
Subjects held the handle of a 1-D manipulandum while seated in front of a computer display. The position of a cursor (red ring) was manipulated by rotating the manipulandum handle about the elbow joint. The cursor (or arm) was continuously perturbed (upper right inset) with a zero-mean, band-limited disturbance, and the subject was asked to compensate by bringing the cursor to a target (black circle) presented in the center of the display. The arm was occluded by an opaque screen (shaded region) so that the cursor provided the only visual cue of arm movement.

2.2.4. Target Tracking Tasks

Continuous visual or torque perturbations were applied to the cursor, target, or arm, respectively, during the 1-D target tracking tasks described below and summarized in Table 2-1. During compensatory tracking (stabilization against an external perturbation), subjects were asked to compensate for low- or high-frequency visual and torque perturbations (low-frequency: 0-1Hz, band-limited white noise; high-frequency: 0-10Hz, band-limited white noise, low-pass filtered at 1 Hz) by bringing the cursor or arm to the desired (stationary) target location as quickly and accurately as possible. During pursuit tracking (target tracking), subjects were asked to track a target with low- or high-frequency visual perturbations (low-frequency: 0-1Hz, band-limited white noise; high-frequency: 0-10Hz, band-limited white noise, low-pass filtered at 1 Hz such that higher frequencies are attenuated but still present) by bringing the cursor to the moving target as quickly and accurately as possible. Subjects performed between 10 and 25 trials per task. Trial lengths varied by task and ranged from 8-32 seconds, with 15-30 seconds of rest between trials. During the rest period, the screen displayed the instruction "relax". Two seconds before the start of the next trial, subjects were cued to "get ready". The trial then began when the cursor and target appeared on the screen.

Table 2-1: Summary of experimental tasks and analysis

Task	Input	Parameter measured		Analysis method
Task 1	Low frequency visual perturbation	T_v	Visual response delay	Cross correlation of subject response with input
		T_v^*	Predicted response delay	
Task 2	Low-frequency torque perturbation	T_p	Proprioceptive response delay	Cross correlation of subject response with input
		T_p^*	Predicted proprioceptive response delay	
Task 3	Fixed levels of isometric torque	α	Multiplicative motor noise	Linear fit of variance vs. average torque
Task 4	High-frequency visual perturbation	J, B, K	Inertia, viscosity, stiffness of elbow	Bootstrapped model fit to the subject's measured frequency response function (FRF)
		J^*, B^*, K^*	Predicted inertia, viscosity, stiffness of elbow (matched to J, B, K)	
		K_v, K_d, K_{pr}, K_i	Controller gains	
		$\sigma_v^2, \sigma_p^2, a_v, a_p$	Sensory noise parameters	
Task 5	Visual offset	RMSE	Movement error	Kinematic analysis

Tasks 1 and 2: Compensatory tracking with low-frequency perturbations

Visual *(T_v, T_v*)* and proprioceptive *(T_p, T_p*)* delays were characterized in separate compensatory tracking tasks. Subjects performed 10 trials per task and trial duration was 20 seconds in each case. In the first task (Task 1), visual response delays *(T_v, T_v*)* were characterized by applying continuous pseudorandom visual displacements (0.05 – 1 Hz; RMS = 10° visual angle) to the cursor position while subjects applied counter movements to the manipulandum so as to maintain the cursor on a stationary target presented at the center of the display.

In the second task (Task 2), proprioceptive response delays *(T_p, T_p*)* were characterized by applying continuous pseudorandom torque perturbations (0.05 – 1 Hz;

RMS = 0.3 Nm) to the manipulandum while subjects applied counter torques to keep the manipulandum aligned perpendicular to the computer monitor. No visual feedback of arm position was provided during the torque perturbations so as to constrain sensory feedback to the proprioceptive path. To account for passive dynamics of the arm in the measured torque response during the second task, an additional five "control" trials (30 sec. each) were collected during which subjects were instructed not to apply corrective torques (i.e. subjects were instructed to maintain the same posture and level of stiffness as in the other tasks, but to not otherwise interfere with the task). During these trials, a high frequency torque perturbation was applied to the arm (0-30Hz, RMS = 1 Nm; first-order zero-phase Butterworth filter with 1Hz cutoff). The contribution of the passive mechanical impedance of the arm to the measured torque was estimated from the least-squares linear regression between the passive torque applied by the arm and externally applied torques during the passive trials ($R^2 > 0.75$). The contribution of the passive mechanical impedance of the arm was then subtracted from the measured torque to estimate subjects' voluntary corrective torque during proprioceptive task trials.

Task 3: Tracking of step torque

Signal-dependent motor variability ("motor noise"), was assessed using an isometric task adapted from Jones et al [113], which measured joint torque variability as a function of average joint torque. During the task, the manipulandum position was fixed parallel to the subject's sagittal plane while subjects produced several isometric torque contractions. Displacement of the cursor from the center of the screen scaled in

proportion to the torque applied to the manipulandum. The subject was required to place the cursor on one of five targets (desired elbow joint torques of 4, 6, 8, 10, and 12 Nm flexion) by applying the appropriate isometric contraction. Five trials were collected at each of the five torque levels (25 trials total). During each eight-second trial, visual feedback of the target and cursor was shown for the first three seconds. Visual feedback was then removed, while subjects attempted to maintain the specified torque level for remaining five seconds.

Task 4: Compensatory tracking with high-frequency perturbations

High-frequency, visual compensatory, visual pursuit, and proprioceptive compensatory tracking tasks were used to characterize the remaining elements of the sensory feedback control model including the controller gains (K_d, K_{pr}, K_i), visual and proprioceptive feedback gains (K_v, K_p), task gain (K_s), arm dynamics (J, B, K, J^*, B^*, K^*), and noise (N). During the task, high frequency, continuous, pseudorandom visual and torque perturbations (0-10 Hz, RMS = 20°, first-order zero-phase Butterworth filter with 1 Hz cutoff) were applied to the cursor, target, or manipulandum, respectively. During visual tasks, subjects were asked to bring the cursor to the target (whether moving or stationary) as quickly and accurately as possible; during the proprioceptive task, subjects were asked to continuously return their elbow to a neutral (90° flexion) position. Ten 32-second trials were obtained for each subject.

Task 5: Pursuit tracking of step displacements

A step displacement task was used to characterize changes in motor output during aging. Subjects performed ten trials of the task. Each 10-second trial started with the target and cursor located at the same screen position. After a one second delay, the target was randomly displaced to the left or right by a randomly selected distance ranging ±24.4 cm along the horizontal midline of the display (corresponding to ±11.5 degrees of visual angle). Subjects were instructed to center the cursor on the target as quickly and accurately as possible and to maintain the cursor position until the end of the trial.

2.2.5   Data Analysis

Sensory delays (Tasks 1 & 2)

We used cross correlation analysis to estimate delays in the visual and proprioceptive feedback-driven responses to band-limited low-frequency perturbations applied in the two low-frequency compensatory tracking tasks (Tasks 1 & 2). The visual response delay, T_v, was estimated as the trial-wise average of the temporal offset (lag) between the perturbations in cursor position applied in Task 1 and the subject's corrective responses measured by the robot's handle position. The proprioceptive response delay was obtained by correlating the subject's voluntary corrective torque response in Task 2 with the applied torque perturbations. The proprioceptive response delay, T_p, was estimated as the trial-wise average of the temporal lag between the continuous torque

perturbations applied to the arm in Task 2 and the subject's voluntary corrective responses. For the purposes of this study, delays and their forward estimates (T_v, $T_v{}^*$, T_p, $T_p{}^*$) were assumed to be equivalent.

Signal-dependent motor noise (Task 3)

The gain of the multiplicative (signal-dependent) motor noise, α, was estimated using the torques measured during Task 3, which involved pursuit tracking of step torque targets. For each target torque level, the mean and variance in the applied torque was measured during the last five seconds of each trial (i.e. after visual feedback was removed). The gain of the multiplicative noise α was estimated as the slope of the linear regression between the mean and the variance of the trial-averaged torque as a function of target torque level.

Frequency response analysis (Task 4)

For each subject, we estimated the remaining model parameters (K_s, K_d, K_{pr}, K_i, K_v, K_p, J, B, K, N) using the transfer functions of our model. The analysis consisted of a two-stage frequency response analysis, which related the experimentally-imposed cursor, target, and torque perturbations to changes in arm position. During the analysis, each subject's sensory delays and motor noise parameters were held constant at values derived during the analysis of data from the first three tasks. Forward model parameters (J^*, B^*, K^*, $K_v{}^*$, $K_p{}^*$) were constrained to be identical to their corresponding model parameters (T_v,

T_p, J, B, K, K_v, K_p). The remaining model parameters were fit to each subject's responses in the frequency domain using the simplex method (Matlab: `fminsearch`).

In the first stage of the analysis, the second-order model of musculoskeletal dynamics (Eq. 2) was fit to the magnitude of the frequency response function (FRF) relating the subject's arm position to the applied torque. To reduce measurement noise prior to the model fit, FRFs were computed for all pair-wise combinations of trials as the ratio of the trial-wise differences between the applied torque (τ) and measured arm position (θ_a) (See Appendix A), and then averaged:

$$FRF(s) = \frac{1}{M}\sum_{i=1}^{N}\sum_{\substack{j=2\\j>i}}^{N}\frac{\theta_{a_i}(s)-\theta_{a_j}(s)}{\tau_i(s)-\tau_j(s)} \tag{3}$$

where N is the number of trials and M is the total number of trial-wise pairs.

In the second stage of the analysis, the remaining model parameters were estimated from the transfer function relating the applied visual perturbation (D_{ext}) and measured arm position (θ_a):

$$\theta_a(s) = -\left[\frac{K_v C(s)P(s)e^{-T_v s}}{1+C(s)P^*(s)-C(s)P^*(s)*\left(K_v^* e^{-T_v^* s}+K_p^* e^{-T_p^* s}\right)+C(s)P(s)\left(K_v e^{-T_v s}+K_p e^{-T_p s}\right)}\right]D_{ext}(s) \tag{4}$$

which, when forward model parameters are matched to their feedback model counterparts, simplifies to:

$$\theta_a(s) = -\left[\frac{K_v C(s)P(s)e^{-T_v s}}{1+C(s)P(s)}\right]D_{ext}(s) \tag{5}$$

the transfer function relating the applied target perturbation (θ_d) and measured arm position (θ_a):

$$\theta_a(s) = \left[\frac{C(s)P(s)e^{-T_v s}}{1+C(s)P^*(s)-C(s)P^*(s)*\left(K_v^* e^{-T_v^* s}+K_p^* e^{-T_p^* s}\right)+C(s)P(s)\left(K_v e^{-T_v s}+K_p e^{-T_p s}\right)}\right] D_{ext}(s) \tag{6}$$

which simplifies to:

$$\theta_a(s) = \left[\frac{K_s C(s)P(s)e^{-T_v s}}{1+C(s)P(s)}\right]\theta_d(s) \tag{7}$$

and the applied proprioceptive perturbation (D_{torque}) and measured arm position (θ_a):

$$\theta_a(s) = \left[\frac{P(s)\left(1+C(s)P(s)\left(1-K_p*e^{-T_p s}\right)\right)}{1+C(s)P(s)}\right] D_{torque}(s) \tag{8}$$

where P(s) and C(s) are the Plant and Controller transfer functions, respectively, defined by Equations 1 and 2.

The remaining transfer functions related the internal noise sources to the subject's arm position for all three tasks. The effect of sensory noise on limb position was estimated for each task using a subtraction analysis (see Appendix A) that removed the contributions of the perturbation signal. In this study, internal visual and proprioceptive noises were assumed to be statistically independent. The source(s) of sensory noise were assumed to be common across tasks such that the model transfer function was the same for each task (Eq. 9):

$$N(s) = \frac{1}{s+a_v} * \frac{K_v C(s)P(s)}{1+C(s)P(s)} * \sigma_v^2 + \frac{1}{s+a_p} * \frac{K_p C(s)P(s)}{1+C(s)P(s)} * \sigma_p^2 \tag{9}$$

where N(s) is the effective sensory noise at the output, σ_v^2 and σ_p^2 are the variance of the visual and proprioceptive noise sources, respectively, and a_v and a_p are filter constants

associated with the independent noise sources. For the proprioceptive compensatory tracking task, K_v (visual gain) was assumed to be 0 since no visual feedback of limb position was provided.

The six FRFs defined across the three task conditions (effects of perturbation and effective sensory noises on subject responses during visual compensatory tracking (Eqs 5, 9); visual pursuit tracking (Eqs. 7, 9); proprioceptive compensatory tracking (Eqs. 8, 9)) were fit to model transfer functions simultaneously. Parameters defining the noise sources for the noise FRFs (σ_v^2, σ_v^2, a_v, a_p) were assumed to be common across all tasks, but noise spectra could be altered by task-specific sensory weights, controller gains, and plant dynamics. During the fits, α (motor noise), T_v and T_p (delays) and J, B, and K (plant dynamics) for each task were fixed at the values calculated in previous analyses.

A bootstrap analysis was applied at each stage of the model fitting procedure to quantify uncertainty in parameter estimates of the FRF associated with measurement noise and model initial conditions. For each bootstrap, 10,000 model fits were performed (with random sampling of the initial conditions for each parameter and of the FRF data points included in each fit): Initial conditions for each parameter were selected from a uniform distribution spanning one order of magnitude centered on nominal values estimated across subjects in a previous analysis [6]; Three hundred data points were selected randomly with replacement across the three-decade range of the FRF. Model fits that did not converge to a solution within 400 iterations due to poor initial parameter estimates (~10% of cases) were discarded from subsequent analysis. For the remaining fits, the mean and standard deviation of the fitted parameters were used to estimate the nominal best-fit value and magnitude of uncertainty in the model parameters. For the

second-stage bootstrap, plant parameter triplets (J, B and K) were randomly sampled from the first-stage FRF analysis to propagate the accumulated error across sequential model fits. During the second stage fits, these triplets were held constant.

Pursuit tracking of step target displacements (Task 5)

For each subject, target acquisition time and mean squared endpoint error were calculated and averaged across trials. Target acquisition time (AT) was calculated as the time required for the subject to move within two degrees of the target after the target appeared. Endpoint error was calculated as the mean-square error (MSE) from the moment of target acquisition to the end of the trial. AT and MSE were used to quantify changes in motor performance with aging.

Statistical Analysis

Statistical analysis was performed using MATLAB and IBM SPSS Amos (IBM, Armonk, NY, USA). Basic statistical analysis (mean, variance, linear regressions) was performed (using MATLAB) in order to examine simple correlations between parameters and to compare parameter values across tasks. Model parameters and noise were related via a piece-wise function in which parameters were fit by a constant value (up to a certain age) followed by a linear increase/decrease.

Amos was used to perform structural equation modeling (SEM) to directly test specific models of age-related changes in sensorimotor control. Structural equation

modeling is a statistical method that tests a theoretical model of relationships between variables; the goal is to determine the extent to which the model accounts for the covariance of the data. Specifically, we used path analysis (also called causal modeling), a type of SEM that tests directional dependencies between variables, to examine the mechanisms of age-related changes in sensorimotor control. In constructing a path analysis, directed relationships are hypothesized between variables. A model covariance is generated, and this model is compared against the covariance matrix of the sample data. These two covariance matrices are compared statistically using the χ^2 test of independence to determine whether the model covariance and data covariance can be considered to be different.

In an initial analysis, model parameters were divided into three groups by task, resulting in 7 parameters for proprioceptive compensatory tracking, 11 parameters for visual compensatory tracking, and 12 parameters for visual pursuit tracking. Limb inertia was not included in the SEM, as it was assumed to be independent of both age and strategic movement choices. Age was assumed to be an exogenous (independent, no measurement error), uncorrelated factor; all other variables (sensory gains, controller gains, plant parameters, noise, movement error, target acquisition time) were assumed to be endogenous (dependent, possible measurement errors). During SEM for proprioceptive compensatory tracking, movement error and target acquisition time were excluded, since these movement outcomes were calculated from a visual, not proprioceptive, task. For the purposes of this study, we assumed that there were no latent (unmeasured) variables underlying endogenous parameters. The probability that each class of model described the changes in parameters was estimated by comparing the

theoretical covariance matrix of the model against the covariance matrix of the supplied data; statistical measures were the chi-squared test, which quantifies the probability that the model and data covariance matrices differ, and the goodness-of-fit index (GFI), which measures the amount of variance and covariance accounted for by the model covariance matrix. A specification search was performed using Amos to examine all possible combinations of paths within each model class in order to determine the path combinations that best account for the observed changes in sensorimotor control with age.

2.3   RESULTS

2.3.1   Participants

Twenty-four subjects were included in the final analysis and ranged in age from 20-76 years old (mean: 41 ± 18 years; N(18-30) = 11; N(31-50) = 5; N(51-60) = 3; N(61-70 = 4; N(71-80) = 1). Ages were evenly distributed within genders; the age of the women (39 ± 16 years; range: 20-63 years) did not differ significantly from the age of the men (43 ± 21 years; range: 20-76 years) (t(22) = 0.41; p = 0.68). A full table of task parameters can be found in Appendix B.

2.3.2   Sensory response delays

The mean visual response delay across subjects was 448.7.4±60.2 ms. Visual response delays exhibited a significant linear correlation (Figure 2-3, left) with age (r =

0.43; p = 0.029); delay was constant until age 25, after which it increased by approximately 1.5 ms per year of age. The mean proprioceptive response delay across subjects was 228.9±88.4 ms (Figure 2-3, right). Proprioceptive response delay was not well fit by the piece-wise function (r = 0.29; p = 0.15).
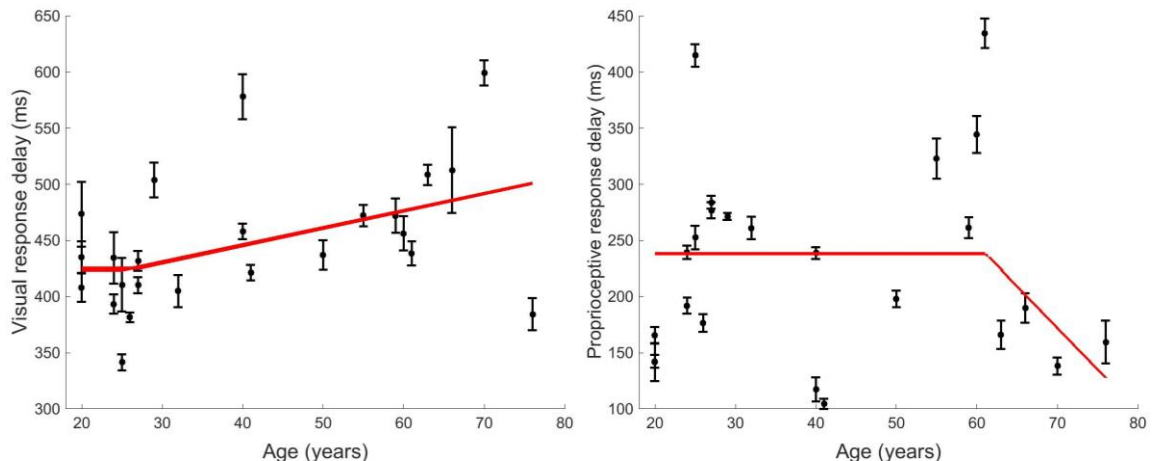
Figure 2-3: Visual (left) and proprioceptive (right) response delays vs. age.
Individual subject data (black circles) and the best-fit piece-wise regression (red). Error bars denote standard error. Visual response delay is positively correlated with age, while proprioceptive response delay is not significantly correlated with age.

2.3.3 Feedforward Motor Noise and Plant Dynamics

Feedforward motor noise did not change significantly with age (mean = 0.067±0.026; increase after age 20; r = 0.35; p = 0.11). Elbow joint dynamics exhibited systematic changes with age; as our model is linearized, changes in muscle tension and co-contraction can affect both the lumped plant viscosity and lumped plant stiffness. Plant viscosity increased with age during visual compensatory tracking (mean = 1.14±1.01; increase after age 32; r = 0.70; p < 0.001), visual pursuit tracking (mean = 0.69±.0.58; increase after age 40; r = 0.63; p < 0.001), and proprioceptive compensatory tracking

(0.89±0.30; increase after age 63; r = 0.68; p < 0.001). Plant stiffness also increased significantly during visual compensatory tracking (mean = 5.48±3.00; increase after age 29; r = 0.59; p = 0.0027), pursuit tracking (4.30±1.48; increase after age 41; r = 0.42; p = 0.039), and proprioceptive compensatory tracking (13.97±7.57; increase after age 66; r = 0.83; p = 0.027). The change in viscosity with age was greatest during visual compensatory tracking; for stiffness, the change was greatest during proprioceptive compensatory tracking. Across subjects, elbow viscosity was significantly higher during visual compensatory tracking than during visual pursuit tracking (paired t-test; t(22) = 3.18; p = 0.0042) but there was no significant difference in viscosity between visual pursuit tracking and proprioceptive compensatory tracking or between visual compensatory tracking and proprioceptive compensatory tracking (paired t-test; t(22) > 2.0; p > 0.05). Significant differences in elbow stiffness were observed between the three tasks for elbow stiffness such that stiffness was highest during proprioceptive compensation and lowest during visual tracking (paired t-test; t(22) > 1.9; p < 0.05).

Plant inertia was not expected not to change with age or task type. However, during compensatory tracking, limb inertia was found to positively correlate with age (mean = 0.057±0.024; r = 0.51; p = 0.011). Changes are most likely due to un-modeled non-linearities in the elbow system. Limb inertia did not change significantly with age during either visual pursuit tracking or proprioceptive compensatory tracking (p > 0.05). Across subjects, limb inertia was significantly lower during visual pursuit tracking than during proprioceptive compensatory tracking (paired t-test; t = 3.28; p = 0.0032).

2.3.4 Neural Controller Gains

All FRFs were well-fit by the sensorimotor control model ($r^2 > 0.80$). FRFs for both the perturbations and the noise are shown in Figure 2-4.
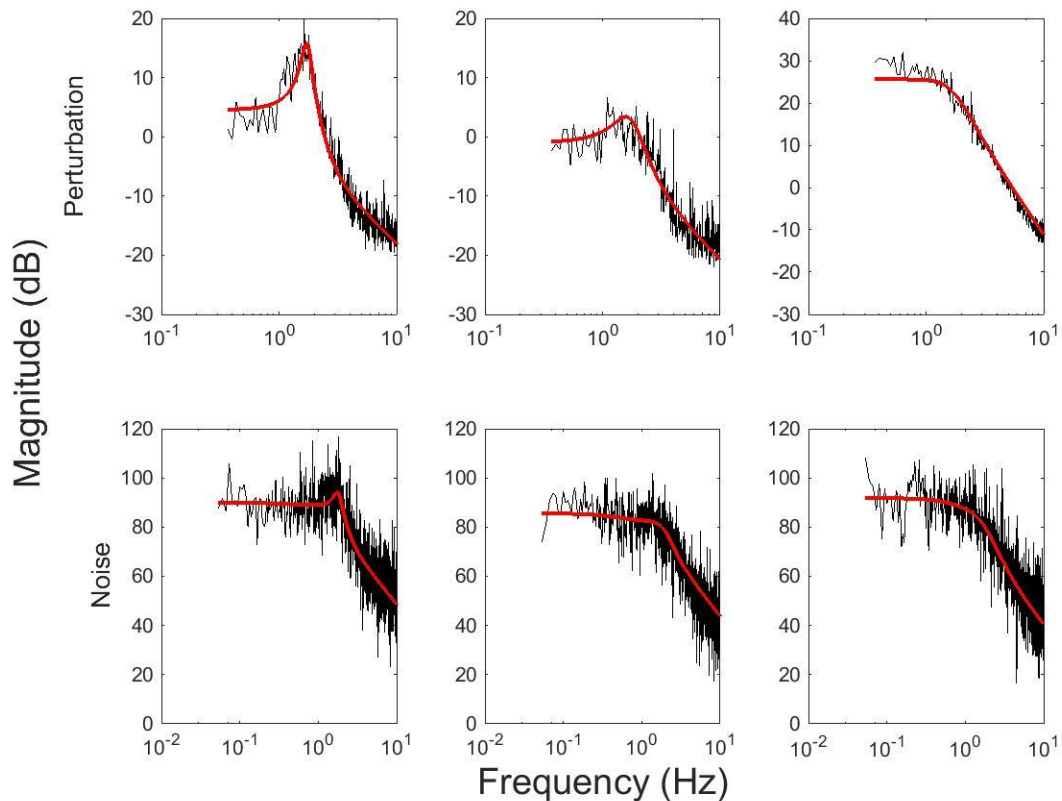
Figure 2-4: Frequency response functions relating subject responses to external perturbations (top) and noise (bottom).
Left: visual compensatory tracking; center: visual pursuit tracking; right: proprioceptive compensatory tracking. Subject FRFs for a representative (age = 25 years) subject are shown in black the best model fits for each FRF are shown in red.

During visual compensatory tracking, derivative (mean=0.0052±0.0055; increase after age 50; r = 0.62; p = 0.0011) and proportional (mean=0.29±0.33; increase after age 55; r = 0.79; p < 0.001) and integral gains increased with age (mean=2.54±6.82; increase

after age 59; r = 0.42; p = 0.039). During visual pursuit tracking, derivative (mean =

0.0045±0.0029; increase after age 20; r = 0.53; p = 0.0079) and proportional gain (mean =

0.20±0.20; increase after age 40; r = 0.63; p <0.001) increase with age. During

proprioceptive compensatory tracking, none of the controller gains varied consistently

with age (p < 0.05). Across tasks, there was no difference in any controller gains between

the three tracking tasks (paired t-test, t(22) > 2.0; p > 0.05).

2.3.5   Sensory gains

Visual gain decreased with age (mean=0.68±0.43; decrease after age 29; r = 0.65;

p < 0.001) for visual compensatory tracking, but not for visual pursuit tracking

(mean=0.95±1.32; r = .16; p = 0.45). During proprioceptive compensatory tracking, all

visual gains were assumed to be zero. Proprioceptive gains exhibited a similar trend,

decreasing during visual compensatory tracking (mean=0.78±0.57; decrease after age 32; r

= 0.58; p = .0028) and visual pursuit tracking (mean=0.50±0.52; decrease after age 29; r =

0.52; p = 0.0092). Proprioceptive gain also decreased during proprioceptive compensatory

tracking but the change was not significant (mean=2.35±2.27; decrease after age 27; r =

0.45; p = 0.026). Task gain during visual pursuit tracking also decreases; this decrease also

does not quite reach statistical significance (mean=0.84±0.53; decrease after age 40; r =

0.53; p = 0.0071). Across subjects, visual gain did not change between visual

compensatory and visual pursuit tracking (paired t-test; t(22) = 1.25; p = 0.22).

Proprioceptive gain did change with task such that the highest proprioceptive gain was

observed during proprioceptive compensatory tracking, and lowest proprioceptive gain during visual pursuit tracking (paired t-test, $t(22)>1.9$; $p < 0.05$).

2.3.6 Variance of Sensory Noise

The sensorimotor control model fit to the noise FRFs was unable to distinguish between visual and proprioceptive noise in subjects where the noise profiles (filter coefficients) were similar between visual and proprioceptive noise. For this reason, visual and proprioceptive noises were combined into a single sensory noise term for each task using a Bayes optimal weighting of sensory noises (Eq. 10):

$$N = \frac{Kv*Dv+Kp*Dp}{Kv+Kp} \tag{10}$$

The log of the combined sensory noise term (Figure 2-5) increased significantly with age for visual (mean=9.51 ± 0.75; increase after age 32; $r = 0.73$; $p < 0.001$) and proprioceptive (9.88 ± 1.05; increase after age 24; $r = 0.69$; $p < 0.001$) compensatory tracking. Increases in sensory noise during visual pursuit tracking did not quite reach statistical significance (8.98 ± 0.68; increase after age 29; $r = 0.39$; $p = 0.061$).
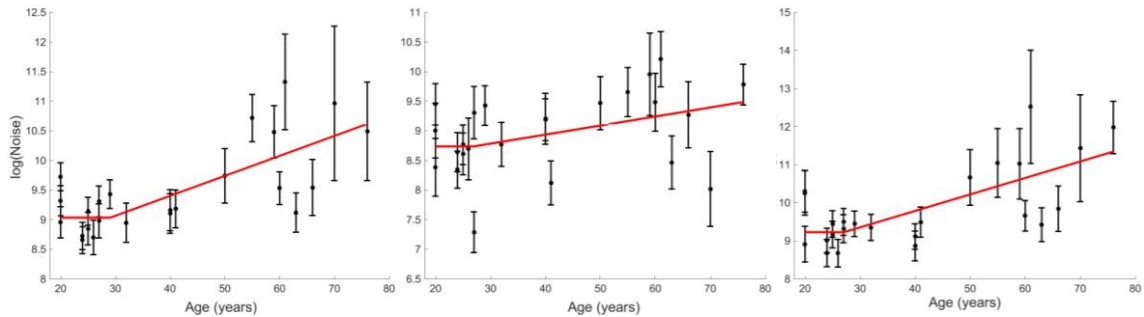
Figure 2-5. Sensory noise vs. age.
Sensory noise vs. age for visual compensatory tracking (left), visual pursuit tracking (middle),
proprioceptive compensatory tracking (right). Subject data is shown in black; best-fit piece-wise fits are
shown in red. Error bars denote standard error.

2.3.7   Movement error and target acquisition time

During the visually guided reach-and-hold task, average mean squared endpoint

error (MSE) across subjects was 0.0061 ± 0.0027 deg^2/ms. MSE did not increase with age

(Figure 2-6, left), until after age 66; as this only included two subjects, it is difficult to say

whether the piece-wise fit was fitting noise ($r = 0.81$; $p < 0.001$). Average target

acquisition time (TAT) across subjects (Figure 2-6, right) was 834.1 ± 179.0ms. TAT was

significantly correlated with age (increase after age 50; $r = 0.69$; $p < 0.001$).
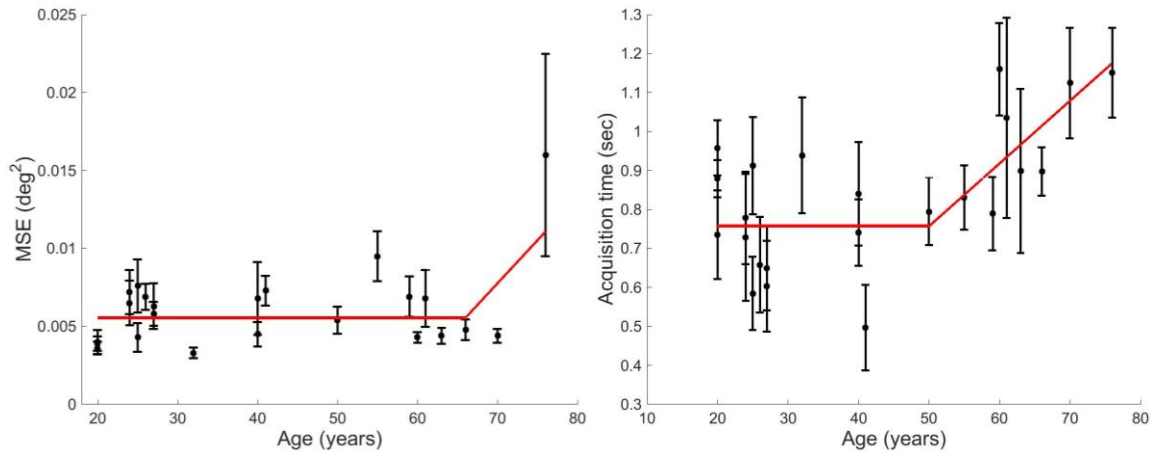
Figure 2-6: Mean square movement error (left) and target acquisition time (right) vs. age.
Error bars denote standard error. Best-fit piece-wise functions are shown in red over subject data.

2.3.8   Changes in parameters with age

We fit model parameters with a piece-wise function that assumed that parameters remained relatively constant in younger subjects before increasing or decreasing linearly with age in older subjects. In examining the age at which this change takes place, we noticed several characteristics that were consistent across tasks; results are summarized in Figure 2-7. First, sensory noise (N) begins to increase at a relatively young age (24-32 years); sensory gains (K_v, K_p) and visual delay (T_v) also begin to change around the same time for all tasks. During visual compensatory tracking, a linear increase in plant dynamics (B, K) occurs around the same time as increases in noise and sensory gains, while the controller gains (K_d, K_{pr}, K_i) change later (50-59 years). During visual pursuit tracking and proprioceptive compensatory tracking, in contrast, controller gains change around the same time as sensory noise and sensory gains, while plant dynamics change later. Finally, target acquisition time (AT) begins to increase around age 50, while

movement error (MSE) begins to increase much later, around age 66. These results may indicate direct impacts of aging on a limited number of parameters, while later changes are the result of strategic changes due to alterations in other movement parameters.
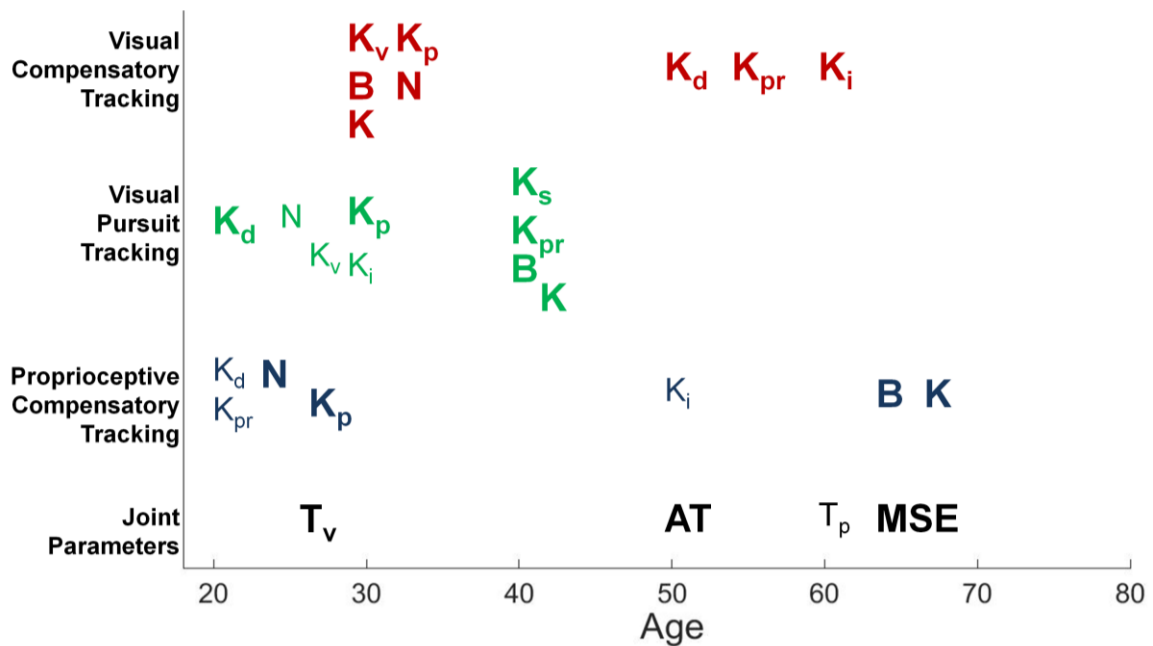
Figure 2-7. Ages at which sensorimotor control parameters begin to change.
Parameter names are plotted against the age at which they begin to change. Red: visual compensatory tracing parameters; green: visual pursuit tracking parameters; blue: proprioceptive compensatory tracking parameters; black: delays and movement outcomes. Bold lettering: statistical significance ($p < 0.05$).

2.3.9 Structural Equation Modeling

An initial analysis of sensorimotor control parameters across subjects identified significant correlations between a large number of sensorimotor control parameters (Table 2-2). In visual compensatory tracking, 21 of the 36 parameter pairs were correlated ($r > 0.40$; $p < 0.05$). In visual pursuit tracking, 11 of 45 parameter pairs were correlated ($r > 0.40$; $p < 0.05$). During proprioceptive compensatory tracking, 4 of 28 possible

correlations were statistically significant (r > 0.40; p < 0.05).To further parse the

interactions between model parameters (e.g. direct vs. indirect effects) structural equation

modeling was used to examine directional relationships between parameters.

Table 2-2: Correlations between model fitted parameters across subjects.
Correlations are shown for visual compensatory tracking (top), visual pursuit tracking (middle) and proprioceptive compensatory tracking (bottom). Significant correlations are highlighted in red. Values shown are Pearson's correlation coefficient (r).

	Kv	Kp	Kd	Kpr	Ki	N	J	B	K
Kv	1.00								
Kp	0.80	1.00							
Kd	-0.49	-0.38	1.00						
Kpr	-0.68	-0.60	0.67	1.00					
Ki	-0.38	-0.29	0.35	0.65	1.00				
N	-0.57	-0.61	0.30	0.59	0.33	1.00			
J	-0.33	-0.29	0.18	0.14	0.11	0.50	1.00		
B	-0.68	-0.63	0.77	0.81	0.34	0.51	0.07	1.00	
K	-0.57	-0.52	0.21	0.50	0.00	0.71	0.55	0.51	1.00

	Ks	Kv	Kp	Kd	Kpr	Ki	N	J	B	K
Ks	1.00									
Kv	0.30	1.00								
Kp	0.00	-0.13	1.00							
Kd	-0.55	-0.13	-0.08	1.00						
Kpr	-0.49	-0.23	-0.41	0.67	1.00					
Ki	-0.34	-0.18	-0.17	0.29	0.25	1.00				
N	-0.27	-0.79	-0.20	0.29	0.49	0.35	1.00			
J	0.01	0.16	0.20	0.52	0.05	-0.24	-0.31	1.00		
B	-0.31	-0.16	-0.29	0.15	0.31	-0.12	0.18	0.09	1.00	
K	-0.31	-0.19	0.00	0.55	0.48	0.12	0.09	0.50	0.47	1.00

	Kp	Kd	Kpr	Ki	N	J	B	K
Kp	1.00							
Kd	0.02	1.00						
Kpr	0.10	0.20	1.00					
Ki	0.00	0.44	0.24	1.00				
N	-0.41	0.11	-0.38	0.12	1.00			
J	-0.01	0.15	0.17	0.19	-0.18	1.00		
B	-0.38	-0.12	0.00	0.08	0.39	-0.22	1.00	
K	-0.39	-0.10	0.00	0.05	0.59	-0.22	0.67	1.00

Structural equation modeling applied to the fitted parameters was used to test specific hypotheses regarding the impact of age on sensorimotor control (Figure 2-8, below). Parameters were grouped by parameter type – sensory noise (lumped noise term), sensory gains (K_v, K_p), neural controller (K_d, K_{pr}, K_i), plant (B, K), and movement performance parameters (MSE, AT). Each task was tested separately, so that separate models of parameter relationships were generated for visual compensatory tracking, visual pursuit tracking, and proprioceptive compensatory tracking.

For the purposes of the modeling, each parameter type was assumed to have the same inputs and outputs. The first model tested whether aging is the direct cause of changes in all sensorimotor control and performance parameters (aging model). Three additional models tested specific hypotheses from the literature: (1) aging alters limb dynamics (plant), which alters all other parameters (plant-first model) [81]; (2) aging alters controller gains via changes in task strategy and goals, which alters all other parameters (controller-first model) [78]; and (3) aging alters sensory noise via loss of fidelity in sensory transmission and processing, which alters all other parameters (noise-first model) [77]. For the controller-first and plant-first models, we assumed that changes in sensory noise were due to age, since noise is an external input in the sensorimotor control model and thus is independent of other model parameters.

We also tested a hybrid model structure in which aging causes changes in sensory noise and either the plant (noise-plant model) or the controller (noise-controller model). Sensory noise then modulates sensory gains, while the plant and controller are causally linked. In both cases, both paths modulate the model output characterized by MSE and AT. Finally, we tested a "cascade" model in which age causes changes only in sensory

noise in order to see whether alterations in sensory noise could explain further changes in

movement control. In this model, sensory noise is modulated by age, followed by

changes in sensory gains, the controller, the plant, and movement parameters (controller-

plant cascade); alternatively, age causes changes in sensory noise, followed by changes in

sensory gains, the plant, the controller, and movement parameters (plant-controller

cascade).
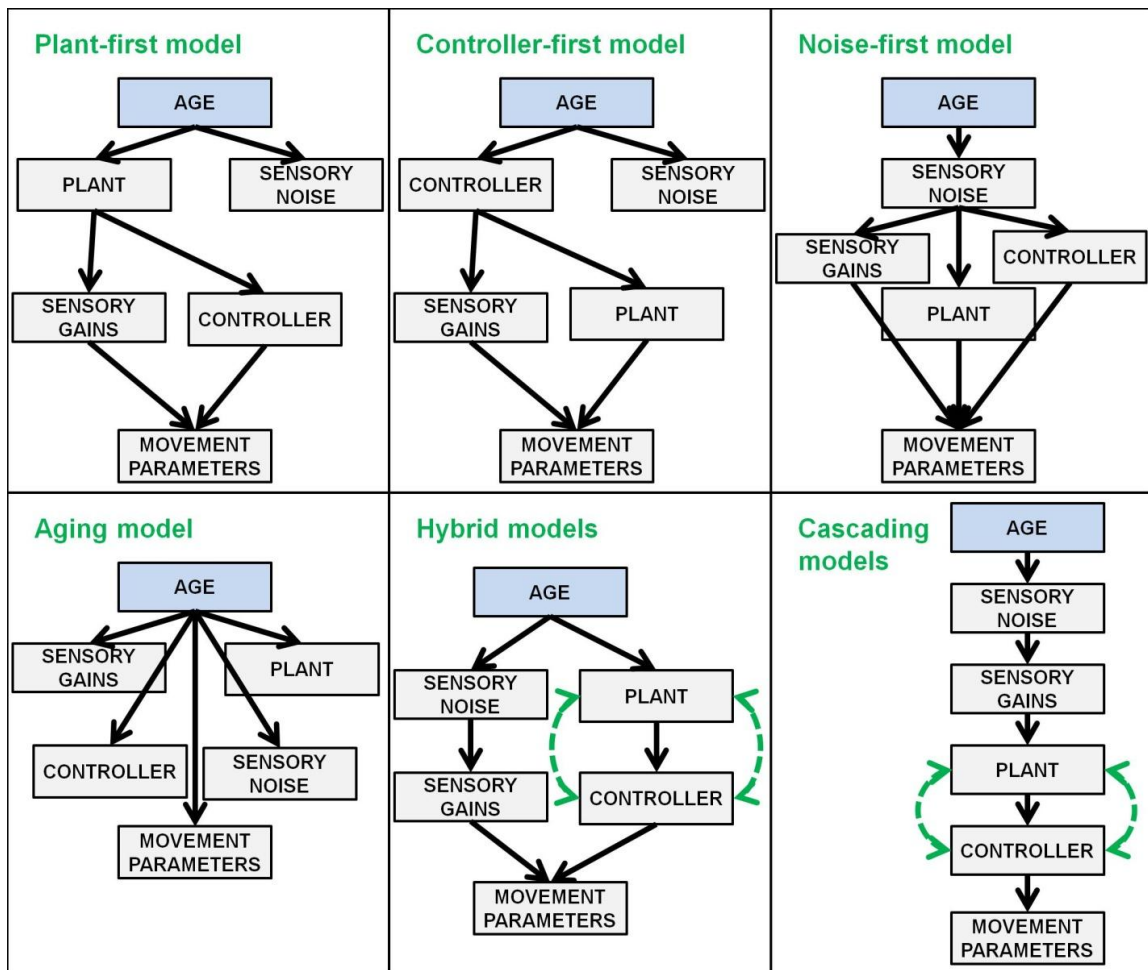
Figure 2-8. Proposed models of age-related changes in sensorimotor control
Independent (exogenous) parameters are shown in blue, while dependent (endogenous) variables are shown
in gray. Parameters are shown grouped by type here so that all 10 parameters are in five groups. Black
arrows indicate hypothesized causality. Green dashed arrows indicate that models were also tested with
these parameters swapped.

Each model was set up for visual compensatory, visual pursuit, and proprioceptive compensatory tracking to search for the most likely theoretical model of parameter relationships such that each parameter was connected to every parameter "below" it (as shown in Figure 2-8), resulting in a minimum of 10 possible paths (aging model) and a maximum of 65 possible connections (cascade models). Correlation coefficients between connected parameters were examined, and those with a p-value over 0.30 (r^2 approximately 0.05) were excluded from further analysis. The p-value of 0.30 was deliberately used to prune the model while minimizing the chances that a potentially beneficial path might be discarded. A "specification search" was then performed; this method searches all possible path combinations (by removing and adding path connections) to determine the best-fit model (based on the χ^2 statistic) of parameter relationships. This analysis was performed for each model class for the best-fit model. Best-fit path combinations for each model class were then compared across classes to determine the best overall model. The models' ability to account for age related changes in sensorimotor control was tested for visual compensatory, visual pursuit, and proprioceptive compensatory tracking.

The null hypothesis tested by SEM is that the model is able to account for the covariance of the data. Significant p-values ($p < 0.05$), therefore, indicate that the proposed model is *rejected* at the $\alpha < 0.05$ level, while p-values greater than 0.05 indicate that the model cannot be rejected, and can be considered as a possible candidate model. For visual compensatory tracking, all model classes were rejected ($p < 0.05$) except for the cascade model. The best fit path combination for the controller-plant cascade model ($df = 29$; $\chi^2 = 28.6$; $p = 0.49$); is shown in Figure 2-9 (left). The goodness-of-fit index

(GFI) for this path combination was 0.90; that is, it accounted for 90% of the variance and covariance of changes in model parameters. Age directly correlated with sensory noise, which modulates sensory gains, controller gains, arm stiffness, and movement error. Visual gain alters derivative and proportional gains and arm stiffness, while proprioceptive gain alters arm viscosity and target acquisition time. Controller gains modify movement error and arm viscosity; proportional gain specifically also alters acquisition time, while integral gain alters arm stiffness. Stiffness is correlated with movement error.

The best-fit path combination for the plant-controller cascade model (df = 28; χ^2 = 26.3; p = 0.56) is shown in Figure 2-9 (right). Changes in sensory noise are directly attributed to age. The best-fit path combination for this model accounts for 91% of the covariance in the parameters. Again, variations in sensory noise modulate sensory gains, arm stiffness, and target acquisition time. Visual gain is directly correlated with arm dynamics and proportional and integral controller gains, while proprioceptive gain modulates derivative gain and movement error. Arm viscosity is correlated with derivative and proportional gains and movement error; stiffness is correlated with integral gain and acquisition time. Controller gains are correlated with movement error.
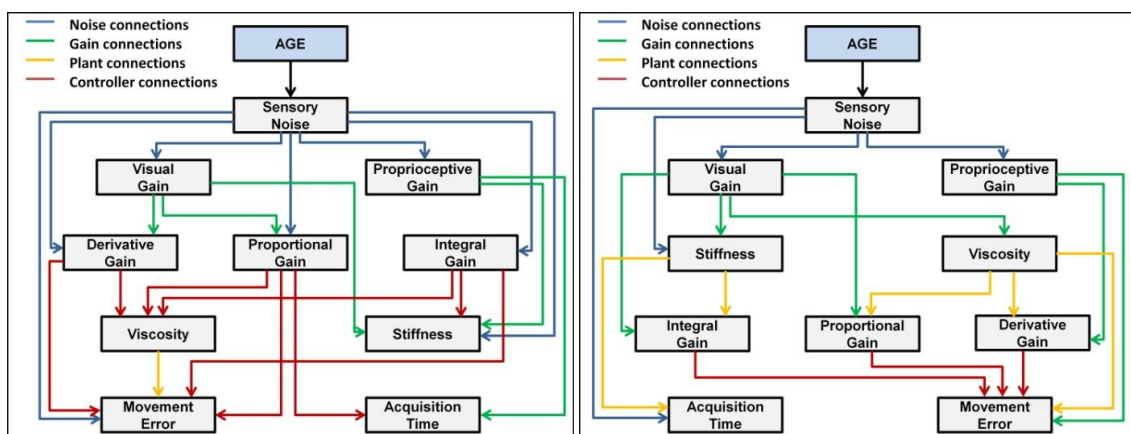
Figure 2-9: Cascade models of visual compensatory tracking.
The controller-plant cascade model is shown on the left and the plant-controller cascade model is shown on the right. Neither model was rejected (p > 0.05) by the SEM analysis. In each case, the model accounted for >90% of the covariance in parameters. Arrows denote directed (causal) relationships between sensorimotor parameters (blue: sensory noise paths; green: sensory and task gain paths; yellow: plant paths; red: controller paths).

For visual pursuit tracking, all model classes were again rejected (p < 0.05), with the exception of the cascade model (p > 0.40). The best-fit path combination for the controller-plant model (df = 35; χ^2 = 34.0; p = 0.514) is shown below in Figure 2-10 (left). The model GFI was 0.78; that is, it accounts for 78% of the covariance in the data. In the model, variations in sensory noise are altered by age and modulate sensory and task gains and elbow stiffness. Task gain, visual gain, and proprioceptive gains in turn modulate the controller gains. Task gain also alters limb viscosity while visual gain alters limb stiffness. Controller gains all alter limb viscosity, while only derivative gain and proportional gain are correlated with limb stiffness. Derivative gain, proportional gain, and limb viscosity are all correlated with target acquisition time. The best-fit path combination for the plant-controller model (df = 36; χ^2 = 35.68; p = 0.48) is shown in Figure 2-10 (right). The model accounts for 77% of the covariance in the data (GFI = 0.77). As in the controller-plant model, age alters sensory noise, which modulates sensory

and task gains as well as derivative gain. Proprioceptive and task gains modify arm

viscosity; task gain modifies arm stiffness. Task gain, sensory gains, limb viscosity and

limb stiffness modulate controller gains. Proprioceptive gain and task gain alter target

acquisition time.
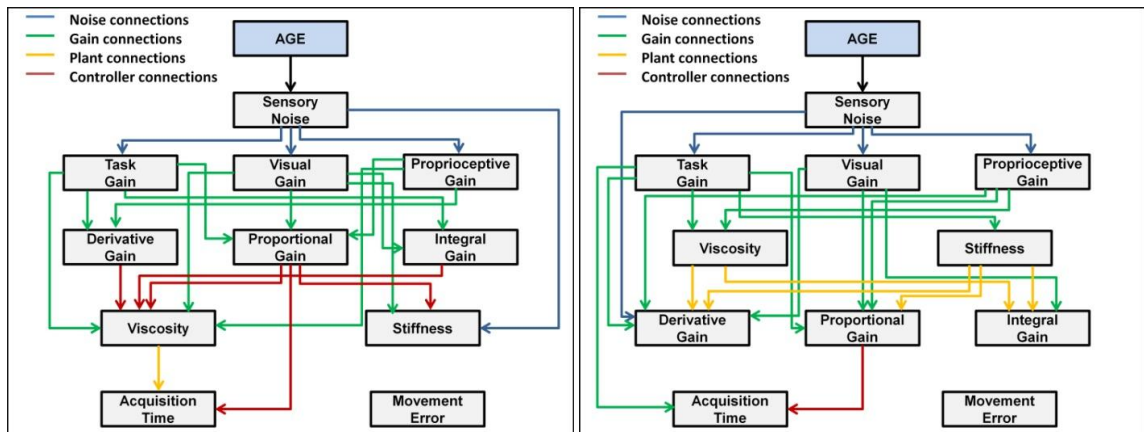

Figure 2-10: Cascade model of visual pursuit tracking.
The controller-plant cascade model is shown on the left and the plant-controller cascade model is shown on the right. Both models were not rejected (p > 0.05) by our analysis; models accounted for >75% of the covariance in tracking parameters. Arrows (blue: sensory noise paths; green: sensory and task gain paths; yellow: plant paths; red: controller paths) indicate paths that were not discarded during the specification search.

While modeling proprioceptive compensatory tracking, movement outcomes

MSE and AT were excluded from analysis since they were calculated from subject data

during a visual, rather than proprioceptive, task. As there were fewer correlations

between parameters, most relationships between parameters were eliminated and no

model was rejected at the p<0.05 level. However, similar to the visual task, the best path

models were Models 7 and 8 (cascade models). Best-fit path models are shown in Figure

2-11. The best fit model (df = 18; χ^2 = 15.1; p = 0.65) for the controller-plant cascade is

shown in Figure 2-11 (left). Aging alters sensory noise, which modulates proprioceptive

gain, plant viscosity, plant stiffness, and proportional gain. Plant stiffness also modulates

proportional gain. Model GFI is 0.79; the model accounts for 79% of data covariance.

The best-fit plant-controller model (df = 17; χ^2 = 15.5; p = 0.56) is shown in Figure 2-11

(right). Aging alters sensory noise, which modulates proprioceptive gain, plant stiffness,

and plant viscosity. Plant viscosity and stiffness are also altered by derivative and

proportional gains. Model GFI is 0.79; again, the model accounts for 79% of data

covariance.
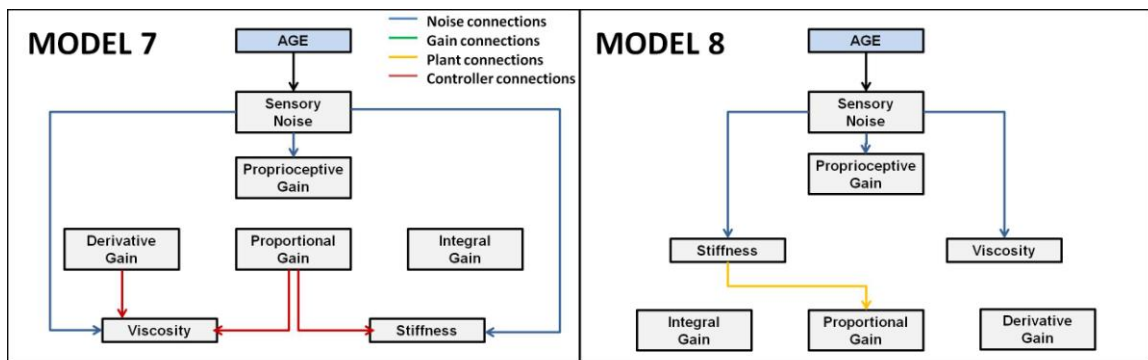
Figure 2-11: Cascade model of proprioceptive compensatory tracking.
The controller-plant cascade model is shown on the left and the plant-controller cascade model is shown on the right. Both models were not rejected (p > 0.05) by our analysis; models accounted for >75% of the covariance in tracking parameters. Arrows (blue: sensory noise paths; green: sensory and task gain paths; yellow: plant paths; red: controller paths) indicate paths that were not discarded during the specification search.

2.4   DISCUSSION

Here, we used systems identification techniques applied to pursuit and

compensatory tracking tasks to examine the effects of aging on motor control about the

elbow during goal-directed movement. Characterization of sensorimotor control within

subjects revealed a large number of model parameters that were significantly correlated

with age, including those associated with movement planning and sensory noise. To better

understand the specific impact of aging on these elements of motor control, either directly

(as an immediate effect of age) or indirectly (in response to age related changes elsewhere in the system), structural equation modeling was used to test specific hypotheses regarding the causal effects of age-dependent changes in motor control. Four classes of models were examined: (1) a direct aging model, in which all sensorimotor parameters are directly altered by aging; (2) specific hypotheses from the literature, including changes in strategy (controller) [81], changes in limb dynamics (plant) [78] and changes in sensory noise [77]; (3) a hybrid model, which combine two separate hypotheses – that sensory gains are altered as a result of changes in sensory noise, and that aging directly affects either the controller or plant; (4) a "cascade" model, in which age directly affects only sensory noise, which, in turn, alters sensory gains, and the neural controller/plant.

The first model tested whether aging could directly account for all changes in model parameters and was rejected for visual compensatory and visual pursuit tracking, indicating that changes in age alone could not adequately account for the covariance between model parameters. Although aging is significantly correlated with a large number of parameters, the SEM analysis indicates it is not the direct cause of the observed changes, suggesting indirect effects of age on model parameters. We further tested a series of mixed-path models in which each major element of the sensorimotor control model (e.g. the neural controller) was modulated by aging, and in turn modulated other parameters. As an external model input, sensory noise was assumed to be modulated directly by age in all mixed path models. Each of these models was also rejected ($p <$ 0.05) for visual compensatory and pursuit tracking.

These results suggest that changes in strategy with aging are not simply due to altered movement goals (controller-first hypothesis model) and therefore changes in

movement strategy may be the result of underlying movement deficits. Further, the rejection of the plant-first hypothesis model, taken with the result that feedforward motor noise does not increase with age, suggests that changes in motor noise or in effective limb dynamics are not primarily responsible for changes in movement planning; changes in limb dynamics may therefore be a deliberate strategic choice. Finally, the rejection of the noise-first hypothesis model suggests that age-related changes in sensory noise are unable to directly account for the widespread changes in sensorimotor control characterized here.

The hybrid model postulated that sensory noise and sensory gains would be inversely related, while aging directly affected either the neural controller or the plant. This class of models was also rejected ($p < 0.05$), suggesting that a model in which aging affects multiple model parameters independently may not be able to account for our data. Finally, we tested a "cascade" model – one in which aging alters sensory noise, which modulates sensory gains; sensory gains then alter either the plant or the neural controller, which are responsible for changes in movement speed and accuracy (as measured by MSE and AT). This model class was not rejected for visual compensatory tracking, visual pursuit tracking, or proprioceptive compensatory tracking, indicating that the covariance of subject parameters did not differ significantly from the covariance predicted by the structural equation model. For visual compensatory tracking, the cascade models accounted for > 90% of the parameter covariance with age. During visual pursuit tracking, the models accounted for > 75% of the covariance with age. Finally, for proprioceptive compensatory tracking, these models accounted for 79% of the covariance of the sample data.

These models are supported by the results from our piece-wise function fits; the ages at which parameters change correspond with the parameter ordering of the best-fit cascade models. This analysis supports the theoretical structure tested by the structural equation modeling. These results suggest that noise and sensory gains are altered simultaneously, indicating that sensory re-weighting may occur on relatively short time scales. For visual compensatory tracking, effective plant dynamics are altered at approximately the same time, while controller gains begin to change much later. During visual pursuit tracking and proprioceptive compensatory tracking tasks, controller gains are altered first, while effective plant dynamics change later. This may indicate that altering a single facet of movement strategy (either effective plant dynamics or neural controller gains) may be effective in the short term, but ultimately not sufficient to compensate for continued changes in sensorimotor control.

In the cascade structural model, only sensory noise was directly modulated by age; age-related modulation of all other sensorimotor parameters occurred indirectly in response to the changes in sensory noise. In conjunction with the finding that visual response delays increased with age, this result implies that changes in sensory feedback may be a significant contributing factor to age-related changes in movement control. Since we did not see significant changes in proprioceptive response time, it seems unlikely that time delays related to sensory conduction are a significant factor in increased response time. The increases in response time and sensory noise may instead reflect deficits in sensory and/or cognitive processing. Previous research has shown that older adults take more time to process complex information than younger adults [90, 91, 115]. Visual processing is a complex task involving multiple stages of processing across visually-

responsive areas of cortex which may be particularly susceptible to the effects of cognitive slowing; increases in sensory noise during proprioceptive compensatory tracking suggest that sensory processing may be impacted more generally.

In the cascade model, changes in sensory noise led to decreases in sensory gains. From a Bayesian perspective, the decrease in sensory gains reflects an effort to maximize movement accuracy while minimizing feedback noise [49, 52]. In support of this, changes in gains are largest during compensation tasks (both visual and proprioceptive), which rely most heavily on accurate sensory feedback. The SEM analysis suggests that the combination of sensory noise and sensory gains drives changes in controller gains and effective limb dynamics, which in turn interact to impact changes in movement error and target acquisition time during visual tasks. In contrast, the relative lack of parameters correlated with age during proprioceptive compensatory tracking may indicate that proprioceptive control of movement is less susceptible to the effects of aging than visual control of movement.

In the best-fit cascade model of visual compensation, controller gains modulate movement error. For visual pursuit tracking, controller gains are not correlated with movement error; instead proportional gain (for both models) and derivative gain (for one model) are both correlated with target acquisition time. In our task paradigm, pursuit tracking may correspond to an open-loop movement strategy, while compensatory tracking corresponds to closed-loop movement control. In this case, open-loop control corresponds to the early part of the movement, particularly that which alters target acquisition time, while closed-loop control takes over to guide endpoint acquisition. This supports a theory of movement control in which reach-and-hold tasks encompass two-

stages of motor control, composed of a transport phase – corresponding to open-loop control strategies – and a stabilization phase – corresponding to closed-loop control strategies [43, 44, 114]. In both cascade models for visual compensatory tracking, changes in effective joint dynamics contribute to movement error and/or acquisition time, while error and acquisition time are much less dependent on the limb dynamics in the visual tracking task, suggesting that limb stiffness may play a larger role strategically during the closed-loop phase of movement than during the open-loop phase of movement.

In our analysis, models in which controller parameters directly modulate limb dynamics (i.e. the plant) and vice versa did not differ significantly and could suggest that changes in both the controller and limb dynamics are modulated jointly, possibly by an additional latent variable that governs movement strategy. In the current SEM analysis the contribution of latent variables was not directly tested due to the limitations of our data; due to the small sample size and large number of possible correlations, additional path combinations could result in an underconstrained model. Future analyses could seek to increase the number of subjects in order to perform more rigorous analyses of the path models defining within the cascade model.

In our analysis, models in which age-related changes in sensory noise modulate all other sensory and motor parameters are candidate models that best explain the observed relationships between aging, motor control, movement error and target acquisition time, accounting for a significant percentage of the age-related covariance of our data. These results suggest a model of aging in which increases in sensory noise caused by deficits in sensory processing are the primary driver of changes in motor control, including changes in sensory gains, movement strategy, and limb dynamics. These changes in sensorimotor

control in turn account for changes in movement speed and accuracy. This result suggests that changes in sensory feedback systems during aging may underlie altered visual compensatory and pursuit tracking during goal-directed movements [65, 80]. As sensory feedback becomes less reliable, sensory gains are reduced in order to reduce the detrimental effects of erroneous feedback [49, 52]. The neural controller, which governs movement strategy, and the plant are then altered in response to these changes, which may indicate that changes in movement strategy are a compensatory mechanism to cope with age-related deficits in sensory feedback [73, 81].

CHAPTER 3: INTENTION TREMOR AND DEFICITS OF SENSORY FEEDBACK CONTROL IN MULTIPLE SCLEROSIS[2]

[2]A form of this work was published in the Journal of NeuroEngineering and Rehabilitation [57]; authorship: M.Heenan; R.A. Scheidt; D. Woo; S.A. Beardsley.

3.1   INTRODUCTION

Accurate arm and hand movements are the key to performing many daily tasks, but in individuals with Multiple Sclerosis (MS), the processes that control these movements are disrupted due to demyelination of the axonal projections that transmit information within and between brain areas. Upper extremity motor dysfunction in MS most often manifests as kinetic tremor (uncontrolled rhythmic motion of the joints during goal-directed movements) or dysmetria (a lack of coordination of movements typified by the under- or overshoot of the intended position of the hand or arm). Up to seventy-five percent of individuals with MS experience tremor in the arms and hands, with as many as 27% of those reporting tremor-related disability [93-95, 116]. Drug therapies [117-121] and surgical treatments [94, 122-124] can mitigate some effects of tremor, although their effectiveness decreases over time [96] (for review see [125]). Recently, rTMS has been used to reduce tremor [97], however, the effects are short-lived.

Because neural lesions that develop in MS are distributed throughout the central nervous system, similar movement deficits (i.e. tremor) may result from differing impairments in the sensory feedback control pathways. Consequently, the specific neuroanatomical etiology of tremor and dysmetria remain unclear. Tremor and dysmetria are most often associated with lesions in the cerebellum and/or the thalamic nuclei,

suggesting impairment of the cortico-cerebellar sensorimotor control loops used for the planning and adaptive control of movement [126, 127]; for review see Koch, et al. [95]. Recent studies also implicate impairments of the predictive mechanisms used to guide movement and/or degradation of the sensory information upon which such predictions are based, including impairment in sensory transmission of information, which is lengthened in those with MS [93, 94, 104, 108, 128, 129]. The many-to-one mapping of the source of impairment onto clinical symptoms poses significant challenges for developing effective therapies. For example, a therapy designed to compensate for one patient's dysmetria caused by increased sensory processing delays may not be effective for another patient whose dysmetria is due to impaired prediction of limb dynamics.

In this study, we describe a systems-level computational model and an experimental technique that parameterizes subject-specific deficits in sensory feedback control of the elbow joint [6, 20, 22, 62] in individuals diagnosed with MS. We used this approach to test the hypothesis that tremor in MS results from subject-specific impairments in the adaptive feedback processes that guide movement. Specifically, we fit the parameters of a dual-feedback, sensorimotor control model to the kinematic data obtained from each subject's responses to perturbations during a series of continuous elbow flexion/extension tasks [6, 22]. We compared the parameters obtained from subjects with MS to those of age- and gender-matched, neurologically-intact control subjects to identify the sensory and/or motor processes affected by MS, and the extent to which they correlate with intention tremor. Future studies using this approach to characterize changes in sensory feedback control induced by therapeutic intervention may

advance understanding of how to best mitigate individuals' deficits of motor function as they evolve with progression of the disease.

3.2   METHODS

3.2.1   Participants

Sixteen subjects participated in the study. Eight subjects had clinical diagnoses of MS and exhibited mild to severe tremor (ages 25-68 years old, 6 female, 7 right-handed). Eight healthy participants served as age- (±7 yrs) and gender-matched control subjects (ages 26-61 years old, 6 female, 8 right-handed). All participants provided written, informed consent in accordance with the Declaration of Helsinki and as approved by institutional review boards at Marquette University and the Medical College of Wisconsin.

Subjects with MS were assessed clinically in a session conducted at the Medical College of Wisconsin prior to participating in the primary study (Table 3-1). Disease duration ranged from 6 to 30 years. Six subjects with MS had received disease-modifying therapy with either an immune-modulator or immunosuppressant, with four subjects continuing therapy at the time of the study. Severity of disability on the Expanded Disability Status Scale (EDDS) ranged from 1 to 7 (out of 10), with three subjects confined to a wheelchair. All of the subjects exhibited motor strength in the upper extremities of 4 or greater on the Medical Research Council system of grading, and all demonstrated normal tone and normal proprioceptive sensation in the upper extremities upon exam. Visual acuities were 20/40 or better in all subjects. Scores on the Ataxia

Scale for Dysmetria and the Tremor Assessment Scale ranged from 1 to 3 (scale 0-4;

score of 0 indicates no tremor; score of 4 indicates severe tremor).

Table 3-1: Clinical characteristics of MS subjects
Disease type (RR: relapsing remitting, PP: primary progressive, SP: secondary
progressive, PR: progressive relapsing), expanded disability status scale (EDSS), tremor
and ataxia scores obtained during a separate clinical evaluation. Nine Hole Peg Test
(NHPT) times were obtained the day of testing (*right hand only; DNC: did not complete
in time allotted).

Subject #	Age	Gender	Dominant Hand	MS Type	EDSS	Tremor Score*	Ataxia Score*	NHPT* (sec)
1	45	F	R	RR	2	1	1	27.9
2	57	F	R	PP	7	1	1	18.9
3	31	F	R	RR	2	2	1	27.0
4	29	F	R	SP	7	2	2	81.6
5	55	F	R	-	6	2	2	DNC
6	25	M	R	PR	7	3	2	75.1
7	41	M	R	RR	6	3	2	77.2
8	68	F	L	RR	1	3	3	141.0

3.2.2 Sensory Feedback Control Model

Based on previous work [12, 20, 112], we have developed a closed-loop model of

sensory feedback control during goal-directed movement (Figure 2-1) [6, 22]. In the

current study, we use this sensory feedback control model to examine how MS impacts

sensory feedback control. In the model, the difference between desired position (θ_d) and

the weighted (K_v, K_p) sum of visual and proprioceptive estimates of the actual arm

position (θ_a) (i.e. performance error) drives the system [6, 13, 20, 22, 62]. Delays in

visual and proprioceptive processing are modeled as lumped-parameter delays (T_v ,T_p)

that account for time lost due to signal conduction and sensory information processing.

The model also includes an internal feedback path (forward model), which provides

predictions of movement dynamics and the sensory consequences of those actions. In the forward path, actual performance error is compared to the predicted performance error to generate an instantaneous prediction error. Prediction error gives rise to a set of muscle activations via a neural controller, which for simplicity we model using a Proportional-plus-Integral-plus-Derivative (PID) controller, C(s):

$$C(s) = K_d s + K_{pr} + \frac{K_i}{s}. \tag{1}$$

This generic controller contains separate derivative (K_d) proportional (K_{pr}) and integral (K_i) gains to allow the controller to minimize transient response errors as well as steady state errors [20]. The output of the controller represents the intended net muscle activations, which act through the musculoskeletal geometry to generate a net torque applied to the physical plant (lower arm rotating about the elbow). We simplify the plant model by discounting muscle activation/contraction dynamics, which are assumed to be dominated by the second-order dynamics of the arm. We account for variations in muscle fiber recruitment [113] by reducing the precision of the intended torque with a multiplicative motor noise (α).

The arm's dynamic response to the applied torque is estimated using a second-order model, P(s),

$$P(s) = \frac{1}{Js^2 + Bs + K} \tag{2}$$

which contains separate inertia (J), viscosity (B), and stiffness (K) terms.

3.2.3 Experimental Setup

All subjects participated in a single, two-hour experimental session during which they performed a series of visual compensatory tracking tasks to characterize sensory feedback control about the elbow. Tasks and analysis are summarized in Table 2-1. All subjects also performed a spiral tracing task to quantify tremor frequency and amplitude [130]. Subjects with MS additionally performed the 9-hole peg test (9HPT) at the beginning of the experimental session for comparison with clinical assessments (9HPT, EDSS [131], ataxia and tremor scores [132]). Subject performance during single-joint elbow tracking tasks was used to quantify and validate an individualized estimate of the sensory feedback control parameters depicted in Figure 2-1. The order of task presentation was counterbalanced across subjects to prevent ordering effects.

During single-joint tracking tasks, subjects held the handle of a 1-D robotic manipulandum with their right hand (Figure 2-2). Additional details of the robot implementation, control, and experimental design can be found in Chapter 2 and in [114]. Joint angle (limited to $\pm 40^o$ relative to the sagittal plane) was yoked to a cursor (a red ring) displayed on a 19-inch computer monitor approximately 60cm from the subject. Direct view of the arm was blocked so that the cursor provided the sole visual cue of arm position.

Continuous, visual or torque perturbations were applied to the cursor or manipulandum, respectively, during the 1-D target tracking tasks described below. Subjects were asked to compensate for external perturbations (low-frequency: 0-1Hz, band-limited white noise; high-frequency: 0-10Hz, band-limited white noise, low-pass

filtered at 1 Hz) by returning the cursor or arm back to the desired location as quickly and accurately as possible.

3.2.4 Target Tracking Tasks and Data Analysis

2D spiral tracing task

A digitized spiral tracing task (adapted from Feys and colleagues) [130], was used to characterize the frequency and signal power of each subject's tremor. During the task, subjects used a digital pen to trace the line of an Archimedes spiral (center-out) overlaid on a Wacom digital tablet (12x18.2 inch drawing surface; Wacom Technology Corporation, Vancouver, WA). Throughout the task, subjects self-supported their arm against gravity and were instructed not to rest their arm or hand on the table while they traced the spiral in the transverse plane. Pen location data was collected at 200 samples/second in Matlab ver. 8.2 using the Cogent 2000 toolbox (Laboratory of Neurobiology, University College London, London, UK). The spiral was labeled with tick marks every 3 cm. To prevent the adoption of strategies that would compensate for tremor during the task, subjects were instructed to adjust their tracing speed according to a metronome such that they crossed one tick mark per beat, while keeping the movement as smooth as possible. During practice trials, subjects were instructed to avoid "stopping and starting" movements as they crossed each tick mark. Metronome speeds were adjusted based on the subject's ability to maintain the target speed, and ranged from 60 beats per minute (bpm) (3 cm/sec) to 240 bpm (12 cm/sec). Prior to the task, subjects

performed five practice trials to familiarize themselves with the task and timing requirements. The first two practice trials were completed at the subjects' self-selected speeds without the metronome. In the remaining practice trials, subjects performed the task with the metronome, starting at 60 bpm and increasing the metronome speed by an additional 40 bpm in each subsequent trial to identify a comfortable base speed. Following the practice trials, subjects completed ten "test" trials limited to 20 seconds each. During the first eight test trials, task difficulty was increased from the base speed on every second trial by incrementing the metronome speed an additional 40 bpm (2 cm/sec) until the subjects' tracing speed fell below 90% of the metronome speed. During the last two trials, subjects were told to move as quickly as possible while accurately tracing the entire spiral.

Tremor frequency and power were quantified using each subject's performance during the spiral drawing task. For each spiral trace, we performed a least-squared-error linear regression of the pen-tip trace angle vs. radial distance from the spiral's center (Matlab command: `polyfit`) to remove the linear relationship between angle and radius associated with the spiral. The best-fit regression was subtracted from the pen-tip data to obtain the variation in the subject's movement about the spiral trajectory. The power spectrum of the residual pen-tip data was calculated for each trace and the best-fit (1/f) frequency spectrum was subtracted to account for low-frequency (<1 Hz) drift and to isolate the spectral power due to tremor. Tremor frequency was not correlated with movement speed, and frequency was therefore averaged across trials. Tremor power was correlated with movement speed (tremor increased as speed increased), and so only the fastest trial was used to gauge tremor power. Tremor frequency was defined as the

frequency that contained the maximum power in each trial; frequencies were averaged

across trials to estimate the average tremor frequency. Tremor amplitude was defined as

the maximum power in the tremor frequency range (2-6 Hz) for the trial performed at

each subject's fastest speed; this frequency range was chosen from the distribution of

upper limb tremor frequencies associated with kinetic tremor (Alusi, 2001).

Tasks 1 and 2: Compensatory tracking with low-frequency perturbations

Visual (T_v, T_v^*) and proprioceptive (T_p, T_p^*) delays were characterized in separate

compensatory tracking tasks. Subjects performed 10 trials per task and trial duration was

20 seconds in each case. Visual response delays (T_v, T_v^*) were characterized by applying

continuous pseudorandom visual displacements (0.05 – 1 Hz; RMS = 10° visual angle) to

the cursor position; proprioceptive response delays (T_p, T_p^*) were characterized by

applying continuous pseudorandom torque perturbations (0.05 – 1 Hz; RMS = 0.3 Nm) to

the manipulandum. In both cases subjects applied counter movements to the

manipulandum to maintain the cursor on a stationary target (visual) or to keep the

manipulandum aligned at 90º of elbow flexion (proprioceptive). No visual feedback of

arm position was provided during the torque perturbations. To remove the passive

dynamics of the arm from the torque response during the proprioceptive task, an

additional five "control" trials (30s each) were collected. A high frequency torque

perturbation was applied to the arm (0-30Hz, first-order zero-phase Butterworth filter

with 1Hz cutoff) while subjects were instructed to not interfere with the perturbation (i.e.

not try to correct). The contribution of the passive mechanical impedance of the arm to

the torque was estimated as a percent of the applied torque calculated from the least-squares linear regression between the measured and applied torques during the passive trials ($R^2 > 0.75$). The contribution of the "passive torque" was then subtracted from the measured torque to estimate subjects' voluntary corrective torque.

We used cross correlation to estimate delays in the visual and proprioceptive feedback-driven responses during compensatory tracking tasks (Tasks 1 & 2). The visual and proprioceptive response delays T_v, T_p, were estimated as the trial-wise average of the temporal offset (lag) between the perturbations in cursor/manipulandum position applied in Tasks 1 and 2 and the subject's voluntary corrective responses measured by the robot's handle position.

Subjects' internal prediction of their visual and proprioceptive response delays (T_v^*, T_p^*) were estimated based on the timing of corrective submovements in Tasks 1 & 2 respectively. Submovements have been associated previously with a discretization of corrective movements during closed-loop sensorimotor control which acts to minimize energy expenditure and movement error [9, 63, 67, 133]. Timing of corrective submovements has been linked to the visual response delay [48] and other neuromotor processes associated with movement planning and execution. Here, submovement intervals were defined as the times between zero-crossings of elbow angular velocity. We accounted for event detection failures in each task using a sum of Gaussians fit to the distribution of submovement intervals across trials. In each task, the means (and variances) of the component Gaussians were constrained to be integer multiples of the primary (i.e. shortest) interval, thus reflecting a doubling (one missed submovement) and tripling (two missed submovements) of interval durations (and variability in their

estimates). The internal estimate of the visual and proprioceptive response delays were taken as the means of the primary distributions of submovements in Tasks 1 & 2, respectively.

Task 3: Tracking of step torque

Signal-dependent variability in torque ("motor noise") was assessed using an isometric task adapted from Jones et al [113]. Joint torque variability was measured as a function of average joint torque. During the task, the manipulandum position was fixed at 90º of elbow flexion while subjects performed several isometric torque contractions to reach a displaced cursor. Displacement scaled with torque, such that the subject was required to place the cursor on one of five pseudorandomly displayed targets (desired elbow joint torques of 4, 6, 8, 10, and 12 Nm flexion) and then maintain that same level of torque once the cursor and target disappeared (after 3 seconds) by applying the appropriate level of isometric torque (for an additional 5s). Five trials were collected at each of the five torque levels (25 trials total).

The gain of the multiplicative (signal-dependent) motor noise, α, was estimated as the slope of the linear regression between the mean and the variance of the trial-averaged torque as a function of target torque level. For each target torque level, the mean and variance in the applied torque was measured during the last five seconds of each trial (i.e. after visual feedback was removed).

Task 4: Compensatory tracking with high-frequency perturbations and model fits

A high-frequency (0-10 Hz, RMS = 20°, first-order zero-phase Butterworth filter with 1 Hz cutoff) compensatory tracking task was used to characterize the remaining elements of the sensory feedback control model including the controller gains (K_d, K_{pr}, K_i), visual and proprioceptive feedback gains (K_v, K_p), and arm dynamics (J, B, K) together with their internal estimates (K_v^*, K_p^*, J^*, B^*, K^*), vis-à-vis the forward model. Subjects were instructed to correct for visual perturbations movements "as quickly and accurately as possible" so as to maintain the cursor on a central stationary target. Ten 32-second trials were obtained for each subject.

We estimated the remaining model parameters (K_d, K_{pr}, K_i, K_v, K_p, J, B, K), and their internal estimates (K_v^*, K_p^*, J^*, B^*, K^*) using fits to the transfer function of the model. This analysis was performed using a two-stage frequency response analysis. Model parameters were fit to each subject's responses in the frequency domain using the simplex method (Matlab: `fminsearch`). In the first stage of the analysis, the second-order model of plant dynamics (Eq. 2) was fit to the magnitude of the frequency response function (FRF) relating the subject's arm position to the applied torque. To reduce measurement noise prior to the model fit, FRFs were computed for all pair-wise combinations of trials as the ratio of the trial-wise differences between the applied torque (τ) and measured arm position (θ_a) (See Appendix A), and then averaged. In the second stage of the analysis, the remaining model parameters were estimated from the closed-loop transfer function relating the applied visual perturbation (D_{ext}) and measured arm

position (θ_a):

$$\theta_a(s) = -\left[\frac{K_v C(s)P(s)e^{-T_v s}}{1+C(s)P^*(s)-C(s)P^*(s)*\left(K_v^* e^{-T_v^* s}+K_p^* e^{-T_p^* s}\right)+C(s)P(s)\left(K_v e^{-T_v s}+K_p e^{-T_p s}\right)}\right] D_{ext}(s) \qquad (3)$$

where P*(s) is the same form (second-order low-pass filter) as P(s):

$$P^*(s) = \frac{1}{J^* s^2 + B^* s + K^*} \qquad (4)$$

characterizes the forward model prediction of arm kinematics. The closed-loop model

(Eq. 3) was fit to a separate FRF formed from the ratio of trial-wise differences between

the applied perturbation (D_{ext}) and measured arm position (θ_a) computed for all pair-wise

combinations of trials (See Appendix). Visual and proprioceptive feedback gains (K_v^*,

K_p^*) were assigned using the subject's fitted sensory gains (K_v, K_p). Motor noise (α),

visual (T_v, T_v^*) and proprioceptive (T_p, T_p^*) response delays were calculated based on

experimental data, not model fits, and were fixed at the mean values estimated from tasks

1-3.

Phase data was excluded from the model fit due to the noise in FRF phase

estimates, particularly at higher (> 2 Hz) frequencies where the power of both the input

signal and the subject response were attenuated. For frequencies below two hertz, the

model and FRF phase profiles were driven primarily by the visual delay in the system,

which was more accurately estimated using the cross-correlation between the applied

perturbations and the subject's corrective response.

To quantify uncertainty in the model fits, we performed a bootstrap analysis for

each stage of analysis (described in Chapter 2 in more detail). For each bootstrap, 10,000

model fits with resampled FRFs and randomized initial conditions were performed. The

mean and standard deviation of the fitted parameters were used as nominal parameter values. For the second-stage bootstrap, plant parameters were randomly sampled from the first-stage FRF analysis to propagate the accumulated error across sequential model fits. During the second stage fits, these triplets were held constant.

For completeness, model and FRF phases for each subject were compared post-hoc using the best-fit model parameters to the FRF magnitude. Due to the noise in FRF phase estimates at higher frequencies, phase profiles could not be reliably "unwrapped" – corrected so that phases could fall outside the range $\pm\pi$ – using a one sample unwrapping procedure. Instead, a multi-sample unwrapping procedure was implemented using a linear regression of phase estimates across the preceding 20 frequency samples to generate a 95% confidence interval around the location of the next "unwrapped" phase value. The FRF phase was then unwrapped by adding or subtracting multiples of 2π until the estimate fell within the confidence interval. In cases where the phase estimate could be unwrapped to two or more locations within the confidence interval, the median was chosen. Uncertainty in the phase profile resulting from the interaction between the unwrapping procedure and the occurrence of multiple phase estimates for confidence intervals exceeding 2π were quantified using a bootstrap analysis. During the bootstrap analysis, the unwrapping procedure was applied to the FRF phase estimates 1000 times, randomly sampling the phase at each frequency containing two or more unwrapped phase estimates within the confidence interval. The 95% confidence interval associated with the unwrapped phase profile was defined at each frequency from the distribution of samples obtained from the bootstrap analysis.

Task 5: Pursuit tracking of step displacements

A step displacement task was used to characterize the functional impact of subjects' deficits during a reach and hold task and compare target capture movements invoked by the subjects to those predicted by the sensory feedback control model of Figure 2-1. Subjects performed ten trials of the task. Each 10-second trial started with the target and cursor located at the same screen position. After a one second delay, the target was randomly displaced to the left or right by a randomly selected distance ranging ±24.4 cm along the horizontal midline of the display (corresponding to ±11.5 degrees of visual angle). Subjects were instructed to center the cursor on the target as quickly and accurately as possible and to maintain the cursor position until the end of the trial.

We evaluated the ability of each subject's best-fit model to characterize sensory feedback control in a separate task that required pursuit tracking in response to step displacements. For each subject, the trial-wise measures of target acquisition time and mean squared endpoint error were calculated. Target acquisition time was calculated as the time required for the subject to move within two degrees of the target. Endpoint error was calculated as the mean-square error (MSE) from the moment of target acquisition to the end of the trial. Target acquisition time and endpoint error were then compared with those of the best fit model to determine the extent to which subject performance was constrained by limitations of sensory feedback control as identified by the model of Figure 2-1.

3.2.5 Statistical Testing

Healthy subjects were matched to patients by age and gender to control for differences in movement control due to factors unrelated to MS. Group differences in the measurements of visual and proprioceptive response delays, submovement intervals, motor noise, and best-fit estimates of the model parameters were tested for statistical significance using a paired, two-sample t-test. Within-subject comparisons of the parameters characterizing internal (predicted) and actual passive limb dynamics were tested for statistical significance using the paired samples z-score of the bootstrap distributions to evaluate the distribution difference from zero (i.e., no difference between distribution means). Pearson's correlation coefficient was applied across participants with MS to identify significant linear relationships (p<0.05) between all combinations of best-fit model parameters and the quantitative clinical assessments of movement performance (e.g. 9HPT, TAS). Post-hoc analysis of the relationship between spiral tremor power and the difference between the internal (predicted) and actual passive limb dynamics was characterized empirically using a least-squares fit to a saturating exponential function of the form

$$\Delta\left(p\right) = \; C * (1 - e^{-r*x})$$

where C is a scaling factor, r is a constant, and x is tremor power.

3.3   RESULTS

3.3.1   Tremor Frequency and Power

Figure 3-1A shows selected spiral traces (insets) and corresponding power spectra for a subject with MS (Subject 6; TAS = 3) and an age-matched control subject. In the spiral drawing task, tremor frequencies for subjects with MS ranged from 2.36-5.01 Hz (mean±SD: 3.38±0.91Hz). Within the 2-6 Hz range associated with tremor, maximum power increased with the speed of movement (data not shown) and ranged from 0.22-5.31 cm^2-s (mean±SD: 1.48±1.82 cm^2-s) across MS subjects for their fastest tracings (Figure 3-1B). The power in the 2-5 Hz band corresponded roughly with TAS, with subjects 5 (TAS = 2) and 8 (TAS = 3) exhibiting the worst tremor and subjects 1, 2 (TAS = 1), and 4 (TAS = 2), exhibiting the least tremor on the day of testing. Tremor power was significantly correlated with 9HPT score on the day of testing (r = 0.80; p = 0.006).
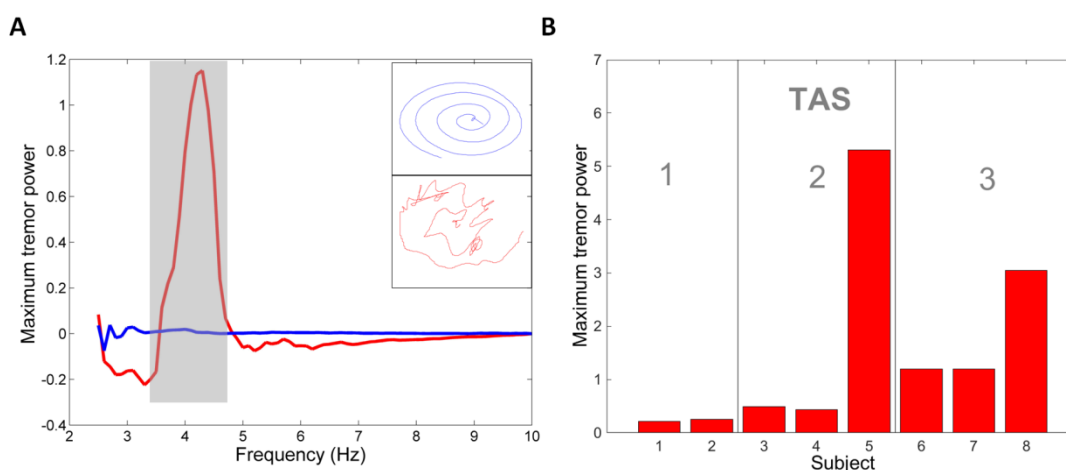
Figure 3-1: Tremor assessment using the spiral drawing task [57].
(A) Power spectra (with low-frequency (<0.5 Hz) drift removed vis subtraction of exponential function described in section 3.2.5) and sample spiral drawings (inset) for Subject 6 with MS (red; TAS = 3) and an age-matched control subject (blue). The shaded area highlights the range of frequencies associated with the subject's tremor. (B) Maximum power within the 2-5 Hz frequency range for subjects with MS together with their corresponding tremor assessment score (TAS).

3.3.2 Visual and proprioceptive response delays (Tasks 1 & 2)

Figures 3-2A and 3-2B (right) show the average visual and proprioceptive response delays for individual subjects with MS and the corresponding range (±SD) for control subjects (shaded bands). The average visual response delay measured across subjects (Figure 3-2A-left), was significantly higher in subjects with MS (647.1±192.3 ms), compared with control subjects (450.9±38.2 ms) (t(7) = 2.63, p = .034). In contrast, the average proprioceptive response delay (Figure 3-2B-right) did not differ significantly between groups (MS: 201.7±56.5 ms; Controls: 175.1±31.9 ms) (t(6) = 1.39, p = 0.21). In four of the eight MS subjects with elevated TAS scores (subjects 4, 5, 6, and 8), visual response delays were >3σ above the range of control subjects. Across subjects, visual response delay times were not significantly correlated with either TAS or spiral tracing performance (p > 0.25), likely due to the "outlier effect" of subject 7 (low visual response delay, high tremor power) on the small population sample. Individual proprioceptive response delays for subjects with MS fell within the control group range - excepting subject 4, whose proprioceptive delay was >2σ from the control average.
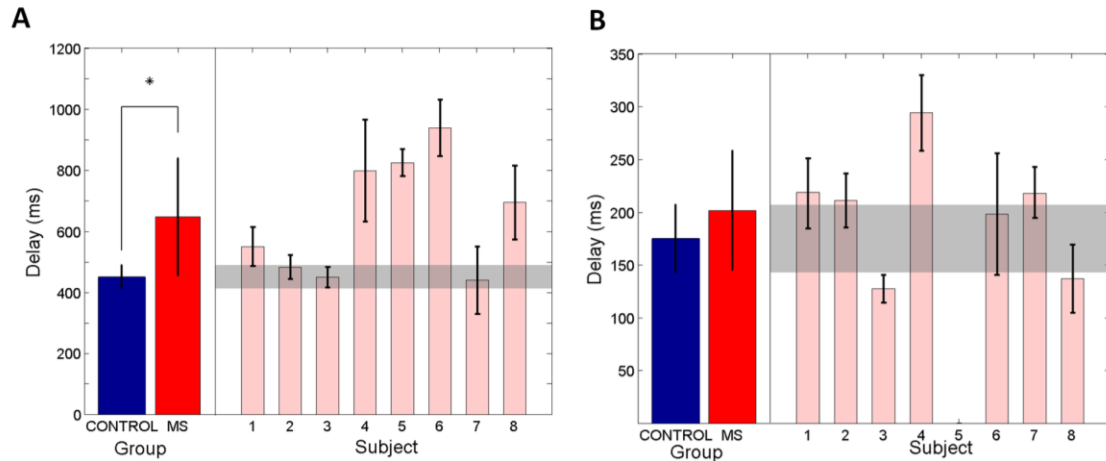
Figure 3-2 Visual and proprioceptive response delays for control subjects (blue) and subjects with MS (red) [57].
(A) Group and individual proprioceptive response delays for subjects with MS. (B) Group and individual visual response delays. Error bars denote ±SD for group and individual measures respectively. Shaded regions denote the corresponding ranges (±SD) for the control group.

Figure 3-3 shows representative single-trial velocity profiles within trial and the distributions of visual (T_V^*) and proprioceptive (T_p^*) submovement intervals across trials for a representative subject with MS in Task 1 (left), which included visual perturbations and in Task 2 (right), which included physical perturbations. For all subjects, distributions were well fit by the Gaussian mixtures model ($r^2 > 0.70$ $p < 0.001$ with 3 Gaussians) wherein the mean of each Gaussian was centered at an integer multiple of the interval associated with the primary distribution. For each subject, internal (predicted) visual and proprioceptive response delays were estimated as the mean submovement interval of the primary distribution.
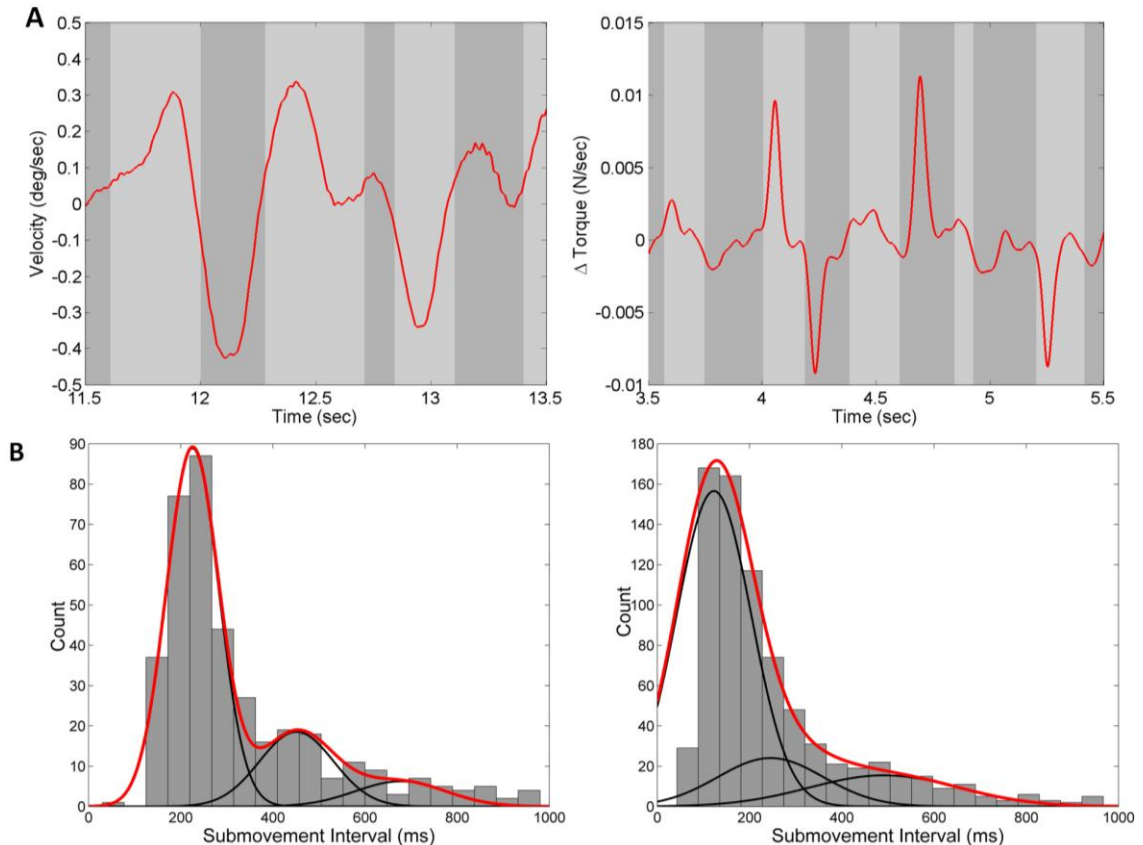
Figure 3-3: Characterization of visual and proprioceptive submovement intervals [57].
(A) Movement velocity profiles used to calculate visual (left) and proprioceptive (right) submovment intervals for Subject 4 (MS, TAS = 2). Examples of individual submovements are highlighted (gray) (B) Distribution of submovement intervals across trials for vision (left) and proprioception (right) for a representative subject with MS (Subject 4). The submovement interval for each subject was characterized by the mean and standard deviation of the best-fit gaussian mixtures model (red line) formed from successive gaussian functions whose means and variances are constrained to be integer multiples of the primary distribution (black lines).

Figure 3-4A shows the average visual and proprioceptive submovement intervals across subjects. Proprioceptive submovement intervals did not differ significantly between the MS and age-matched control groups (t(6) = 1.88, p = 0.11). Visual submovement intervals tended to be shorter in subjects with MS compared to controls, however, the difference did not reach statistical significance (t(7) = -1.92, p = 0.097). Figure 3-4B compares the duration of visual and proprioceptive response delays for each participant with their corresponding submovement intervals. Proprioceptive

submovement intervals and response delays were approximately equal for both control

and MS subjects (t(9) < 1.6, p > 0.05). Similarly, visual response delays and

submovement intervals did not differ for control subjects (t(9) < 1.4, p > 0.05). By

contrast, four of the eight MS subjects exhibited a dramatic mismatch between their

visual submovement interval and corresponding visual response delay (Figure 3-4B;

bottom right corner). In these subjects, visual response delays increased markedly

compared to control subjects, resulting in a significant group difference between visual

response delay and visual submovement interval (t(7)=2.55 p = 0.038).
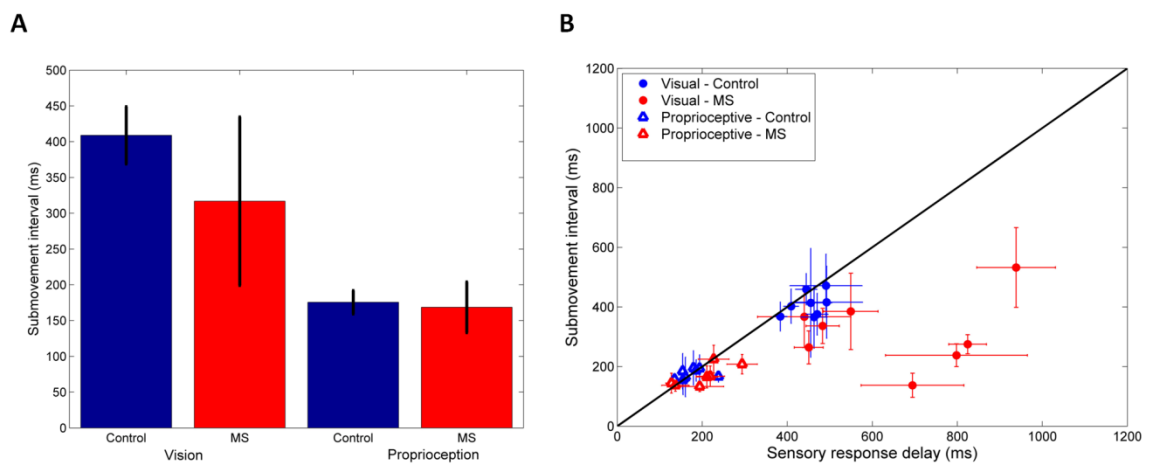
Figure 3-4. Comparison of submovement intervals and task response delays [57].
(A) Group average submovement intervals (±SD) for control subjects (blue) and subjects with MS (red).
(B) Visual (filled circles) and proprioceptive (open triangles) response delays (±SD) as a function of submovment interval for control subjects (blue) and subjects with MS (red). The diagonal line (black) represents equivalency between response delay and submovement interval.

3.3.3 Feedforward Motor Noise (Task 3)

One subject with MS (Subject 5) was unable to complete the task due to time

constraints. For the remaining subjects, the scaling of elbow torque variability with mean

elbow torque showed no significant differences between groups (control subjects: 0.021 ± 0.010; subjects with MS: 0.025 ± 0.011; paired samples: $t(6) = 0.72$, $p = 0.48$).

3.3.4   Frequency Response Analysis (Task 4)

The frequency response functions (and corresponding model transfer function fits) relating corrective changes in arm position to the perturbation of cursor position are shown in Figure 3-5 for subject 4 with MS (right) and the corresponding age-matched control (left). For subject 4, the empirical frequency response function and corresponding model fit both contain a marked resonance peak between 2-4 Hz, closely approximating the tremor frequency observed in the subject's spiral tracing task (i.e., 2.4-5 Hz). The peak frequency identified in the compensatory tracking task was slightly lower than in the spiral tracing task, likely due to the additional inertia of the manipulandum handle and robot (inertia $= 0.008$ kg-m^2), which would act to reduce the resonant frequency of the combined arm+robot system. The magnitude of the FRFs for all subjects (control and MS) were well approximated by the model of Figure 2-1 ($R^2 > 0.80$ in every case). The phase of the FRF was well approximated by the model until approximately 2Hz and 6Hz in the MS patients and control subjects respectively. Within this range, the phase profile was dominated by the phase lag associated with the visual delay (Figure 3-5B – gray line). At higher frequencies, phase estimates became too noisy to unwrap (correct phase range to include values outside the range $\pm\pi$) reliably; however, model responses fell within the 95% confidence interval of possible phase profiles unwrapped from the FRF phase.
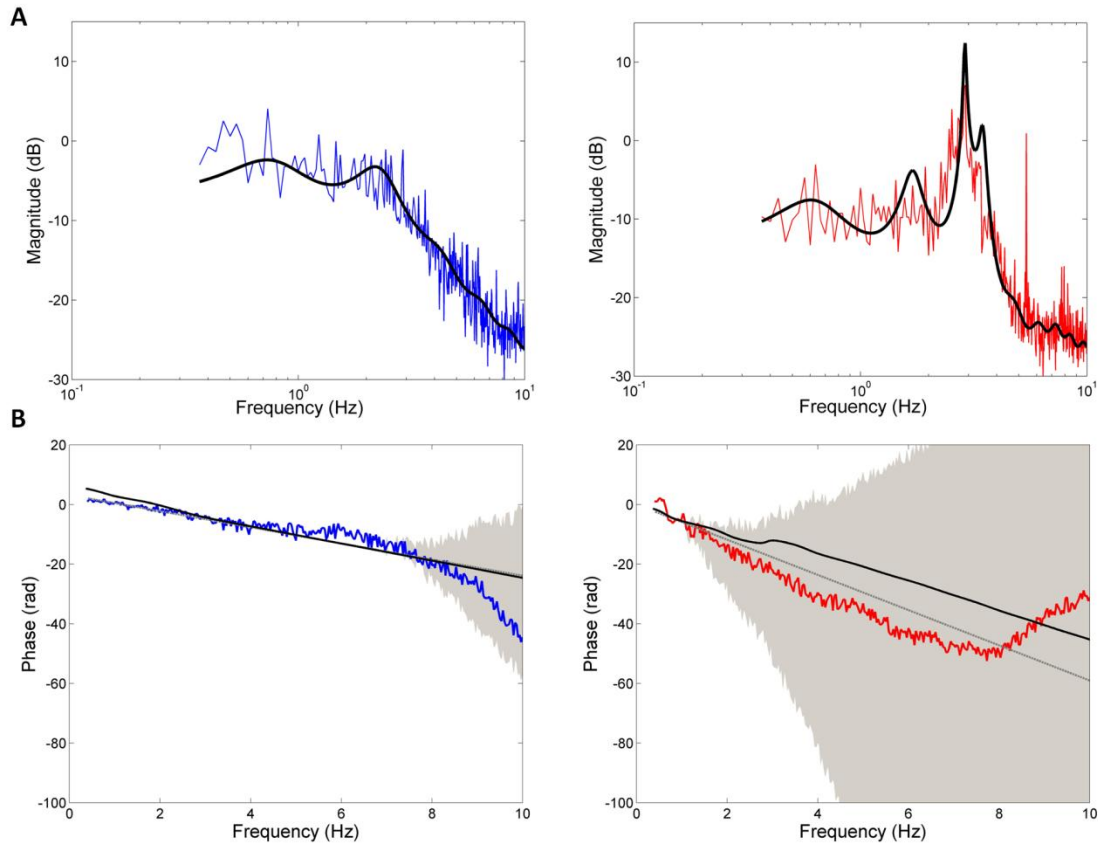
Figure 3-5: Magnitude and phase of frequency response functions [57]
(A) Magnitude of the frequency response function (colored traces) relating applied cursor perturbation to corrective change in arm position for subject 4 with MS (TAS = 2; right) and the age-matched control subject (left). The best-fit model for each subject is denoted by the solid black line. (B) Phase of the FRF (colored traces) with 95% confidence intervals (grey shading) for subject 4 with MS (right) and age-matched control subject (left). The solid black line denotes the best-fit model to the subject's magnitude FRF (Eq. 3). The grey line denotes the phase profile associated with the subject's visual delay.

Of the ten parameters estimated using the frequency responses analysis (full results shown in Appendix C), significant differences between groups were observed only for the integral and derivative gains of the generic feedback controller. Subjects with MS exhibited higher integral gains than control subjects (6.86 ± 4.71 vs. 4.71 ± 2.39 Nm/deg-s; $t(7) = -3.62$, $p < 0.01$) and higher derivative gains than control subjects ($8.3\text{x}10^{-3}\pm3.8$ $\text{x}10^{-3}$ vs. $3.3 \text{ x}10^{-3} \pm1.8 \text{ x}10^{-3}$ Nm-s/deg; $t(7) = -3.38$, $p < 0.05$). In control subjects, the derivative gain was significantly correlated with integral gain, musculoskeletal viscosity,

and musculoskeletal stiffness (r = 0.81, 0.71, and 0.75 respectively; p < 0.05). In subjects

with MS, these correlations were absent; derivative gain was not correlated with actual

(or predicted) musculoskeletal viscosity or stiffness and it was not correlated with tremor

assessment score and tremor amplitude measured by the spiral tracing task (r < 0.50; p >

0.25). Instead, the best-fit derivative gain was significantly correlated with visual

response delay in subjects with MS (r = 0.77; p = 0.024). This shift in coupling from the

plant (in controls) to the visual delay (in subjects with MS) is interesting in light of the

derivative gain's traditional role in modulating the transient response of the system. This

finding suggests the increased visual processing delay seen in MS may play a central role

in causing subjects to alter the effective closed-loop dynamic response of the arm during

goal-directed movement.

We next analyzed the best-fit sensory feedback control models from subjects with

MS to identify systematic covariations between model parameters and clinical

performance measures. We found that subjects with MS displayed a consistent mismatch

between the model parameters characterizing predictive arm dynamics (eq. 4) and the

actual arm dynamics (eq. 2). The degree of parameter mismatch - quantified by the

mismatch magnitude normalized by the corresponding parameter value from the actual

arm dynamics - varied systematically with tremor assessment score (TAS). Mismatches

in all three dynamical parameters (J, B and K) increased with tremor severity, although

mismatches in the effective viscosity were evident only in subjects with severe tremor

(TAS = 3), (Figure 3-6A). By contrast, control subjects showed no mismatch between the

parameters characterizing internal and actual passive joint dynamics (two-tailed Z < 1.9,

p >.05 for each parameter).

A

B
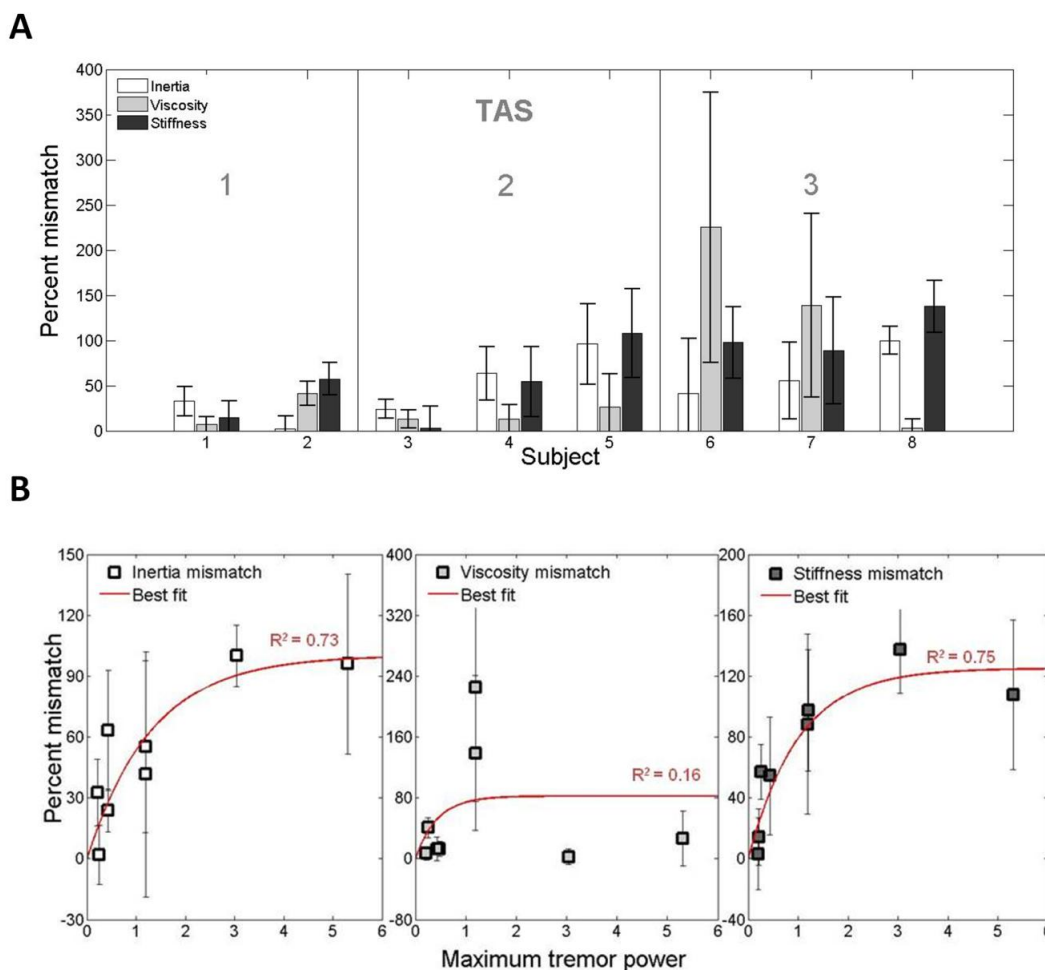
Figure 3-6: Percent mismatches in limb dynamics [57]
(A) Percent mismatch between predicted versus actual estimates of passive joint dynamics (inertia, viscosity, stiffness) as a function of tremor severity (TAS score) in subjects with MS. Mismatch between actual and predicted limb dynamics increased with tremor assessment score. Error bars denote ±SD of the bootstrap distribution. **(B)** Percent mismatch between the parameters characterizing internal (predicted) and actual effective joint dynamics for subjects with MS (±SD) vs. tremor power characterized using the spiral-tracing task. Percent mismatch saturated with tremor magnitude and was well fit by an exponential function (red) for inertia and stiffness ($R^2 > 0.70$; $p < 0.01$) but not for viscosity ($R^2 = 0.16$; $p = 0.32$).

Mismatches in effective limb inertia and stiffness varied systematically with tremor power characterized by the spiral tracing task; in both cases, this relationship was well-approximated by a saturating exponential function ($R^2 > 0.73$). In contrast, no systematic relationship was observed between mismatches in effective viscosity and tremor power (Figure 3-6B).

3.3.5 Pursuit tracking of step target displacements

We required subjects to perform a final tracking task to characterize the impact of sensory feedback control deficits on a 1-D reach and hold task similar to transporting a cup of water along a tabletop. The task also enabled us to compare movements generated by the subjects to those predicted by the sensory feedback control model of Figure 2-1. Subject and model performance were examined using measures of target acquisition time from the onset of the step displacement and steady-state endpoint error following the displacement. Control subjects' performance tended to cluster into one of two general task strategies characterized by either larger endpoint errors and faster response times or smaller endpoint errors and slower (and more variable) response times (Figure 3-7; note the two distinct peaks in the bivariate distribution of control subjects' performance represented by the dark shading). Approximately 25% of subject responses exhibited higher error, lower response time; 95% of these trials took less than 1200 ms to reach the target (Figure 3-7, top shaded distribution) and resulted in an endpoint MSE's up to 0.02 degrees^2. Remaining responses were slower and had high endpoint accuracy; 95% of these trials were completed within 2000 ms with endpoint MSE's less that 0.008 degrees^2 (Figure 3-7, bottom shaded distribution).

Subjects with MS exhibited similar trends in step-tracking performance, with the exception that the four subjects with high visual delays (Figure 3-7, dark red circles) exhibited performances that fell outside the 95% confidence interval bounds of the bivariate distribution of the response times and endpoint MSEs exhibited by control subjects. The subjects with high visual delays all had high TAS and high tremor power.

Three of the four subjects (S4, S5, and S6) had significantly higher response times when performing the step-tracking task. Endpoint MSE was also increased, falling within the range of control responses emphasizing speed over accuracy. The fourth subject (S8) showed the reverse pattern with an increase in endpoint MSE but no apparent increase in response time. For all subjects with MS, the corresponding performance of the best-fit model, averaged across trials, is shown for comparison (Figure 3-7, triangles). In all cases, model-predictions underestimated actual response times and in all but two cases, model-predictions over-estimated actual terminal mean-squared errors.
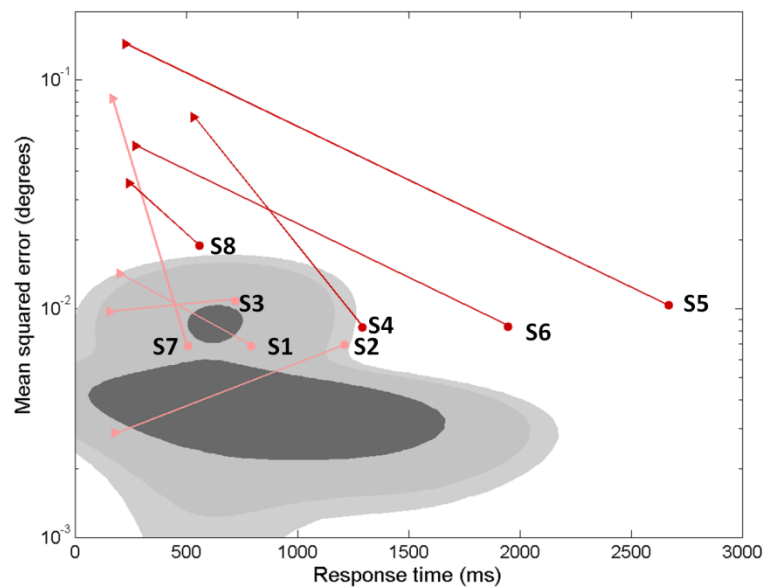
Figure 3-7: Log mean squared steady state error (degrees) vs. response time (ms) during a reach and hold task (step displacement) [57].
Shaded regions (dark, medium, and light gray) denote the 50, 90, and 95% confidence intervals estimated from a mixture of Gaussians fit to control subjects' response across all trials. For subjects with MS, trial-averaged response times and MSEs are shown individually for clarity (filled circles). Dark red symbols denote MS subjects with "high" (>3SD above the control mean) visual delays, and pink symbols denote MS subjects with "low" (<3SD) visual delays. The average best-fit model performance to the same trials is also shown for each MS subject (filled triangles). In all cases, the best-fit sensory feedback control model for subjects with MS (filled triangles) reacted more quickly to a target perturbation than the subjects' actual responses (filled circles).

3.3.6 Functional impact of mismatch between actual and predictive limb dynamics

We examined the functional consequence of the mismatch between actual and predictive arm dynamics in a subsequent, post-hoc simulation analysis. For each MS subject we performed two forward dynamic simulations that characterized the model's performance on the step displacement task using (a) the best-fit model parameters, including mismatches between actual and predictive limb dynamics; and (b) "corrected" model parameters wherein the predictive limb dynamics of the forward model were forced to match the actual limb dynamical parameters. Figure 3-8 shows representative results for a subject with MS with moderate tremor (TAS=2). The step response of the model *with* a mismatch in limb dynamics (black) actually decreased the time to target acquisition and resulted in lower endpoint error than simulated responses with no mismatch in plant dynamics (gray), suggesting that mismatches in plant dynamics may be an adaptive response to the instability caused by mismatches in actual and predicted delays.
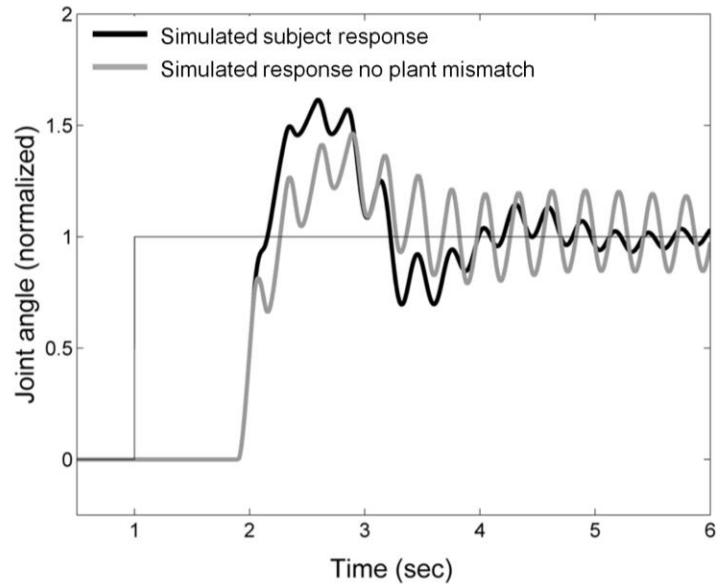
Figure 3-8. Step response of the sensory feedback control model [57]
Response for the best-fit model containing a mismatch between the actual and expected elbow kinematics (black line) and for a model in which the actual and expected kinematics are matched (gray line).

3.4 DISCUSSION

We used a multisensory model of sensory feedback control to individually characterize sources of sensorimotor dysfunction in subjects with MS performing a series of goal-directed stabilization and movement tasks about the elbow. In contrast to the initial supposition that MS might impact sensory feedback control uniquely in each subject, the results suggest that upper extremity tremor and dysmetria may result from systematic changes in sensory feedback control. Specifically, subjects with moderate to severe tremor (TAS $\geq$ 2) exhibited increased visual response delays relative to normal control subjects. They also exhibited systematic mismatches between predictions of arm dynamics (vis-à-vis the forward model) and actual arm dynamics which were not present in normal control subjects; the degree of mismatch in subjects with MS correlated with tremor signal power measured in our spiral tracing task. We also observed group-wise

differences in the integral and derivative gains of a generic model of the neural feedback controller. Whereas the controller gain parameters covaried with the dynamic properties (i.e., apparent viscosity and stiffness) of the musculoskeletal system in normal control subjects, the derivative gain parameter in subjects with MS correlated instead with the visual delay; the increase in derivative gain may therefore be a response to the increase in instability related to increases in visual delay.

A comparison of actual and simulated responses to step changes in desired performance suggests that the apparent mismatch between subject predictions of arm dynamics and actual arm dynamics may actually serve to improve response times in subjects with MS, despite their long visual delays. Taken together, our results suggest that tremor and dysmetria in MS may be caused by a combination of two factors: an inability of the brain to adequately adapt to increases in the time required to process visual information related to movement and by compensatory – but maladaptive – errors in predictions of arm dynamics.

An increased visual delay such as the one observed here is consistent with reductions in the conduction speed of action potentials due to disease-induced demyelination in MS [134] and it agrees well with the increased time required by MS subjects to perceive visual information and perform visually-guided tasks [103, 134, 135]. Proprioceptive conduction time in the lower extremities has also been shown to increase in MS [100], although we did not find a corresponding increase in proprioceptive response delay for the upper extremity. This may be due to the longer path length in the spinal cord for the transmission of motor control signals to the lower extremities.

Interestingly, the increased visual response delay in subjects with MS was not accompanied by an increase in the latency of submovements (i.e. their submovement interval). Submovements have been used previously to study impairments in movement control [136, 137]. Current theories of intermittent control during goal-directed movement associate individual submovements with discretization of sensorimotor control, such that each submovement represents a complete "primitive" movement profile comprised of movement planning, movement execution and sensory feedback phases [9, 63, 67, 133]. For the purpose of characterizing feedback control in MS, we have assumed that the combined time delays associated with these three submovement phases form the basis of the expected response delays characterized by the model (Figure 2-1). Correspondingly, the submovement intervals measured experimentally in response to corrective movements mediated by visual or proprioceptive motion cues (Exp. 1a and 1b respectively) reflect internal estimates of the open-loop sensory processing delays. This interpretation is supported by the consistent match in control subjects between visual and proprioceptive response delays and the measured submovement intervals (Figure 3-4B).

In subjects with MS, submovement interval and visual response delay differed significantly in four of the eight subjects, suggesting that they failed to adjust (or were unable to adjust) their expectations of visual processing delays to compensate for the full increase in visual processing time resulting from the disease. A previous study by Miall and Jackson has demonstrated that it is possible to adapt to increases in extrinsic feedback delays [48]. However, the visual delays seen here in subjects with MS were markedly larger than those that Miall and Jackson used to adapt their neurologically intact subjects (<300ms). Moreover, the delays experienced by MS subjects reflect

intrinsic, rather than extrinsic sources. It is possible that intrinsic sources of delay may not engage adaptive mechanisms that respond to task-specific changes in the environment (cf. [138]); our results suggest that subjects with MS may adapt their forward models of plant dynamics (creating a mismatch) in response to these increases.

Although continuous control models, such as the one used here, make simplifying assumptions that neglect the impact of intermittent feedforward control actions, continuous control models have been shown to accurately predict human performance in a variety of single joint motor tasks that minimize the predictability of environmental or target perturbations [6, 20, 22, 62]. Additional simplifications of our model include the use of a 1-D task to characterize movement control and the use of a second-order musculoskeletal plant model. These simplifications were made because the plant model of the arm becomes much more complicated with the inclusion of additional joints or by including higher-order models of muscle activation contraction dynamics [28]. We believe these simplifications are justified because the bandwidth limitations of the plant are dominated by the effects of the arm's inertia and mechanical viscoelasticity rather than by low-pass filter properties of the activation/contraction dynamics - at least in quasi-isometric conditions such as the stabilization tasks studied here.

For subjects with MS, the pattern of mismatch in the limb dynamics (stiffness and inertia) co-varied with tremor assessment score and tremor power calculated from the spiral-tracing task (Figure 3-6). This was despite marked differences in task design; the model was characterized using single-joint compensatory tracking movements with the arm supported against gravity whereas the clinical assessments and spiral tracing required the subject to generate motion at multiple joints without arm support. Correspondence in

the results of these disparate tasks is to be expected; a disease-related increase in visual processing time is expected to impact motor performance in any visuomotor task. The simulation results of Figure 3-8 suggest that the observed mismatch between internal estimates of plant dynamics and actual plant dynamics may actually help subjects with moderate tremor reduce steady-state movement error despite an inability to compensate for long visual delays. This form of compensation would not be unreasonable, particularly for adaptive mechanisms in the brain that seek to minimize discrepancy between the predicted and realized sensory consequences of actions (cf. [139]). Uncompensated increases in visual delay would yield lagged perceptions of arm position, compromising limb state estimation [108]. Considering that a delay in the limb's response to descending motor commands also occurs when the hand grasps an object that is heavier than expected, an uncompensated lag in the visual perception of limb motion could be misconstrued as an unexpected increase in limb inertia. Therefore, increasing the internal estimate of limb inertia (Figure 3-8) could, within narrow limits, partially compensate the functional impact of inaccurate predictions of sensory delay. Beyond those limits, changes in the estimated limb dynamics could lead to increased joint torque production (intended to overcome an environmental load that is not in fact present) and inappropriate compensatory responses to the perceived error. This notion is consistent with the suggestion that intention tremor in MS is due, in part, to inaccurate voluntary corrections to errors in position [135]. From a neurological standpoint, cerebellar damage, which has been linked with tremor in previous studies ([24, 126, 127, 140]), could degrade pathways necessary for effective sensorimotor adaptations, causing

inappropriate compensatory responses to become more likely, and exacerbate tremor severity.

During the reach-and-hold task, subjects with MS tended to move more slowly than the control subjects. They also moved more slowly than the performance predicted by best-fit models of Figure 2-1. These results are consistent with a favoring of accuracy over speed in the pursuit tracking of step changes in target location and may reflect a strategic choice by subjects to minimize endpoint errors associated with delay and kinematic mismatches. This bias toward accurate (rather than fast) movements is not surprising since in many daily activities (e.g. eating, dressing) it is more important to bring the hand accurately to a desired spatial location than to do so with speed.

Our results suggest a possible reinterpretation of results of prior studies seeking to reduce tremor in MS. Tasks which force subjects to adapt to novel force fields or to perturbations [105-107] could allow subjects to "reset" maladaptive models and form a new model that is better able to compensate for long visual delays. Our results also suggest novel rehabilitative strategies for reducing intention tremor in subjects with MS. We envision at least two possibilities: one approach would require subjects to hold the handle of a rehabilitation robot while making goal directed movements within a simple virtual-reality environment. As training progresses, subjects would be required to adapt to slowly-increasing visuomotor delays while the robot would simulate mechanical loads that vary unpredictably from trial to trial, thus discouraging compensatory mal-adaptation of musculoskeletal property estimates. We speculate that providing practice in compensating for visuomotor delays while discouraging adaptation of limb dynamics will

favor appropriate adaptive compensations for physiological visual processing delays, thereby mitigating tremor.

A second approach centers on the idea that the brain's effort to minimize performance error hinders the ability to adapt to changes in the physiological visual delay. That is, we speculate the presence of a non-monotonic relationship between performance error and increases in predictive delay such that small increases in predictive delay would lead to increased errors, while large changes in expected delay could lead to optimal performance. This non-linear relationship may preclude the inherent adaptive mechanisms from matching the predictive delay to the true physiological delay. Rehabilitation under this approach would involve using the feedback control model (Figure 2-1) to identify and tailor the visual feedback to gradually shift the minimum performance error to the actual visual delay [141].

The preliminary findings presented here demonstrate that systems identification techniques provide an informative framework for investigating how neuromotor disease affects motor control and the neuromotor causes of motor disability. Specifically, we have done so by examining deficits in the neural processes underlying upper extremity motor dysfunction in a small cohort of individuals with clinical diagnoses of Multiple Sclerosis. We found evidence that tremor and dysmetria may be caused by an inability of the brain to adequately adapt to increases in the time required to process visual information related to movement as well as by compensatory mal-adaptations of internal estimates of arm dynamics. Future studies should seek to confirm the findings reported here with a larger cohort of individuals with MS. Subsequent studies could then seek

effective ways to reduce intention tremor by identifying strategies that mitigate motor

instability due to slowed visual processing caused by MS.

CHAPTER 4: DELAY ADAPTATION TO REDUCE INTENTION TREMOR IN MULTIPLE SCLEROSIS: A CASE SERIES[3]

[3]This work is intended for publication. Authorship: M.Heenan; R.A. Scheidt; S.A. Beardsley.

4.1   INTRODUCTION

4.1.1   Background

Persons with multiple sclerosis (PwMS) often experience severe neuromotor symptoms that significantly impact their quality of life. Because MS is degenerative, these symptoms can often be difficult to manage and treat. One particularly difficult symptom to manage is intention tremor, which affects approximately 15% of those with MS [94]. Intention tremor –tremor about the endpoint of a voluntary movement – affects many activities of daily living, including reaching, eating, driving and writing, and significantly impacts the ability of PwMS to maintain independence [95].

Although there are several medical options available, including drug therapies and surgical treatments, most do not result in significant, long-term improvement due to either increasing drug tolerance or to increasing symptom severity. Physical therapy has been used successfully to reduce select motor symptoms in MS, including posture and balance deficits [100]. Recent, more targeted studies by Feys et al. have shown that intention tremor in MS can be reduced through alteration of computer-generated visual feedback [102], while motor training using robotic devices to introduce proprioceptive and visual perturbations has been shown to reduce motor impairment in persons with MS [105-107]. These short-term improvements in motor function suggest robot-assisted training may provide a viable approach to reduce motor dysfunction in MS. Maximizing

the impact of retraining on motor performance and functional outcomes requires a better understanding of the sensorimotor control mechanisms specifically impacted by MS.

4.1.2   Sensorimotor deficits in Persons with Multiple Sclerosis

Our recent work suggests that intention tremor may be due to an inability to adapt movement predictions to account for an increase in the time required to process visual feedback [57]. In the intact neuromotor control system, sensory delays can be compensated by predicting the future outcome of movement. This prediction process can be characterized as a form of model predictive control, such that the effect of the time delay on the system transfer function is minimized by subtracting a prediction of the delayed feedback from the instantaneous error (Figure 4-1). When the actual feedback delay τ(s) and predicted feedback delay $\hat{\tau}$(s) become mismatched, the system oscillates and can become unstable.
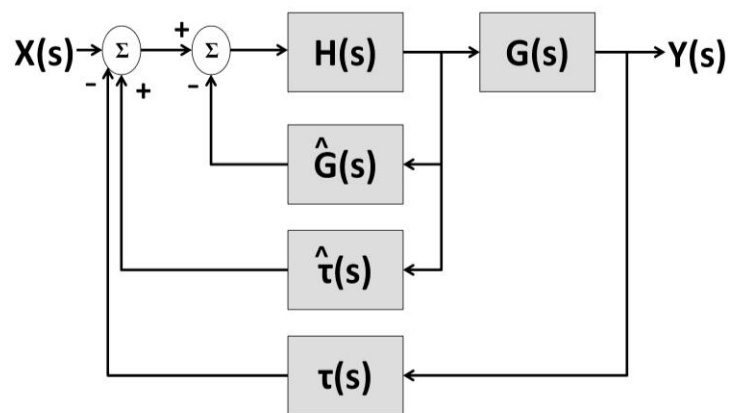
Figure 4-1. Model Predictive Control.
The effects of long feedback delays on system control can be reduced by using a predictive feedback controller to cancel the effects of the delay. The controller (H(s)) acts on the total error between the delayed τ(s) feedback of output Y(s) and the predicted, delayed error through the feedback loops of the estimated plant ($\hat{G}$(s)) and the estimated time delay $\hat{\tau}$(s).

It remains unclear why subjects with MS do not adapt directly to increases in visual delay, which would be the most effective method of reducing motor instability. Previous studies examining delay adaptation have found that healthy subjects are able to adapt to small increases in feedback delay, but are unable to adapt to large, sudden increases in feedback delay [19, 48]. Subjects with MS are able to correct movement trajectories in force fields, indicating that their ability to adapt is not completely lost due to neurological changes resulting from MS [105]. These results suggest that subjects with MS should be able to adapt successfully to gradual increases in visual delay. In subjects with MS, we have previously shown that the mismatch between actual and predicted visual feedback can create a mismatch between actual and predicted limb dynamics that may become maladaptive as motor dysfunction progresses [57]. Subjects may therefore attempt to first compensate for delay mismatches by altering predictions of limb dynamics. Once these changes become insufficient to compensate for increases in visual delay, the additional feedback delay may be too large for subjects to be able to adapt to directly. However, instability is reduced when $\tau(s)$ is an exact multiple of $\hat{\tau}(s)$ because frequency multiples (harmonics) maximize destructive interference with the fundamental frequency. In individuals with MS, visual delays in subjects with severe tremor are approximately twice the delays of healthy control subjects [57]. Here, we hypothesize that that PwMS are reducing oscillation by maximizing destructive interference within the feedback loop and are unable to increase their predicted delay away from the first harmonic because doing so would increase instability. Further, we hypothesize that *increasing* visual feedback delay will shift the location of this first harmonic, resulting in

an increase in the optimal value of $\hat{\tau}$(s) and inducing delay adaptation in subjects with MS.

We have previously proposed a framework for investigating movement deficits leading to tremor on an individualized basis [57]. In the current study, we use this framework together with subject-specific simulations of sensorimotor control to investigate the barriers to delay adaptation in PwMS. Simulation results suggest that delay adaptation in PwMS can be facilitated by further delaying visual feedback; we test this hypothesis in three subjects to determine whether this presents a viable rehabilitation strategy. Finally, we examine the extent to which adaptive changes in subjects' internal estimate of their visual delay can reduce intention tremor and improve motor performance in MS.

4.2   SIMULATIONS

4.2.1   Methods

Model

Sensorimotor control of joint angle was modeled as a multi-input single-output linear time-invariant system described in detail in previous work [6, 56, 57]. Three model inputs corresponded to external sensory perturbations to the cursor and limb ($D_{vision;}$ D_{torque}), and to the desired cursor/limb position (θ_d) , defined as the visual target; model output corresponded to current cursor/limb position (θ_a). The sensorimotor control model

(Figure 2-1) consisted of a feed-forward control pathway, two feedback pathways corresponding to visual and proprioceptive estimates of limb position, and a "forward model" – here modeled as a Smith Predictor - acts as a predictive controller to minimize the impact of system delays. Perturbations to visual feedback of limb position were combined with estimates of actual limb position which were weighted (K_v, K_p) and delayed (T_v, T_p). This sum was subtracted from desired position (θ_d) to obtain an estimate of performance error. Simultaneously, the forward model generated a prediction of performance error used to account for delays in the feedback pathways. These two signals (performance error and predicted performance error) were summed to produce an overall estimate of prediction error. Prediction errors provided the input to a PID controller (corresponding to a neural controller which acts to minimize error), which commanded the musculoskeletal geometry (not modeled here), to produce a torque that moved the plant by rotating the arm about the elbow. The plant was modeled here as a 2nd order system (inertia, viscosity, and stiffness) which converted command torque to joint angle.

Model characterization

Delay estimation:

To estimate response delays, subjects were asked to respond to a continuous, low frequency (0-1Hz band-limited white noise), pseudorandom perturbation was applied to the cursor or manipulandum. Subjects were asked to return the cursor to the (stationary) target (visual perturbation) or return the elbow joint to 90° of flexion (torque perturbation) during ten, 20-second trials. Response delays were estimated by finding the temporal offset of the cross-correlation between the perturbation and subjects' responses.

Forward predictions of subjects' individual sensory response delays (T_v^*, T_p^*) were

calculated from the same task by examining the average length of individual

"submovements" throughout the task. Submovements have previously been found to

correlate with sensory response delays; this correlation may be related to the

discretization of corrective movements to minimize error and reduce the amount of effort

necessary to continuously process error feedback [57, 67, 133]. For each subject, the

submovement interval and range of uncertainty were measured as the mean (μ) and

standard deviation (σ) from a sum of Gaussians fit to the distribution of submovement

intervals throughout the task [57].

Plant dynamics, sensory weights, controller gains:

Plant dynamics, sensory weights, and controller gains were fit to subjects'

responses to a high frequency (0-10Hz, low-pass filtered at 1 Hz with a 1st order zero-

phase Butterworth filter) pseudorandom perturbation applied to cursor position. As in the

previous task, subjects were asked to use the manipulandum to return the cursor to a

stationary target as quickly and accurately as possible. For each subject's responses, two

frequency response functions (FRFs) were calculated. One FRF related subjects'

command torque to limb position and was used to determine plant dynamics. The second

FRF related the subjects' position response to the input perturbation and was used to fit

the remaining parameters of the sensorimotor control model (K_v, K_d, K_{pr}, K_i, J^*, B^*, K^*)

for each subject. FRFs were averaged across trials using a subtraction analysis (See

Appendix A). Each FRF was fit to the sensorimotor control model transfer equations

(Eqs. 1-4) using the simplex method (Matlab fminsearch). To characterize the uncertainty

in each parameter, model fits were performed 1000 times. On each fit, the FRF data was resampled (with replacement) to provide an estimate of the uncertainty in the FRF calculation. Prior to fitting, model parameters were randomly initialized to span an order of magnitude about the set of nominal parameter values estimated from healthy human subjects (Chapter 2). For each model parameter, the resulting distribution was used to define the best estimate (mean) and uncertainty (SD) in the parameter estimates.

The FRF relating the subject's joint position to their input torque was well fit by a 2nd-order model of joint dynamics (Eq. 1):

$$P(s) = \frac{1}{Js^2 + Bs + K} \tag{1}$$

where J, B, and K correspond to the moment of inertia, viscous damping coefficient, and spring constant, respectively, of the elbow joint.

The FRF relating the subject's joint position relative to the applied perturbation was fit to the corresponding model transfer function

$$\theta_a(s) = -\left[\frac{K_v C(s)P(s)e^{-T_v s}}{1+C(s)P^*(s)-C(s)P^*(s)*\left(K_v^* e^{-T_v^* s}+K_p^* e^{-T_p^* s}\right)+C(s)P(s)\left(K_v e^{-T_v s}+K_p e^{-T_p s}\right)}\right] D_{ext}(s) \tag{2}$$

where P(s) is the transfer function of the plant and C(s) is the transfer function of the neural controller, characterized here as a PID controller:

$$C(s) = K_d s + K_{pr} + \frac{K_i}{s} \tag{3}$$

and P*(s) is the subject's internal dynamics:

$$P^*(s) = \frac{1}{J^*s^2 + B^*s + K^*} \tag{4}$$

Subjects

Subjects were drawn from the population of PwMS with moderate to severe intention tremor accompanied by a significant increase in visual response time (approximately 50% of the subject population [57]). Exclusion criteria included subjects with proprioceptive deficits, cognitive deficits, and eye movement deficits. Two women (41 and 60 years old) and one man (29 years old) participated in the study. All subjects were right handed, according to the Edinburgh Handedness Inventory. No subjects reported neurological deficits (aside from MS) that would interfere with their participation in the study. Two subjects were diagnosed with secondary-progressive MS; the third subject was diagnosed with relapsing-remitting MS. All had been diagnosed > 10 years previously, and two subjects had EDSS > 5. EDSS for the remaining subject was unavailable. All subjects were on immunomodulating drugs at the time of the study. Written, informed consent was obtained from each subject in accordance with the Declaration of Helsinki and approved by the Marquette University Institutional Review Board.

Subject Parameters

Subjects' individual sensorimotor systems were characterized using the methods

described above and in more detail in Chapter 3 and in [57]. Parameters used for each

subject's simulations are shown in Table 4-1.

Table 4-1. Subject parameters used in simulations

Sub	K_v	K_d	K_{pr}	K_i	J	B	K	J^*	B^*	K^*	T_v	T_v^*	T_p
1	0.71	0.008	0.15	1.42	0.034	0.92	2.77	0.059	1.24	2.57	686	301	360
2	0.35	0.023	0.27	10.1	0.043	1.21	1.29	0.066	2.02	9.77	870	402	208
3	0.17	0.025	0.51	16.8	0.087	1.19	14.7	0.12	1.25	30.6	540	320	170

Simulations

For each subject the best-fit sensorimotor control model was implemented in

Simulink (MathWorks, Natick, MA). The step response of the model was used to

simulate the subject's response to a reach and hold task to estimate model movement

error during the "endpoint acquisition" phase of movement – after the "limb" has covered

80% of the target distance. Mean squared error (MSE) during this hold period was

calculated as the average difference between the simulated joint angle and the target

("desired position"). Model MSE was calculated as a function of the predicted visual

response delay (-200ms to 800ms difference from our estimate) defined by the forward

model (Figure 2- 1).This created an "error profile" whose slope mapped changes in the

MSE to corresponding changes in predicted visual delay. In order to investigate the

effects of altering visual feedback, separate error profiles were generated for a range of

external visual delays (50, 100, 150, 200, 250, and 300 ms) which increased feedback delays.

4.2.2   RESULTS

Error Profiles

For each subject, we plotted MSE vs. increase in predicted visual response delay. An error profile for a sample subject (Subject 2) is shown below (Figure 4-3). In all subjects, a local minimum in the error profile existed near zero – near each subject's current predicted delay. Error then increases with an increase in predicted visual delay up to approximately 100ms; this is followed by a decrease in movement error which reaches a global minimum at approximately each subject's actual visual delay.
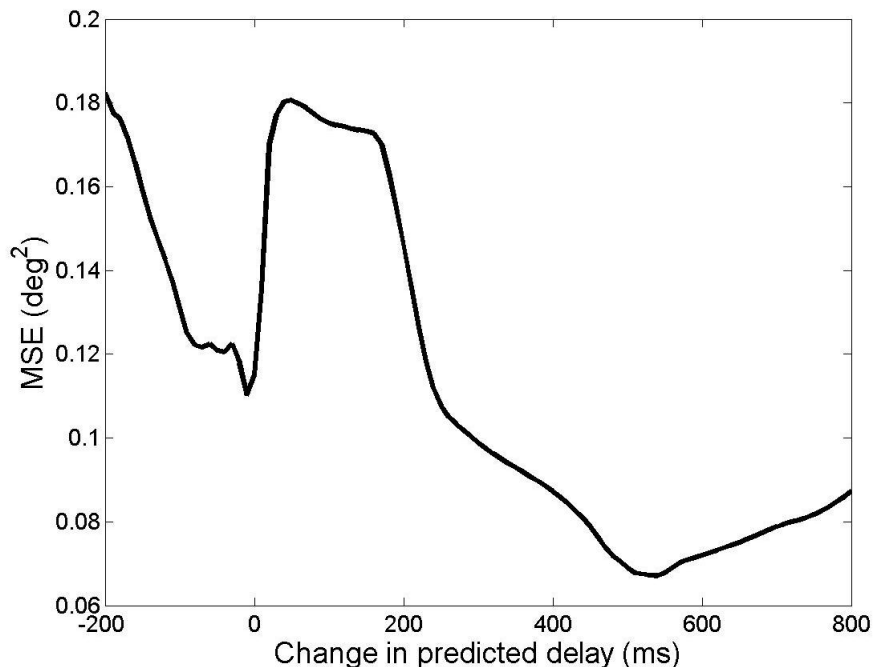
Figure 4-2. Simulated movement error as a function of the change in predicted visual response delay for Subject 2 (Error profile).
Shown is the error profile for subject 2. Zero indicates subject's predicted visual delay. The local minimum is located approximately at 0. Another minimum is located between 500 and 600 ms above the predicted visual delay (approximately the actual visual response delay).

Local minima reported in the table were based on the minimum MSE nearest to the subject's internal estimate of visual response delay. Local minima in the simulated error profiles all fell within one standard deviation of the internal estimates of visual response delay characterized using the submovement interval. Global minima in the simulated error profiles occurred within one standard deviation of the actual visual response delay for two of three subjects, and within two standard deviations of the actual visual response delay for the third subject. Mean differences between local and global minima in the error profiles was 423.3±111.5 ms.

Table 4-2. Actual and expected visual response delays (mean±SD) and model local and global minima.

| Subject	Predicted visual response delay (ms)	Visual response delay (ms)	Model local minimum error (ms)	Model global minimum error (ms)	Difference between local and global error (ms)
1	299.0±105.3	686.0±227.5	361	741	380
2	408.0±162.2	869.0±120.6	398	948	550
3	318.3±131.0	517.2±39.7	280	620	340

Error Profiles with Increasing Feedback Delays

In order to examine the effects of increases in visual feedback delay, we simulated error profiles for three specific delay increases. Error profiles for the sensorimotor control model of Subject 2 are shown in Figure 4-3. When a 100 ms external feedback delay is added, simulation MSE was no longer at a local minimum (blue line). Minimizing movement error in the presence of the 100 ms external delay corresponds to an increase in the internal estimate of the visual response delay of approximately 10 ms. When external feedback delay is increased to 200 ms (cyan), movement error is no longer at a local minimum; minimizing error results in an increase in the predicted estimate of the visual response delay of approximately 60 ms. Finally, when the external feedback delay is increased to 300 ms, the error profile (green) indicates that the minimum movement error will occur when the expected visual response delay is increased by an additional 80 ms – resulting in an overall increase of 140 ms in the internal estimate of the visual response delay. When the 300 ms external feedback delay is removed (and the additional external feedback delay is 0 ms), simulation MSE decreases as predicted visual response

delay increases toward the global error minimum corresponding to approximately the actual visual response delay (idealized path shown in red arrows).
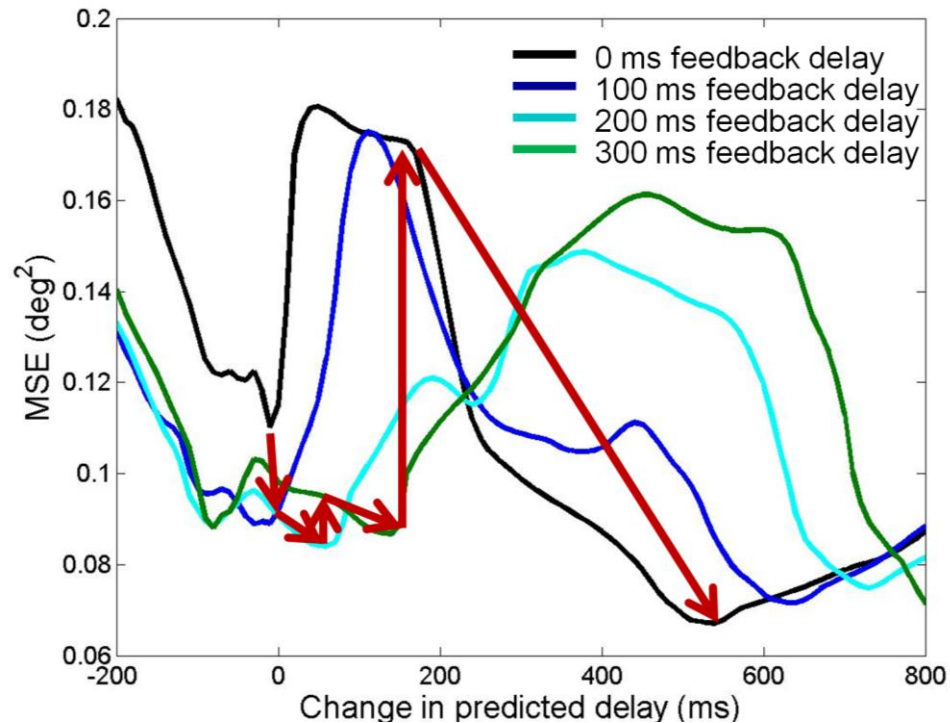
Figure 4-3. Error profiles with increasing feedback delays for Subject 2.
The change in error profile with the addition of an external visual feedback delay are shown in blue (100ms), cyan (200 ms), and green (300 ms). Arrows indicate hypothetical changes in error in a system that seeks to minimize endpoint error.

Here, we assumed that adaptation in subjects' sensorimotor control systems would seek to minimize overall position error. To this end, we generated simulations of changes in predicted visual delay (in the direction of decreasing error) in response to increases in actual visual delay. Based on the simulated error profiles for each subject's sensorimotor control model, three external visual feedback delays were selected to maximize adaptation in the internal estimate of the visual response delay toward the subject's actual visual response delay. For subject 1 external delays of 120, 200, and 200

ms were used during the adaptation sessions. For subjects 2 and 3, the external delays were [100, 200, and 300 ms - shown] and [50m 100m and 150 ms] respectively.

4.3 ADAPTATION

4.3.1 Methods

Outcome Measures

Four outcome measures were used to evaluate the effect of delay adaptation on motor control: the nine hole peg test (9HPT), spiral tracing [130], handwriting, and a reach-and-hold (step) task using the manipulandum [57]. The 9HPT was timed and scored according to the multiple sclerosis functional composite score (MSFC). During the handwriting task, subjects were instructed to copy three sentences (typed with 20pt font). Sentence completion was timed using a stopwatch; timing started as soon as the subject began writing the first letter, and ended when the subject completed the sentence. The sentences chosen were, "I am writing this sentence", "One thousand three hundred and eighty-seven dollars and twelve cents" (to mimic, for example, writing a check), and "The five boxing wizards jump quickly" (a pangram). Subjects were instructed to copy each sentence at a "normal writing speed". Sentence writing speed was calculated (in letters/sec) by dividing the number of letters per sentence by the time (in sec) spent writing the sentence. Writing speed was then averaged across sentences.

During the spiral tracing task (described in detail in Chapter 3 and in [57, 130]), subjects were instructed to trace an Archimedes spiral on a Wacom tablet (Wacom Technology, Vancouver, WA). The spiral was marked every 3 cm with a tick mark. Subjects were instructed to match the speed of their tracing movement to the speed of a metronome by crossing one tick mark per beat. Tracing speeds range from 60bpm (3 cm/sec) to 120bpm (12 cm/sec). Pen position and timing information was collected using Cogent (University of London, London) and MATLAB (MathWorks, Natick, MA). Spiral position was de-trended by subtracting the least-square error liner fit to angle vs. radius, resulting in deviations from the spiral trace. The power spectrum of each tracing trial was calculated and the frequency and magnitude of tremor was calculated by finding the maximum amplitude within the tremor frequency range (2-6Hz) [94]. Tremor frequency was estimated by average frequency across trials. Because tremor amplitude increased with speed, tremor magnitude was averaged across the three fastest trials only.

Finally, target acquisition time (AT) and mean squared error (MSE) were calculated from each subject's responses during the "endpoint acquisition" phase of a reach and hold task. During the task, subjects were seated at the manipulandum. A visual target placed along the midline of the computer display was displaced pseudo-randomly to the left or to the right by 18, 20, or 22 degrees with the restriction that joint angle not exceed ±40° from the midline (90° flexion). Subjects were asked to move to the target as quickly as possible; speed of the movement was emphasized in order to prevent subjects from altering their movement strategies in order to achieve greater accuracy. Subjects performed eight target jumps per trial with the timing between jumps randomized from 3.5 to 4.5 seconds. During analysis, trials were parsed into eight, three second epochs

beginning at each target jump. For each epoch, target acquisition time was calculated by determining the time at which subjects completed 80% of the trajectory (80% of the distance to the target). MSE was calculated using the square of the difference between target and subject position after subjects acquired the target (e.g. at the end of the target acquisition time).

Sham sessions

In order to investigate which effects are due to practice, and which effects are due to adaptation, we had subjects participate in a "sham" adaptation while performing a series of reach and hold tasks using the manipulandum. During the task, the target was located along the horizontal midline of the display and randomly displaced to the left or the right. Subjects were again instructed to move to each target "as quickly as possible". Displacements were randomly selected from ±10, 15, 20, 25, or 30 degrees and occurred pseudo-randomly every 3.5-4.5 seconds with the restriction that elbow joint angle not exceed 40º from the midline. Subjects performed three sets of 10, 64 second trials. Each trial contained approximately 16 target displacements per trial for a total of 480 target displacements during the session. During analysis, step trials were divided into epochs consisting of the first 3 seconds post-target jump and normalized against target distance. Trials where subjects moved too early (<0.1 seconds post-target jump), too late (>1.0 seconds post-target jump), or in the wrong direction were excluded from analysis (<5% of trials). For each jump, MSE and submovement interval were calculated as described above and averaged across trials.
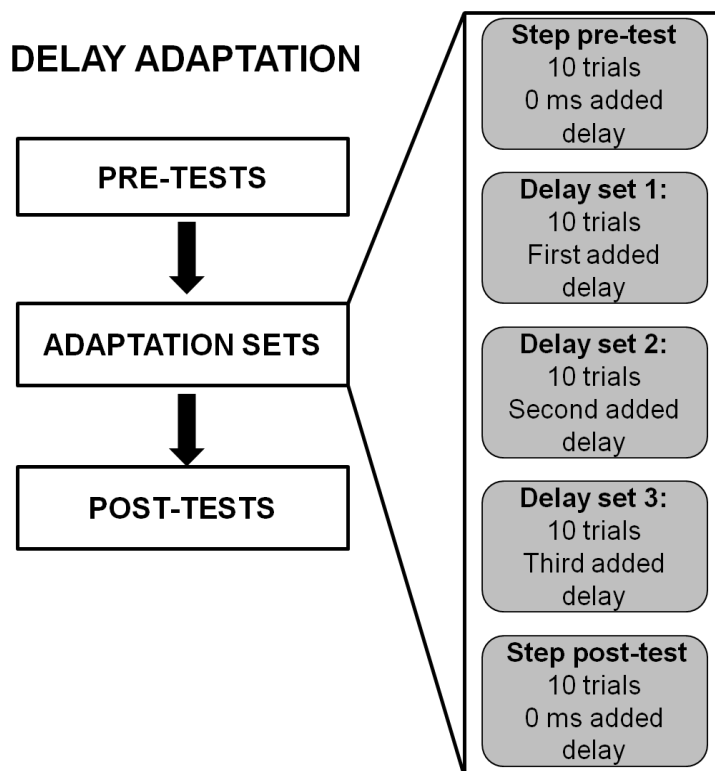
Delay Adaptation

On a separate day, subjects performed the same reach and hold task as described above, but with the goal of facilitating delay adaptation. As in the sham session, each trial lasted 64 seconds. During each trial, the target was randomly displaced by 20 ± 2 degrees, with the caveat that elbow angle not exceed 90 ± 40 degrees. Slightly different target distances were used in order to prevent subjects from learning the task easily.

Unlike the sham session, during adaptation sessions the presentation of the cursor feedback was delayed relative to the arm position. External delays used in the adaptation sessions were individualized for each subject based on the simulation results in order to provide the optimal feedback delays to induce adaptation; successive delays moved the subject's simulated minimum MSE toward a higher internal estimate of visual response delay. All adaptation sessions began with 10 trials (a "set") with 0 ms of added feedback delay, followed by three trial sets with external feedback delays equal to the first-third optimal delays identified by our simulations (Figure 4-4).

Care was taken to ensure that subjects were unaware that the sham and adaptation sets were different; setup and questions asked were identical across days. Before and after the sham and adaptation sessions, subjects performed the pre- and post-tests described above to characterize intention tremor and improvements in functional performance. Finally, 24-48 hours after the adaptation session, subjects performed the pre- and post-tests a final time in order to examine whether changes in motor performance persisted. Performance on the pre- and post- tests was compared within and across sessions to

determine whether changes in movement control were due to visual delay adaptation or simply to practice effects.

DELAY ADAPTATION

| PRE-TESTS |
| ADAPTATION SETS |
| POST-TESTS |

Step pre-test
10 trials
0 ms added delay

Delay set 1:
10 trials
First added delay

Delay set 2:
10 trials
Second added delay

Delay set 3:
10 trials
Third added delay

Step post-test
10 trials
0 ms added delay

Figure 4-4. Delay adaptation experimental design.
During this session, adaptation sets were performed between pre- and post-tests of visually guided reach. Adaptation sets consisted of 5 sets of 10 trials each; during each set, external feedback delay was held constant in order to give subjects time to adapt. External feedback delay was increased between delay sets 1-3, then removed entirely for the post-test.

4.3.2   Sham Results

Across subjects, no significant differences in motor performance were observed before and after the sham adaptation session. Two subjects (subjects 2 and 3) showed decreases in 9HPT completion time (9.1% and 11%, respectively) in their dominant hands. Only one subject (subject 3) had a decrease in 9HPT time for her non-dominant

hand. Across subjects, the changes were not statistically significant for either the dominant (paired t-test; $t(4) = 0.24$, $p = 0.82$) or non-dominant (paired t-test; $t(4) = 0.25$, $p = 0.81$) hands. Only one subject showed a large change ($>70\%$) in tremor power as measured by the spiral tracing task, however, the change was not statistically significant due to high variance between trials (unpaired t-test; $t(4) = 1.41$, $p = 0.23$). No significant changes in handwriting speed was found within (unpaired t-test; $t(4) < 2.0$, $p > 0.05$) or between (paired t-test; $t(16) = 0.54$, $p = 0.59$) subjects. Similarly, movement error did not decrease within (unpaired t-test; $t(68) < 2.0$; $p > 0.05$) or across (paired t-test; $t(4) = 0.52$, $p = 0.63$) subjects. In two subjects, submovement intervals did not change significantly across sets ($t(170) < 2.0$, $p > 0.05$). However, one subject (Subject 3) did show a small ($<$ 70 ms), but statistically significant, increase (unpaired t-test; $t(170) = 4.02$; $p < 0.001$) in submovement interval.

4.3.3   Adaptation Results

Error reduction across trials

Analysis of MSE from the delay adaptation sessions was used to directly probe changes in the internal estimates of the visual response delay. Increases in the external feedback delay were immediately followed by an increase in endpoint error that decreased across trials within a delay set (Figure 4-5). Linear correlations between error and trial number were negative ($r<-0.20$) in three of the four sets, including the final adaptation set, when the external visual delay was set to zero.
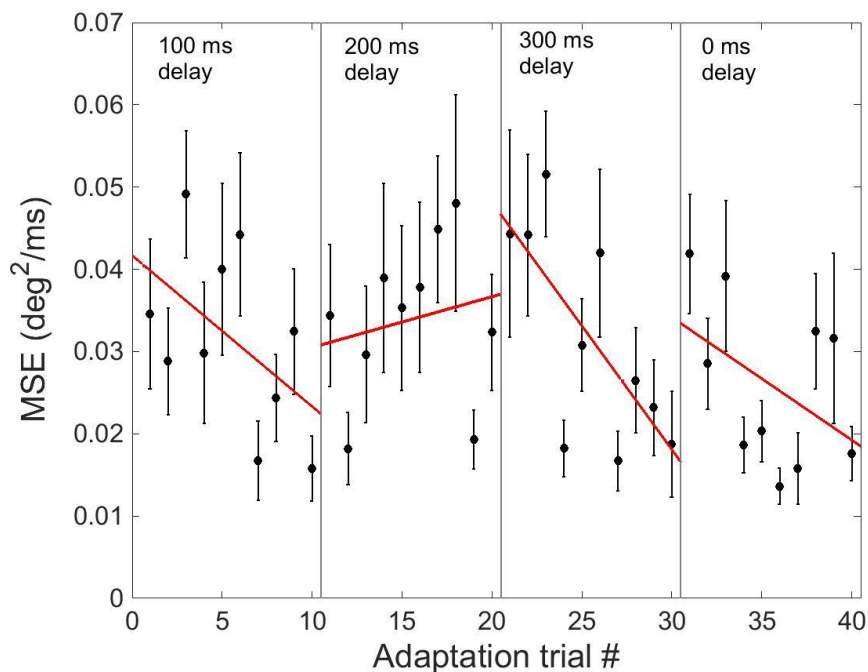
Figure 4-5. MSE across adaptation sets (black circles) and best-fit linear regression within each set (red lines) for Subject 2.
In general, correlations are negative, but only one (300 ms delay; p = 0.02) reaches significance. Error bars denote standard error.

Submovement Interval

Submovement intervals increased throughout the adaptation session for all three subjects (Figure 4-6). Internal estimates of subjects' visual response delays increased significantly ($t(170) > 2.0$; $p<0.05$) across adaptation sets in all three subjects. Only Subject 1 exhibited changes in submovement interval that increased to a value comparable to actual visual response delay. In all three subjects, submovement interval increases significantly ($t(170) > 2.0$; $p < 0.05$) during and after adaptation. In two subjects, the effect is retained 24-48 hours following adaptation ($t(170) > 2.0$; $p < 0.05$).
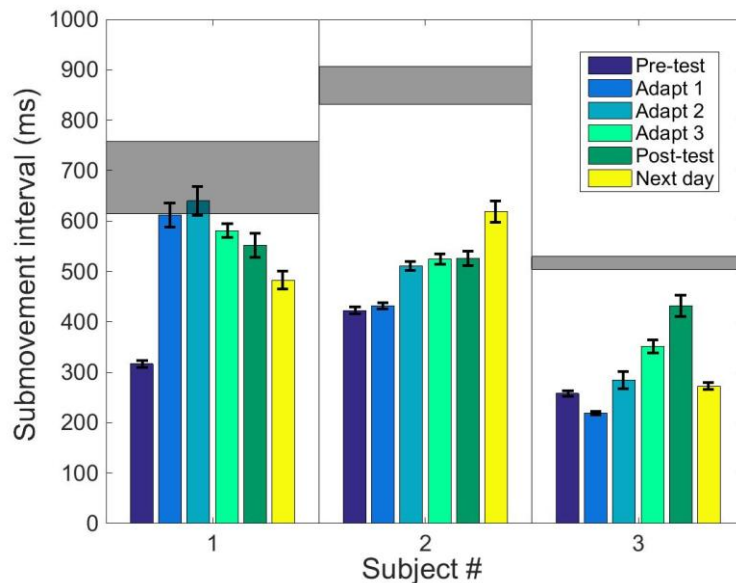
Figure 4-6. Submovement interval across adaptation sets.
Pre-test: dark blue; Delay Set 1: blue; Delay Set 2: light blue; Delay Set 3: light green; Post-test: green; Next-day post-test: yellow. Error bars denote standard error. Actual visual response delay (±SD) is denoted by the shaded region.

Error Reduction

For subject 1, movement error decreased significantly (unpaired t-test; t(138) = 2.54; p = 0.012) following adaptation to the three external delays; movement error decreased slightly from post-adaptation testing to the following day (Figure 4-7 left). Movement error for subject 2 decreased consistently from pre- to post- testing and movement error continued to decrease on the following day, however, the changes did not reach statistical significance (t(138) < 2.0, p > 0.05). Error in subject 3 also decreased from pre- to post- testing, although the change was not significant (t(138) = 0.63, p = 0.53). Error increased significantly from post-adaptation testing to the following day (t(138) = 2.47, p = 0.015). Figure 4-7 (right) shows the average movement profile in response to step displacements of the target (normalized to displacement magnitude)

before and after adaptation for subject 2. Subject 2 shows a tendency to approach the

target more slowly during post-adaptation testing (green), but with fewer direction

changes and lower variance when compared to pre-test performance (t(2998) = 4.33; p <

0.001). During follow-up testing the next day (yellow), subject speed increased, but

endpoint variance has remained lower than pre-adaptation variance (t(2998) = 2.72; p =

0.0065).
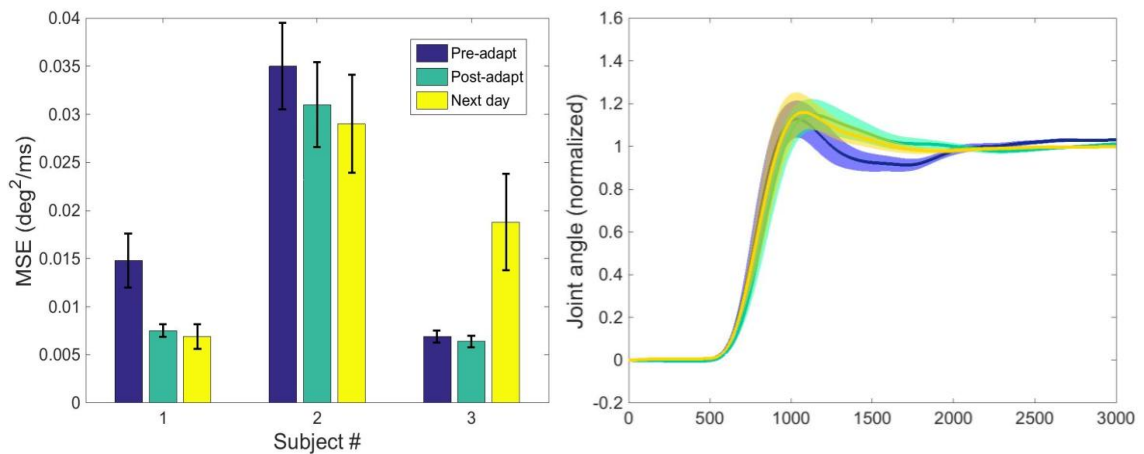
Figure 4-7. Endpoint error and average movement profile
(Left) Endpoint error. Error bars denote ±standard error (Right) Average normalized movement profile
during a reach and hold task before (blue), immediately following (green) and 24-48 hours after delay
adaptation (yellow) for Subject 2. Dashed lines denote variance about the mean movement.

Movement Speed

In addition to examining movement error, we calculated target acquisition time in

order to ensure that subjects were not simply moving more slowly. As feedback delay

increased, subjects moved more slowly, with target acquisition time peaking between the

second (Subjects 1 and 2) and third (Subject 3) delay sets. Once the external feedback

delay was removed, target acquisition time decreased to the times observed before adaptation (Figure 4-8).
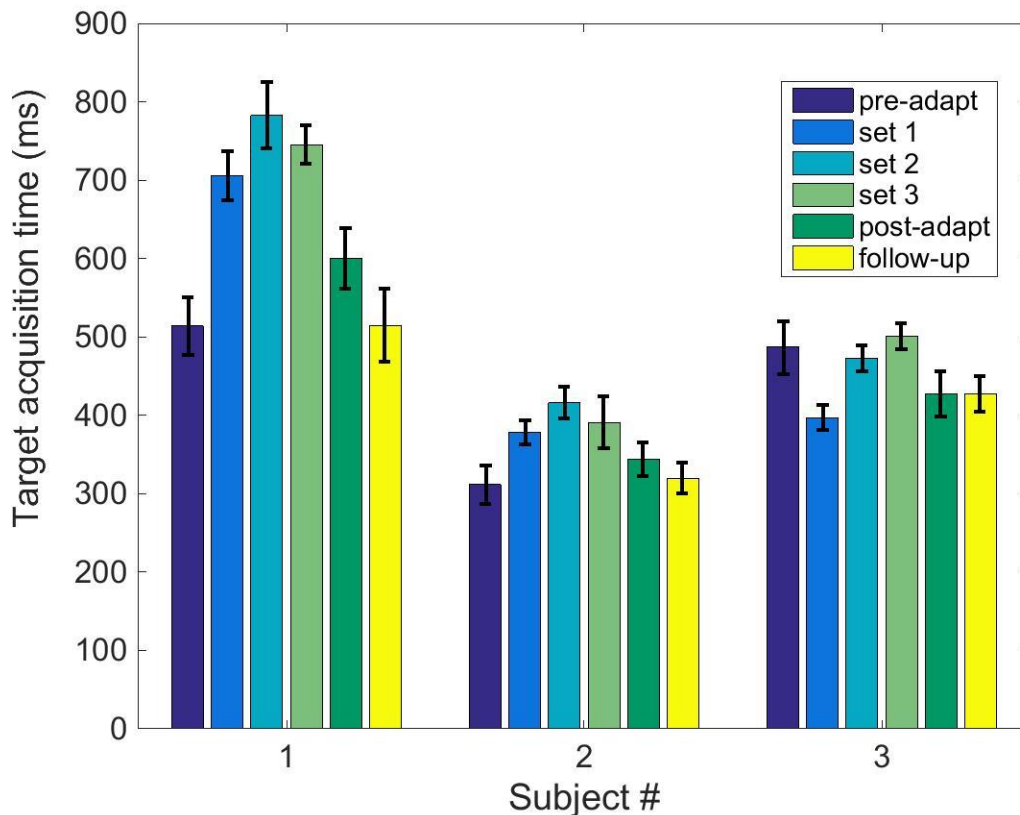
Figure 4-8. Target acquisition time (TAT) across adaptation sets.
TAT before (dark blue), during (blue, turquoise, light green), and after (green) adaptation sets and in the follow-up session (yellow).

9HPT

Time to completion scores on the 9HPT consistently decreased following delay adaptation (Figure 4-9). Decreases in the time to complete the task were observed in subjects 1 and 3 in both their dominant (left) and non-dominant (right) hands. Subject 2 also improved in his dominant, but not his dominant hand. Nine hole peg test score with the dominant arm showed modest improvements of 3.5% and 11.2% for subjects 1 and 2.

Larger improvements were seen across days, resulting in 21.2%, 13.3%, and 10.7%

decreases in 9HPT time for subjects 1-3. Improvements in performance were also seen in

the non-dominant arm, with post-adaptation improvements of 8.3%, and 27.1% in

subjects 1 and 3. Across days, the same subjects had improvements of 15.1% and 29.1%.

Because the 9HPT was only measured twice for each test, within-subject statistical

comparisons could not be made. However, across subjects, there was a significant

improvement in 9HPT time for the dominant hand from pre-adaptation to the following

day (paired t-test; $t = 11.5$; $df = 5$; $p < 0.001$). A similar change was not seen in the non-

dominant hand (paired t-test; $t = 0.30$; $df = 5$; $p = 0.78$).
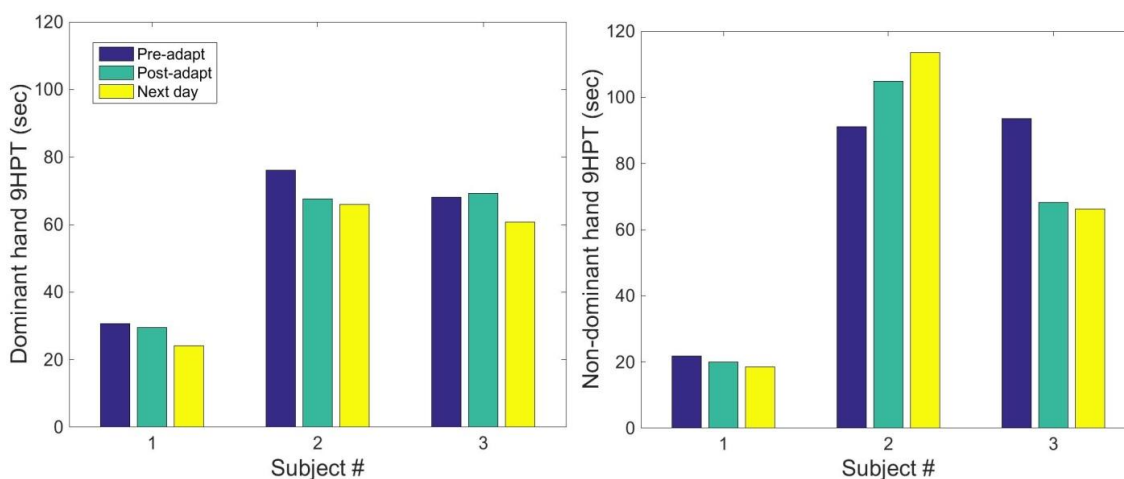
Figure 4-9: 9HPT scores for the dominant (left) and nondominant (right) limb.
Before (blue) and after (green) delay adaptation, and during the follow-up testing after 24-48 hours.

Handwriting

Handwriting speed improved significantly (unpaired t-test; $t(4) = 3.1$; $0 = 0.036$)

following delay adaptation in Subject 2 (Figure 4-10, left). Subjects 1 and 3 both showed

slight increases in handwriting speed but the difference was not significant. The quality

of handwriting samples also improved following delay adaptation (Figure 4-10, right).

Handwriting appeared smoother post-adaptation and the improvements were sustained

into the following day. In the representative writing sample shown in Figure 4-10,

handwriting appears more accurate following adaptation, based on the number of letters

that touched (rather than "floated above") the writing line. Further, handwriting appeared

more fluid post-adaptation; crossbars (e.g. "I" and "t") are straighter, and curved letters

(e.g. "m" and "n") are more rounded.
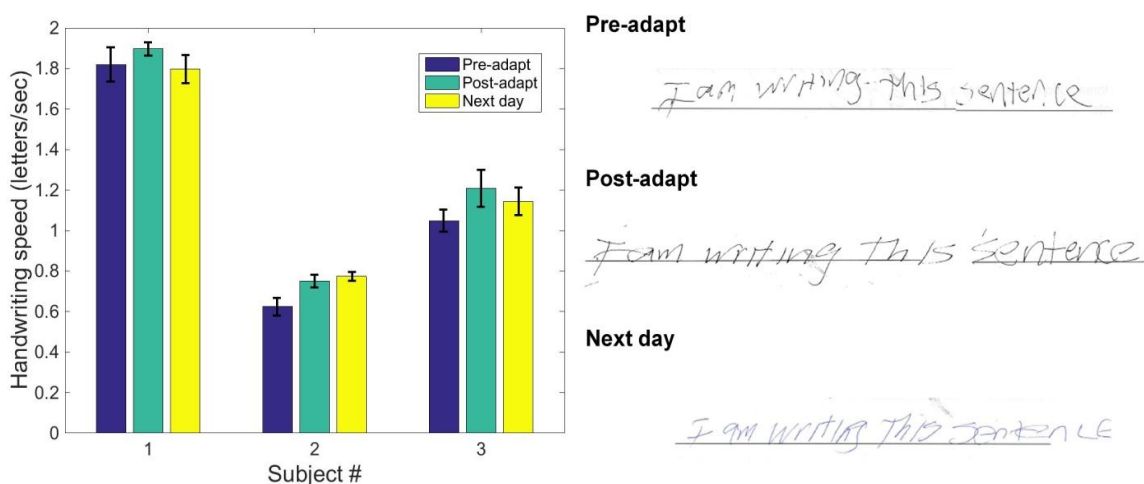
Figure 4-10. Handwriting speed and samples.
(Left) Handwriting before (blue) and immediately after (green) adaptation, and after 24-48 hours. Error bars denote ±1 standard error. (Right) Handwriting sample from a representative subject (Subject 2)

Tremor frequency and power

Tremor power (averaged across the three fastest trials of the spiral tracing task)

decreased in all three subjects (Figure 4-11, left) although the changes were not

significant ($t(2) > 2.0$, $p > 0.10$) due to variance in tremor power across trials of varying

speeds. In subject 1, tremor power decreased by 57.1%; in subject 2, by 36.4%; and in subject 3, by 75.7%. While decreases in tremor power were observed in all subjects the effect across subjects was not statistically significant (paired t-test; $t(4) = 1.87$; $p = 0.13$) due to the small subject sample size. On the following day, tremor power increased in all three subjects from the post-adaptation session. Tremor frequency (Figure 4-11, right) was also altered by delay adaptation. In two of three subjects (Subjects 2 and 3), tremor frequency decreased significantly from the pre-test to the post-test ($t > 1.9$; $p<0.05$) This effect did not last into the follow-up testing ($p > 0.05$).
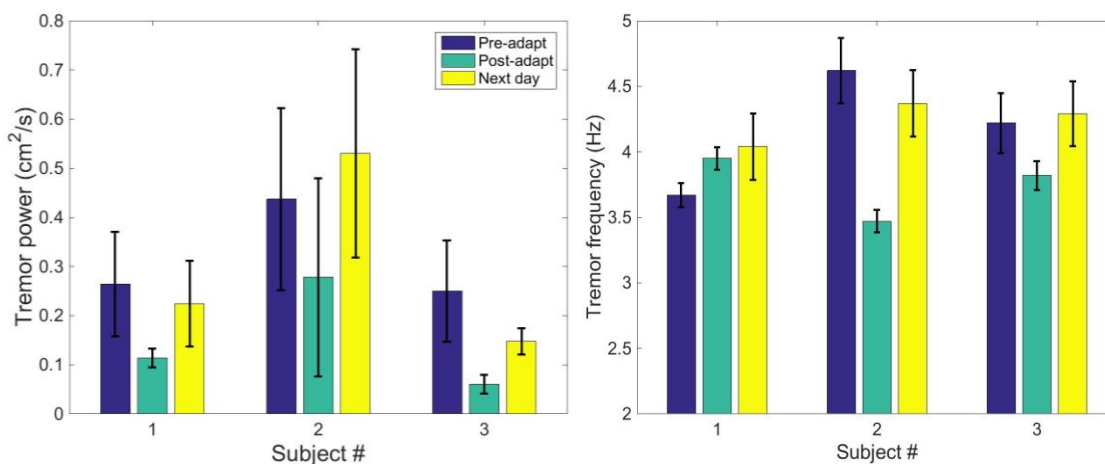
Figure 4-11. Tremor power and frequency.
Tremor power during spiral tracing task before (blue) and after (green) adaptation task and during next-day post-test (yellow). Error bars denote standard error.

4.4   DISCUSSION

We have previously shown that PwMS and intention tremor have high visual response delays but normal submovement intervals; in our model, we link this to an inability to generate an accurate forward model to account for long sensory delays. In

simulations, this results in oscillatory behavior; in human subjects, it can result in tremor during goal-directed movements. These large differences between actual and predicted visual delays are correlated – in our subject population - with large mismatches between the plant and its forward model. Changes in the forward model of the plant, but not the delay, suggest that persons with MS may be unable to adapt directly to the increase in visual response delay [57]. Instead, subjects alter their internal estimates of limb dynamics – a model that is more readily adaptable [49]. The goal of the current study was to investigate the barriers to direct delay adaptation in PwMS and whether delay adaptation can be facilitated through the alteration of visual feedback.

Here, we characterized subjects' individual sensorimotor systems and simulated movement outcomes in order to examine why subjects with MS are unable to adapt directly to increases in feedback delay. The sensorimotor control model for each subject was used to examine the consequences of changes to the internal estimate of visual response delay on movement endpoint error. Model simulations suggest that subjects' ability to adapt their internal estimate of visual response delay may be confounded by the need to minimize endpoint error during movement, which may provide an explanation for our previous results - subjects may be forced to adapt other aspects of the motor control system in order to reduce error. However, model simulations with an externally applied visual feedback delay indicate that the local minimum of endpoint error can be shifted toward higher internal estimates of visual delay by applying specific sequences of external delays. Assuming subjects naturally adapt in the direction of minimum error, these specific sequences of external feedback delays should allow subjects to directly alter predicted visual delay.

To determine whether adaptation of the internal estimate of visual response delay was taking place, movement error and submovement intervals during adaptation sets were examined. Trends toward decreases in movement error occurred across adaptation trials, suggesting that subjects are able to reduce error in response to external feedback delays. Increases in submovement interval, used here to characterize the internal estimate of visual response delay, also occurred during adaptation trials. This suggests that internal estimates in the visual response delay may be changing in response to the targeted adaptation tasks. These factors, taken together, may indicate that subjects were successfully adapting their internal estimates of visual response delay in an effort to reduce movement error.

As an effect of the adaptation task, significant reductions in MSE were observed within one of the three subjects as well as between subjects (between-subject significant results, in the absence of significant within-subject results, is due to large within-subject variance). In addition to the reduction in MSE, improvements in other functional measures of motor control were also found, including handwriting speed, 9HPT score, and tremor power and frequency during spiral tracing (Table 4-3). Subject 2 had the largest tremor initially and had improvement in 4 of 7 metrics: submovement interval, handwriting (speed and accuracy), and 9HPT score. Tremor power and movement error were also reduced, but results were not statistically significant. For subjects 1 and 3, results were similarly mixed; both Subjects 1 and 3 showed improvement in 3 of 7 metrics,. Some of these effects persisted into a second day; submovement interval and improvements in handwriting, in particular, had the largest persistent effects. In contrast,

tremor power and frequency were altered only immediately post-task, suggesting that changes in tremor cannot be explained simply by practice effects.

Although there was a trend towards a generalized improvement in all subjects, small sample sizes and large variations in task performance limited the power of the statistical tests. Comparable changes were not seen in the sham adaptation session, with the possible exception of 9HPT score (improvements in 3/6 hands after sham adaptation vs. improvements in 5/6 hands after delay adaptation). This may indicate that the 9HPT is more susceptible to practice effects and/or that performance on the 9HPT can be improved by performing generic goal-directed tasks.

Table 4-3. Summary of changes in functional performance following delay adaptation. Green arrows indicate significant improvement. Yellow arrows indicate no significant change in performance.

Task	Subject 1	Subject 2	Subject 3
Predicted Visual Delay	⬆ (green)	⬆ (green)	⬆ (green)
Handwriting	⬌ (yellow)	⬆ (green)	⬌ (yellow)
Movement Error	⬆ (green)	⬌ (yellow)	⬌ (yellow)
Movement Speed	⬌ (yellow)	⬌ (yellow)	⬌ (yellow)
Tremor Power	⬌ (yellow)	⬌ (yellow)	⬆ (green)
Tremor Frequency	⬌ (yellow)	⬆ (green)	⬆ (green)
9HPT	⬆ (green)	⬆ (green)	⬌ (yellow)

The predictions of the model simulations were not fully realized while testing the subjects. Specifically, complete adaptation of visual response delay to the subjects' actual visual response delay did not occur. This is likely due to factors that were unaccounted for (by the model), including changes in sensorimotor control not related to the increase in expected visual response delay predicted in simulation. For example, an increase in arm co-contraction, a common response to unanticipated movement errors, would manifest in the model fits to the subject's limb dynamics, potentially altering as many as five model parameters (actual joint viscosity and joint stiffness, predicted joint inertia, viscosity, and stiffness). Significant changes in other model parameters would be expected to alter the "error space" used to select the external delays used to maximize the effects of delay adaptation. Furthermore, subjects may not have adapted fully in the current test paradigm. Changes in movement error during adaptation suggest that this may be the case; in several cases error did not stabilize at a new level before the delay was changed. Additionally, although our model predicts complete adaptation, previous studies have found that learned internal models may be stored for future retrieval [49]. These models (which are more practiced) may interfere with complete adaptation as subjects switch between tasks.

The pilot results reported here suggest that individualized delay adaptation may be successful in reducing intention tremor in PwMS. All subjects showed improvements in motor performance immediately following adaptation to targeted external delays. In two subjects, the functional effects of delay adaptation were retained over 24 hours. More subjects are required to confirm whether targeted delay adaptation can provide an effective approach to reduce tremor across the broader population of PwMS.

Additionally, future studies should seek to increase subjects' internal estimate of their visual response delay over a more extended training period to determine whether the internal estimate of the visual response delay can be fully adapted, and whether such adaptations can be sustained following training.

The results presented here may partially explain previous findings regarding alteration of sensory feedback in subjects with MS. Changes in visual [103, 128, 135, 142] or torque feedback [105, 106] may force subjects who have adapted incorrectly to increases in the visual response delay to re-learn more effective movement strategies. Altering error feedback directly [107] may alter the error profiles relative to the internal estimate of the visual response delay and shift the position of local error minima. Although these studies have seen mixed results, we propose that strategically and individually altering feedback – specifically, visual feedback delays – may be more effective than having all subjects with MS perform identical tasks. Here, our data indicate that subjects do not adapt fully to the additional feedback delays, which may explain why we see only moderate effects.

Visual delay adaptation can reduce intention tremor in PwMS and may provide a new avenue for rehabilitation. Subjects with intention tremor and a visual delay mismatch improved their motor performance after exposure to a series of targeted external visual feedback delays designed to systematically shift minimum endpoint error in relation to the subject's internal estimate of visual response delay. Motor improvement was seen in at least three tasks in subjects with moderate (Subject 1, Subject 3) intention tremor and in a subject with severe (Subject 2) intention tremor. Crucially, increases in submovement interval with training occurred alongside these improvements, suggesting

that visual delay adaptation may be able to reduce or potentially eliminate intention

tremor in PwMS.

CHAPTER 5: SUMMARY OF RESULTS

The goal of the work presented in this dissertation was to develop a quantitative and mechanistic framework for examining atypical neuromotor control and for the development of hypotheses regarding therapeutic measures to reduce motor dysfunction. To this end, we developed a linear model of sensorimotor control whose parameters could be characterized within individual subjects using systems identification techniques. We then investigated motor dysfunction as the result of aging and multiple sclerosis and tested the hypotheses generated by our model by developing and evaluating a rehabilitative strategy for individuals with MS and intention tremor.

We first used our model to characterize the changes in motor control that take place during healthy aging in adults. We characterized three types of task – visual compensatory tracking, visual pursuit tracking, and proprioceptive compensatory tracking – in order to examine the sensorimotor system under multiple sensory and control conditions. Our results show that changes in motor control that take place during aging may be related to losses in the reliability of sensory feedback, including slower sensory response times and increased uncertainty in sensory feedback (sensory noise). We found that increases in sensory variances were correlated with changes in neural control as well as changes in effective limb dynamics (which can be controlled voluntarily as part of the overall motor control system), suggesting that increases in sensory noise may drive changes in task strategy with age.

We then extended the model to examine the underlying causes of intention tremor in multiple sclerosis. We found that subjects with MS and moderate to severe intention

tremor have significantly larger visual response delays than both healthy controls and subjects with MS with no or mild intention tremor. Through the model, we showed that increases in visual response delays associated with the disease are not accounted for by predictive mechanisms that may be used to compensate for long loop delays. At the same time, changes in visual response delays were correlated with changes in the expected limb dynamics, which could be the result of maladaptation to high, uncompensated, visual processing delays.

Based on these results, we developed a rehabilitation strategy for intention tremor centered on adapting the internal estimate of visual response delay to match the subject's actual visual response delay – thus reducing the system instability responsible for intention tremor. Simulations of subjects' sensorimotor control models indicated that the inability to adapt to high visual response delays may be due to the existence of a local minimum in error which would require subjects to accept an increase in movement error in order to adapt their internal estimate of visual response delay. Additional simulations revealed that targeted external visual delays could be used to shift the local error minimum toward higher internal estimates of visual response delay, thereby reducing tremor. Preliminary tests in three subjects with MS have provided support for the model predictions. Increases in feedback delay induce changes in internal estimates of visual response delay that are correlated with reductions in intention tremor across several tasks and can be sustained over a 24-hour period.

Systems identification and modeling is potentially a powerful tool for understanding the processes that guide sensorimotor control. Here, we show that systems identification can be used to describe and quantify the mechanisms that underlie

alterations in motor control due to aging and multiple sclerosis. Further, these models can be used to predict motor behavior in response to external changes in feedback and guide development of targeted rehabilitation strategies to improve motor function. One avenue for future investigation should be to verify and extend the preliminary results shown here and determine whether long-term reductions in tremor due to delay adaptation can be achieved. Additionally, the methods presented in Chapter 4 of this dissertation may be extended to the investigation of several potential avenues for rehabilitation. The methods developed here can potentially be simplified to a continuous motion task with a visual feedback delay increase; these tasks could potentially be performed by subjects on a laptop at a clinic or at home, which would provide a convenient and user-friendly method of rehabilitation for tremor in PwMS. Further, similar sensory deficits have been implicated in balance deficits in PwMS; these results may therefore be applicable to the understanding and rehabilitation of balance dysfunction. The outcomes of these future studies may help reduce motor deficits in PwMS and may provide insight into avenues for future rehabilitation techniques.

BIBLIOGRAPHY

1.   Beuter, A., J. Belair, and C. LaBrie, *Feedback and delays in neurological diseases: a modeling study using dynamical systems.* Bulletin of Mathematical Biology, 1993. **55**(3): p. 525-541.

2.   Chew, J.Z.Z., S.C. Gandevia, and R.C. Fitzpatrick, *Potural control at the human wrist.* J Physiol, 2008. **586**: p. 1265-1275.

3.   Crevecoeur, F., et al., *Movement stability under uncertain internal models of dynamics.* J Neurophysiol, 2010. **104**: p. 1301-1313.

4.   Desmurget, M. and S. Grafton, *Forward modeling allows feedback control for fast reaching movements.* Trends in Cognitive Sciences, 2000. **4**(11).

5.   Goodworth, A.D. and R.J. Peterka, *Contribution of sensorimotor integration to spinal stabilization in humans.* Journal of Neurophysiology, 2009. **102**: p. 496-512.

6.   Heenan, M.L., R.A. Scheidt, and S.A. Beardsley, *Visual and proprioceptive contributions to compensatory and pursuit tracking movements in humans.*, in *Conf Proc IEEE Eng Med Biol Soc.*2011: Boston, MA, USA.

7.   Huisinga, J.M., et al., *Postural control strategy during standing is altered in patients with Multiple Sclerosis.* Neurosci Lett, 2012.

8.   Liu, D. and E. Todorov, *Evidence for the flexible sensorimotor strategies predicted by optimal feedback control.* The Journal of Neuroscience, 2007. **27**(35): p. 9354-9368.

9.   Loram, I.D., et al., *Human control of an inverted pendulum: Is continuous control necessary? Is intermittent control effective? Is intermittent control physiological?* J Physiol, 2011. **589**(2): p. 307-324.

10. Loram, I.D., M. Lakie, and P.J. Gawthrop, *Visual control of stable and unstable loads: what is the feedback delay and extent of linear time-invariant control?* Journal of Physiology, 2009. **587**(6): p. 1343-1365.

11. Loughlin, P. and M. Redfern, *Analysis and modeling of human postural control.* IEEE Eng Med Biol Mag, 2003. **22**(2): p. 18.

12. Magdeleno, R.E. and D.T. McRuer, *Experimental validation and analytical elaboration for models of the pilot's neuromuscular subsystem in tracking tasks.* NASA contrac Rep NASA CR, 1971: p. 1-81.

13. Mahboobin, A., et al., *A mechanism for sensory re-weighting in postural control.* Med Biol Eng Comput, 2009. **47**(9): p. 921-9.

14. Mahboobin, A., P.J. Loughlin, and M.S. Redfern, *A model-based approach to attention and sensory integration in postural control of older adults.* Neurosci Lett, 2007. **429**(2-3): p. 147-51.

15. Mahboobin, A., et al., *Sensory re-weighting in human postural control during moving-scene perturbations.* Exp Brain Res, 2005. **167**(2): p. 260-7.

16.   Merfeld, D.M., L. Zupan, and R.J. Peterka, *Humans use internal models to estimate gravity and linear acceleration.* Nature, 1999. **398**(6728): p. 615-8.

17.   Mergner, T., C. Maurer, and R.J. Peterka, *Sensory contributions to the control of stance: a posture control model.* Adv Exp Med Biol, 2002. **508**: p. 147-52.

18.   Mergner, T., C. Maurer, and R.J. Peterka, *A multisensory posture control model of human upright stance.* Prog Brain Res, 2003. **142**: p. 189-201.

19.   Miall, R.C., et al., *Is the cerebellum a smith predictor?* J Mot Behav, 1993. **25**(3): p. 203-16.
20.   Peterka, R.J., *Sensorimotor integration in human postural control.* J Neurophysiol, 2002. **88**(3): p. 1097-118.

21.   Peterka, R.J., *Comparison of human and humanoid robot control of upright stance.* Journal of Physiology, 2009. **103**: p. 149-158.

22.   Poladia, C., *Systems identification of sensorimotor control for visually guided wrist movements*, in *Biomedical Engineering*2009, Marquette University.

23.   Scheidt, R.A., et al., *Interaction of visual and proprioceptive feedback during adaptation of human reaching movements.* J Neurophysiol, 2004. **93**: p. 3200-3213.

24.   Smith MA, S.R., *Intact ability to learn internal models of arm dynamics in Huntington's disease but not cerebellar degeneration.* J Neurophysiol, 2005 **93**: p. 2809-21.

25.   Suminski, A.J., et al., *Neural and electromyographic correlates of wrist posture control.* J Neurophysiol, 2007. **97**(2): p. 1527-45.

26.   van Beers, R.J., A.C. Sittig, and J.J. Denier van der Gon, *Integration of proprioceptive and visual position information: an experimentally supported model.* J Neurophysiol, 1999. **81**: p. 1355-1364.

27.   van der Helm, F.C.T. and L.A. Rozendaal, *Musculoskeletal systems with intrinsic and proprioceptive feedback*, in *Neural control of posture and movement*, J.M. Winters and P. Crago, Editors. 2000: Springer Verlag, NY. p. 164-174.

28.   Winters, J.M.a.L.S., *Muscle models: what is gained and what is lost by varying model complexity.* Biol Cybern, 1987. **55**: p. 403-420.

29.   Johnston, D.E. and D.T. McRuer, *Investigation of interactions between limb-manipultator dynamics and effective vehicle roll control characteristics.* NASA contrac Rep NASA CR, 1986. **3983**.

30.   McRuer, D.T., W.F. Clement, and R.W. Allen, *A theory of human error.* NASA contrac Rep NASA CR, 1980. **166313**.

31.   Goffredo, M., et al., *A neural tracking and motor control approach to improve rehabilitation of upper limb movements.* J Neuroeng Rehabil, 2008. **5**.

32.   Bhanpuri, N.H., A.M. Okamura, and A.J. Bastian, *Proprioceptive modeling by the cerebellum improves proprioception.* J Neurosci, 2013. **33**(36): p. 14301-14306.

33.   Bhanpuri, N.H., A.M. Okamura, and A.J. Bastian, *Predicting and correcting ataia using a model of cerebellar function.* Brain, 2014. **137**: p. 1931-1944.

34.   Block, H.J. and A.J. Bastian, *Sensory weighting and realignment: independent compensatory processes.* J Neurophysiol, 2011. **106**: p. 59-70.

35.   Verstynen, T., et al., *Ipsilateral motor cortex activity during unimanual hand movements relates to task complexity.* J Neurophysiol, 2005. **93**(3): p. 1209-22.

36.   Bagesteiro, L.B. and R.L. Sainburg, *Handedness: dominant arm advantages in control of limb dynamics.* J Neurophysiol, 2002. **88**: p. 2408-2421.

37.   Bagesteiro, L.B. and R.L. Sainburg, *Nondominant arm advantages in load compensation during rapid elbow joint movements.* J Neurophysiol, 2003. **90**: p. 1503-1513.

38.   Duff, S.V. and R.L. Sainburg, *Lateralization of motor adaptation reveals independence in control of trajectory and steady-state position.* Exp Brain Res, 2007. **179**: p. 551-561.

39.   Haaland, K.Y., et al., *Hemispheric asymmetries for kinematic and positional aspects of reaching.* Brain, 2004. **127**: p. 1145-1158.

40.   Haaland, K.Y., et al., *Ipsilesional trajectory control is related to contralesional arm paralysis after left hemisphere damage.* Experimental Brain Research, 2009. **196**: p. 195-204.

41.   Schaefer, S.Y., K.Y. Haaland, and R.L. Sainburg, *Ipsilesional motor deficits following stroke reflect hemispheric specializations for motor control.* Brain, 2007. **130**: p. 2146-2158.

42.   Schaefer, S.Y., K.Y. Haaland, and R.L. Sainburg, *Hemispheric specialization and functional impact of ipsilesional deficits in movement coordination and accuracy.* Neuropsychologia, 2009. **47**(13): p. 2953-2966.

43.   Scheidt, R.A. and C. Ghez, *Separate adaptive mechanisms for controlling trajectory and final position in reaching.* J Neurophysiol, 2007. **98**: p. 3600-3613.

44.   Scheidt, R.A. and T. Stoeckmann, *Reach adaptation and final position control amid environmental uncertainty after stroke.* Journal of Neurophysiology, 2007. **97**: p. 2824-2836.

45.   Flowers, K., *Visual 'Closed-Loop' and 'Open-Loop' Characteristics of Voluntary Movement in Patients with Parkinsonism and Tremor.* Brain 1976. **99**: p. 269-310.

46.   Poulton, E.C., *On the stimulus and response in pursuit tracking.* Journal of Experimental Psychology, 1957. **53**(3): p. 189-194.

47.   Poulton, E.C., *Tracking a variable rate of movement.* Journal of Experimental Psychology, 1967. **73**(1): p. 135-144.

48.   Miall, R.C. and J.K. Jackson, *Adaptation to visual feedback delays in manual tracking: evidence against the Smith Predictor model of human visually guided action.* Experimental Brain Research, 2006. **172**: p. 77-84.

49.   Wolpert, D.M., R.C. Miall, and M. Kawato, *Internal models in the cerebellum.* Trends Cogn Sci, 1998. **2**(9): p. 338-47.

50.   Mugge, W., et al., *Sensory weighting of force and position feedback in human motor control tasks.* The Journal of Neuroscience, 2009. **29**(17): p. 5476-5482.

51.   Quintern, J., et al., *Influence of visual and proprioceptive afferences on upper limb ataxia in patients with Multiple Sclerosis.* Journal of the Neurological Sciences, 1999. **163**: p. 61-69.

52. Kording, K.P. and D.M. Wolpert, *Bayesian decision theory in sensorimotor control.* Trends Cogn Sci, 2006. **10**(7): p. 319-26.

53. Bialek, W., *Physical limits to sensation and perception.* Annu Rev Biophys Biophys Chem, 1987. **16**: p. 455-78.

54. Faisal, A.A., L.P. Selen, and D.M. Wolpert, *Noise in the nervous system.* Nat Rev Neurosci, 2008. **9**(4): p. 292-303.

55. Neishabouri, A. and A.A. Faisal, *Axonal noise as a source of synaptic variability.* PLoS Comput Biol, 2014. **10**(5): p. e1003615.

56. Heenan, M., R.A. Scheidt, and S.A. Beardsley, *Age-related differentiation of sensorimotor control strategies during pursuit and compensatory tracking.* Conf Proc IEEE Eng Med Biol Soc, 2014. **2014**: p. 3562-5.

57. Heenan, M., et al., *Intention tremor and deficits of sensory feedback control in multiple sclerosis: a pilot study.* J Neuroeng Rehabil, 2014. **11**(1): p. 170.

58. Maurer, C., T. Mergner, and R.J. Peterka, *Multisensory control of human upright stance.* Exp Brain Res, 2006. **171**(2): p. 231-50.

59. Maurer, C. and R.J. Peterka, *A new interpretation of spontaneous sway measures based on a simple model of human postural control.* J Neurophysiol, 2005. **93**(1): p. 189-200.

60. Mehta, B. and S. Schaal, *Forward models in visual control.* Journal of Neurophysiology, 2002. **88**: p. 942-953.

61. Peterka, R.J. and P.J. Loughlin, *Dynamic regulation of sensorimotor integration in human postural control.* J Neurophysiol, 2004. **91**(1): p. 410-23.

62. van der Kooij, H. and R.J. Peterka, *Non-linear stimulus-response behavior of the human stance control system is predicted by optimization of a system with sensory and motor noise.* J Comput Neurosci, 2011. **30**(3): p. 759-78.

63. Gawthrop, P.J., et al., *Intermittent Control: a computational theory of human control.* Biol Cybern, 2011. **104**: p. 31-51.

64. Richardson, M.J. and T. Flash, *Comparing smooth arm movements with the two-thirds power law and the related segmented-control hypothesis.* J Neurosci, 2002. **22**(18): p. 8201-11.

65. Huang, H.J. and A.A. Ahmed, *Older adults learn less, but still reduce metabolic cost, during motor adaptation.* J Neurophysiol, 2014. **111**(1): p. 135-44.

66. Kwon, J. and Y. Choe, *Facilitating neural dynamics for delay compensation: a road to predictive neural dynamics?* Neural Netw, 2009. **22**(3): p. 267-76.

67. Miall, R.C., Weir, D. J., Stein, J. F., *Intermittency in Human Manual Tracking Tasks.* Journal of Motor Behaviour, 1993. **25**(1): p. 53-63.

68. Franklin, D.W. and D.M. Wolpert, *Computational mechanisms of sensorimotor control.* Neuron, 2011. **72**(3): p. 425-42.

69. Smith, M.A. and R. Shadmehr, *Intact ability to learn internal models of arm dynamics in Huntington's disease but not cerebellar degeneration.* J Neurophysiol, 2005. **93**(5): p. 2809-21.

70. Smith, M.A., J. Brandt, and R. Shadmehr, *Motor disorder in Huntington's disease begins as a dysfunction in error feedback control.* Nature, 2000. **403**(6769): p. 544-9.

71. Peterka, R.J., et al., *Postural compensation for unilateral vestibular loss.* Front Neurol, 2011. **2**: p. 57.

72. DeGoede, K.M., et al., *How quickly can healthy adults move their hands to intercept an approaching object? Age and gender effects.* J Gerontol A Biol Sci Med Sci, 2001. **56**(9): p. M584-8.

73. Lee, G., et al., *Efficient control of arm movements in advanced age.* Exp Brain Res, 2007. **177**(1): p. 78-94.

74. Sleimen-Malkoun, R., J.J. Temprado, and E. Berton, *Age-related changes of movement patterns in discrete Fitts' task.* BMC Neurosci, 2013. **14**: p. 145.

75. Sleimen-Malkoun, R., J.J. Temprado, and S.L. Hong, *Aging induced loss of complexity and dedifferentiation: consequences for coordination dynamics within and between brain, muscular and behavioral levels.* Front Aging Neurosci, 2014. **6**: p. 140.

76. Temprado, J.J., et al., *Aging of sensorimotor processes: a systematic study in Fitts' task.* Exp Brain Res, 2013. **228**(1): p. 105-16.

77. Boisgontier, M.P. and V. Nougier, *Ageing of internal models: from a continuous to an intermittent proprioceptive control of movement.* Age (Dordr), 2013. **35**(4): p. 1339-55.

78. Kwon, M., et al., *Aging and limb alter the neuromuscular control of goal-directed movements.* Exp Brain Res, 2014. **232**(6): p. 1759-71.

79. Poston, B., et al., *Movement trajectory smoothness is not associated with the endpoint accuracy of rapid multi-joint arm movements in young and older adults.* Acta Psychol (Amst), 2013. **143**(2): p. 157-67.

80. Sarlegna, F.R., *Impairment of online control of reaching movements with aging: a double-step study.* Neurosci Lett, 2006. **403**(3): p. 309-14.

81. Ketcham, C.J., et al., *Age-related kinematic differences as influenced by task difficulty, target size, and movement amplitude.* J Gerontol B Psychol Sci Soc Sci, 2002. **57**(1): p. P54-64.

82. Stirling, L.A., et al., *Use of a tracing task to assess visuomotor performance: effects of age, sex, and handedness.* J Gerontol A Biol Sci Med Sci, 2013. **68**(8): p. 938-45.

83. Coats, R.O. and J.P. Wann, *The reliance on visual feedback control by older adults is highlighted in tasks requiring precise endpoint placement and precision grip.* Exp Brain Res, 2011. **214**(1): p. 139-50.

84. Toledo, D.R. and J.A. Barela, *Age-related differences in postural control: effects of the complexity of visual manipulation and sensorimotor contribution to postural performance.* Exp Brain Res, 2014. **232**(2): p. 493-502.

85. Tsai, Y.C., L.F. Hsieh, and S. Yang, *Age-related changes in posture response under a continuous and unexpected perturbation.* J Biomech, 2014. **47**(2): p. 482-90.

86. Enoka, R.M., et al., *Mechanisms that contribute to differences in motor performance between young and old adults.* J Electromyogr Kinesiol, 2003. **13**(1): p. 1-12.

87. Bernard, J.A. and R.D. Seidler, *Evidence for motor cortex dedifferentiation in older adults.* Neurobiol Aging, 2012. **33**(9): p. 1890-9.

88. Bernard, J.A. and R.D. Seidler, *Moving forward: age effects on the cerebellum underlie cognitive and motor declines.* Neurosci Biobehav Rev, 2014. **42**: p. 193-207.

89. Bartzokis, G., et al., *Lifespan trajectory of myelin integrity and maximum motor speed.* Neurobiol Aging, 2010. **31**(9): p. 1554-62.

90. Hoffstaedter, F., et al., *Age-related decrease of functional connectivity additional to gray matter atrophy in a network for movement initiation.* Brain Struct Funct, 2015. **220**(2): p. 999-1012.

91. Stewart, J.C., X. Tran, and S.C. Cramer, *Age-related variability in performance of a motor action selection task is related to differences in brain function and structure among older adults.* Neuroimage, 2014. **86**: p. 326-34.

92. Seidler, R.D., J.L. Alberts, and G.E. Stelmach, *Changes in multi-joint performance with age.* Motor Control, 2002. **6**(1): p. 19-31.

93. Alusi, S.H., et al., *Tremor in Multiple Sclerosis.* Journal of Neurology Neurosurgery and Psychiatry, 1999. **66**: p. 131-134.

94. Alusi, S.H., et al., *A study of tremor in Multiple Sclerosis.* Brain, 2001. **124**: p. 720-730.

95. Koch, M., et al., *Tremor in multiple sclerosis.* J Neurol, 2007. **254**(2): p. 133-45.

96. Labiano-Fontcuberta, A. and J. Benito-Leon, *Understanding tremor in Multiple Sclerosis: prevalence, pathological anatomy, and pharmacological and surgical approaches to treatment.* Tremor Other Hyperkinet Mov, 2012. **2012**(2).

97. Koch, G., Rossi, S., Prosperetti, C., Codeca C., Monteleone, F., Petrosini, L. Bernardi, G. Centonze, D., *Improvement of hand dexterity following motor cortex rTMS in multiple sclerosis patients with cerebellar impairment.* Mult Scler, 2008. **14**(7): p. 995-998.

98. Mori, F., et al., *The use of repetitive transcranial magnetic stimulation (rTMS) for the treatment of spasticity.* Prog Brain Res, 2009. **175**: p. 429-39.

99. Quinn, L., et al., *Client and therapist views on exercise programmes for early-mid stage Parkinson's disease and Huntington's disease.* Disabil Rehabil, 2010. **32**(11): p. 917-28.

100. Cameron, M.H., et al., *Imbalance in Multiple Sclerosis: a result of slowed spinal somatosensory conduction.* Somatosens Mot Res, 2008. **25**(2): p. 113-122.

101. Brown, T.R. and G.H. Kraft, *Exercise and rehabilitation for individuals with multiple sclerosis.* Phys Med Rehabil Clin N Am, 2005. **16**(2): p. 513-55.

102. Feys P, R.A., Ruutiainen J, Davies-Smith A, Jones R, Avizzano CA, Bergamasco M, Ketelaer P, *Assistive technology to improve PC interaction for people with intention tremor* J Rehabil Res Dev, 2001. **38**: p. 235-243.

103. Feys, P., et al., *Effects of vision and arm position on amplitude of arm postural tremor in patients with multiple sclerosis.* Arch Phys Med Rehabil, 2004. **85**: p. 1031-1033.

104. Feys, P., et al., *Interaction between eye and hand movements in Multiple Sclerosis patients with intention tremor.* Mov Disord, 2005. **20**(6): p. 705-713.

105. Carpinella, I., et al., *Robot-based rehabilitation of the upper limbs in multiple sclerosis: feasibility and preliminary results.* J Rehabil Med. , 2009. **41**(12): p. 966-970.

106. Carpinella, I.C., D.; Bertoni, R.; Ferrarin, M., *Robot training of upper limb in multiple sclerosis: comparing protocols with or without manipulative task components.* IEEE Trans Neural Syst Rehabil Eng, 2012. **20**(3): p. 351-360.

107. Vergaro, E., et al., *Adaptive robot training for the treatment of incoordination in Multiple Sclerosis.* J Neuroeng Rehabil, 2010. **7**: p. 37.

108. Liu, X., et al., *Analysis of action tremor and impaired control of movement velocity in multiple sclerosis during visually guided wrist-tracking tasks.* Mov Disord, 1997. **12**(6): p. 992-9.

109. Schenk, T., E.U. Walther, and N. Mai, *Closed- and open-loop handwriting performance in patients with multiple sclerosis.* Eur J Neurol, 2000. **7**(3): p. 269-79.

110. Fradet, L., G. Lee, and N. Dounskaia, *Origins of submovements in movements of elderly adults.* J Neuroeng Rehabil, 2008. **5**: p. 28.

111. Ruitenberg, M.F., et al., *Post-error slowing in sequential action: an aging study.* Front Psychol, 2014. **5**: p. 119.

112. Magdeleno, R.E., D.T. McRuer, and G.P. Moore, *Small perturbation dynamics of the neuromuscular system in tracking tasks.* NASA contrac Rep NASA CR, 1968: p. 1-119.

113. Jones, K.E., A.F. Hamilton, and D.F. Wolpert, *Sources of signal-dependent noise during isometric force production.* J Neurophysiol, 2002. **88**(3): p. 1533-54.

114. Scheidt, R.A., C. Ghez, and S. Asnani, *Patterns of hypermetria and terminal cocontraction during point-to-point movements demonstrate independent action of trajectory and postural controllers.* J Neurophysiol, 2011. **106**: p. 2368-2382.

115. Beer, S., F. Khan, and J. Kesselring, *Rehabilitation interventions in multiple sclerosis: an overview.* J Neurol, 2012. **259**: p. 1994-2008.

116. Pittock SJ, M.R., Mayr WT, Rodriguez M, Matsumoto JY., *Prevalence of tremor in multiple sclerosis and associated disability in the Olmsted County population.* Mov Disord, 2004. **19**(12): p. 1482-85.

117. Hallett, M., et al., *Controlled trial of isoniazid therapy for severe postural cerebellar tremor in multiple sclerosis.* Neurology, 1985. **35**(9): p. 1374-7.

118. Morrow, J., et al., *Isoniazid and action tremor in multiple sclerosis.* J Neurol Neurosurg Psychiatry, 1985. **48**(3): p. 282-3.

119. Henkin, Y. and Y.O. Herishanu, *Primidone as a treatment for cerebellar tremor in multiple sclerosis - two case reports.* Isr J Med Sci, 1989. **25**(12): p. 720-1.

120. Sechi, G., et al., *Effects of topiramate in patients with cerebellar tremor.* Prog Neuropsychopharmachol Biol Psychiatry, 2003. **27**(6): p. 1023-7.

121. Goodman, A.D., et al., *Sustained-release oral fampridine in multiple sclerosis: a randomised, double-blind, controlled trial.* Lancet, 2009. **373**(9665): p. 732-8.

122. Mills, R.J., L. Yap, and C.A. Young, *Treatment for ataxia in multiple sclerosis.* Cochrane Database Syst Rev, 2007. **1**: p. CD005029.

123. Striano, P., et al., *Levetiracetam for cerebellar tremor in multiple sclerosis.* J Neurol, 2006. **253**(6): p. 762-6.

124. Nandi, D. and T.Z. Aziz, *Deep brain stimulation in hte management of neuropathic pain and multiple sclerosis tremor.* J Clin Neurophysiol, 2004. **21**(1): p. 31-9.

125. Alan J Thompson, A.T.T., Olga Ciccarelli, *Pharmacological management of symptoms in multiple sclerosis: current approaches and future directions.* Lancet Neurol, 2010. **9**: p. 1182-99.

126. S.J. Hickman; C.M.H. Brierley; N.C. Silver; I.F. Moseley. *Infratentorial hypointense lesion volume on T1 weighted magnetic resonance imaging correlates with disability in patients with chronic cerebellar ataxia due to multiple sclerosis.* Journal of the Neurological Sciences, 2001. **187**: p. 35-39.

127. Feys, P., et al., *Relationship between multiple sclerosis interion tremor severity and lesion load in the brainstem.* Brain Imaging, 2005. **16**(12): p. 1379-1382.

128. Feys, P., et al., *Intention tremor during manual aiming: a study of eye and hand movements.* Mult Scler, 2003. **2003**(9): p. 44-54.

129. Demaree, H.A., et al., *Speed of information processing as a key deficit in Multiple Sclerosis: implications for rehabilitation.* J Neurol Neurosurg Psychiatry, 2007. **67**: p. 661-663.

130. Feys, P., et al., *Diitised spirography as an evaluation tool for intention tremor in multiple sclerosis.* Journal of Neuroscience Methods, 2007. **160**: p. 309-316.

131. Kurtzke, J.F., *Rating neurologic impairment in multiple sclerosis: an expanded disability status scale (EDSS).* Neurology, 1983. **33**(11): p. 1444-1452.

132. Alusi, S.H.W., J; Glickman, S; Findley, L.J.; Bain, P.G., *Evaluation of three different ways of assessing tremor in multiple sclerosis.* J Neurol Neurosurg Psychiatry, 2000. **68**(6): p. 756-60.

133. Fishbach, A., et al., *Deciding when and how to correct a movement: discrete submovements as a decision making process.* Exp Brain Res, 2007. **177**: p. 45-63.

134. Liu, X., et al., *Effects of visual feedback on manual tracking and action tremor in Parkinson's disease.* Exp Brain Res, 1999. **129**: p. 477-481.

135. Feys, P., et al., *Effect of visual information on step-tracking movements in patients with intention tremor due to multiple sclerosis.* Mult Scler, 2003. **9**: p. 492-502.

136. Rohrer, B., et al., *Movement smoothness changes during stroke recovery.* J Neurosci, 2002. **22**(18): p. 8297-304.

137. Rohrer, B., et al., *Submovements grow larger, fewer, and more blended during stroke recovery.* Motor Control, 2004. **8**(4): p. 472-83.

138. Wei, K. and K. Kording, *Relevance of error: what drives motor adaptation?* J Neurophysiol, 2009. **101**(2): p. 655-64.

139. Blakemore, S.J., D. Wolpert, and C. Frith, *Why can't you tickle yourself?* Neuroreport, 2000. **11**(11): p. R11-6.

140. Maschke M, G.C., Ebner TJ, Konczak J, *Hereditary cerebellar ataxia progressively impairs force adaptation during goal-directed arm movements.* J Neurophysiol, 2004 **91**: p. 230-38.

141. Heenan, M.L., R.A. Scheidt, and S.A. Beardsley. *Visual delay adaptation to reduce intention tremor in multiple sclerosis.* in *ACTRIMS/ECTRIMS.* 2014. Boston.

142. Feys, P., et al., *The effect of changed visual feedback on intention tremor in Multiple Sclerosis.* Neuroscience Letters, 2006. **394**: p. 17-21.

APPENDIX A

A subtraction analysis was used to reduce the impact of noise on the estimate of the subjects' frequency response function (FRF). For each trial, the relationship between the input to the sensorimotor control system and joint angle output can be expressed as:

$$\theta_a(s) = H(s) * X(s) + N(s)$$

where X(s) is the power spectrum of the input – either the torque or external perturbation – and N(s) is the power spectrum of all noise sources combined. H(s) is the transfer function relating the input X(s) to the output $\theta_a(s)$. The sum of noise sources n(t) is assumed to be zero mean and characterized by a nominal spectrum N(s). In the frequency domain, the addition of noise results in a frequency dependent offset from the "true" FRF. This offset can be characterized as a random variable $N_i(s)$ with variance $\sigma_n^2(s)$, whose mean corresponds to the average noise spectrum. To eliminate this offset, individual estimates of the FRF were obtained by pair-wise subtraction of the trial-wise input and output spectra. For a pair of trials,

$$\theta_{a_1}(s) = H(s) * X_1(s) + N_1(s)$$

$$\theta_{a_2}(s) = H(s) * X_2(s) + N_2(s)$$

subtraction yields

$$\theta_{a_1}(s) - \theta_{a_2}(s) = H(s) * \left(X_1(s) - X_2(s)\right) + \left(N_1(s) - N_2(s)\right)$$

so that the nominal noise spectrum is removed and the variance is now centered around 0. Rearranging this equation, we get:

$$H(s) = \frac{\theta_{a_1}(s) - \theta_{a_2}(s)}{X_1(s) - X_2(s)} + \frac{N_2(s) - N_1(s)}{X_1(s) - X_2(s)}$$

where the first term characterizes the difference FRF of the system and second reflects the contribution due to noise. The frequency response due to noise has zero mean and variance σ_n^2/σ_X^2.

The transfer function for the system, H(s), was estimated by taking the average of the difference FRFs across all pair-wise trial combinations (i, j),

$$H(s) \cong FRF(s) = \frac{1}{M} \sum_{i=1}^{N} \sum_{\substack{j=2 \\ j>i}}^{N} \frac{\theta_{a_i}(s) - \theta_{a_j}(s)}{X_i(s) - X_j(s)}$$

where M is the number of pairwise trial combinations and the contribution of the (zero-mean) noise spectrum decreases as the inverse square root of M.

Meanwhile, the noise spectrum can be calculated by eliminating the effects of the transfer function (H(s)) through a similar subtraction analysis.

$$\theta_{a_1}(s) = H(s) * X_1(s) + N_1(s)$$

$$\theta_{a_2}(s) = H(s) * X_2(s) + N_2(s)$$

First, system equations are divided by the input (X(s)):

$$\frac{\theta_{a_1}(s)}{X_1(s)} = H(s) + \frac{N_1(s)}{X_1(s)}$$

$$\frac{\theta_{a_2}(s)}{X_2(s)} = H(s) + \frac{N_2(s)}{X_2(s)}$$

and then are subtracted to yield:

$$\frac{\theta_{a_1}(s)}{X_1(s)} - \frac{\theta_{a_2}(s)}{X_2(s)} = \frac{N_1(s)}{X_1(s)} - \frac{N_2(s)}{X_2(s)}$$

assuming that $N_1(s)$ and $N_2(s)$ have the same trial-by-trial statistical properties, we can factor out N(s):

$$\frac{\theta_{a_1}(s)}{X_1(s)} - \frac{\theta_{a_2}(s)}{X_2(s)} = N(s)(\frac{1}{X_1(s)} - \frac{1}{X_2(s)})$$

rearranging, we can see that:

$$N(s) = \frac{\dfrac{\theta_{a_1}(s)}{X_1(s)} - \dfrac{\theta_{a_2}(s)}{X_2(s)}}{\dfrac{1}{X_1(s)} - \dfrac{1}{X_2(s)}}$$

APPENDIX B

Table B-1. Parameter descriptions.

Parameter	Description	Units
Ks	Task gain	Unitless
Kv	Visual Gain	Unitless
Kp	Proprioceptive Gain	Unitless
Kd	Derivative Gain	Nm-s/deg
Kpr	Proportional Gain	Nm/deg
Ki	Integral Gain	Nm/deg-s
N	Lumped noise term	Unitless
J	Limb Inertia	$Kg\text{-}m^2$
B	Limb Viscosity	Nm-s/rad
K	Limb Stiffness	Nm/rad
Tv	Visual Delay	ms
Tp	Proprioceptive Delay	ms
α	Motor Noise Multiplier	Unitless
MSE	Movement Error	Deg^2
AT	Acquisition Time	sec

Table B-2. Model parameters for visual compensatory tracking during aging.

Age	Kv	Kp	Kd	Kpr	Ki	log(N)	J	B	K
			VISUAL COMPENSATORY TRACKING						
20	0.478	0.271	0.006	0.234	2.017	9.322	0.065	0.659	4.556
20	0.613	0.420	0.004	0.158	2.145	9.725	0.023	0.394	2.380
20	0.583	1.036	0.000	0.223	0.639	8.957	0.035	0.269	3.650
24	1.061	2.002	0.003	0.106	0.813	8.657	0.046	0.184	3.083
24	1.386	1.352	0.000	0.094	0.032	8.728	0.048	0.321	5.400
25	0.232	0.417	0.002	0.481	11.982	8.848	0.033	1.872	3.730
25	1.676	1.936	0.002	0.042	0.565	9.143	0.028	0.196	1.411
26	0.806	1.372	0.001	0.167	0.148	8.702	0.062	0.484	7.965
27	0.917	1.152	0.004	0.131	0.160	8.981	0.060	0.687	4.762
27	0.893	0.362	0.005	0.143	0.083	9.311	0.081	0.804	4.832
29	1.483	1.567	0.002	0.055	0.358	9.433	0.045	0.394	2.927
32	0.957	1.037	0.007	0.071	1.203	8.948	0.057	0.207	3.387
40	0.687	0.669	0.003	0.119	1.022	9.106	0.052	0.723	5.039
40	0.962	0.803	0.002	0.048	0.022	9.164	0.014	1.520	3.099
41	0.449	0.855	0.004	0.179	1.719	9.184	0.055	0.732	4.453
50	0.428	0.184	0.004	0.246	0.189	9.742	0.038	1.993	6.659
55	0.415	0.946	0.003	0.029	0.032	10.718	0.093	1.084	7.551
59	0.341	0.408	0.006	0.187	0.535	10.481	0.093	1.345	10.559
60	0.846	0.448	0.004	0.168	0.060	9.533	0.090	0.887	5.101
61	0.156	0.015	0.007	0.864	1.210	11.326	0.085	2.606	15.325
63	0.475	0.920	0.014	0.200	2.732	9.121	0.090	1.349	3.754
66	0.156	0.324	0.025	0.976	0.166	9.543	0.033	4.418	7.149
70	0.085	0.139	0.015	1.278	32.528	10.963	0.078	2.647	6.368
76	0.225	0.057	0.004	0.759	0.814	10.495	0.065	1.572	8.308

Table B-3. Model parameters for visual pursuit tracking during aging.

Age	Ks	Kv	Kp	Kd	Kpr	Ki	log(N)	J	B	K
				VISUAL PURSUIT TRACKING						
20	0.581	1.186	0.225	0.005	0.178	1.688	8.387	0.059	0.545	5.020
20	0.771	0.194	0.281	0.000	0.145	1.017	9.452	0.018	0.361	1.902
20	0.837	0.610	0.469	0.000	0.148	0.906	9.002	0.020	0.266	2.609
24	0.795	0.788	1.230	0.004	0.151	1.293	8.640	0.057	0.385	5.570
24	0.961	0.402	0.974	0.006	0.089	0.831	8.347	0.094	0.089	5.199
25	0.988	0.276	1.004	0.002	0.127	0.129	8.614	0.047	0.849	5.954
25	0.888	2.388	0.466	0.006	0.141	1.374	8.770	0.056	0.654	2.558
26	0.145	0.742	2.174	0.005	0.051	1.074	8.697	0.050	0.218	3.858
27	1.899	5.961	0.182	0.002	0.057	0.051	7.291	0.060	0.295	4.273
27	1.189	0.215	0.210	0.002	0.092	0.487	9.308	0.031	0.299	2.302
29	1.597	0.399	1.279	0.003	0.062	0.194	9.428	0.048	0.609	2.270
32	0.833	1.148	1.129	0.008	0.050	1.140	8.769	0.067	0.340	4.256
40	0.909	0.277	0.379	0.004	0.113	0.956	9.204	0.053	0.484	4.180
40	2.443	0.173	0.417	0.001	0.060	0.027	9.189	0.052	0.518	4.215
41	1.021	2.646	0.095	0.003	0.077	0.645	8.122	0.026	0.201	2.222
50	0.542	0.097	0.151	0.005	0.230	0.210	9.470	0.049	1.433	4.407
55	0.700	0.431	0.249	0.008	0.125	1.688	9.656	0.055	0.569	4.731
59	0.301	0.035	0.136	0.007	0.391	11.378	9.955	0.027	0.568	4.987
60	0.782	0.366	0.144	0.004	0.181	0.099	9.482	0.067	1.822	5.242
61	0.344	0.089	0.010	0.013	1.004	1.351	10.210	0.065	0.441	6.408
63	0.550	1.476	0.505	0.008	0.189	2.151	8.466	0.072	0.807	6.012
66	0.289	0.124	0.342	0.006	0.457	0.357	9.268	0.045	2.536	7.636
70	0.381	2.501	0.082	0.006	0.341	0.223	8.017	0.066	1.495	3.604
76	0.392	0.376	0.068	0.005	0.359	2.325	9.782	0.039	0.845	3.900

Table B-4. Model parameters for proprioceptive compensatory tracking during aging.

Age	PROPRIOCEPTIVE COMPENSATORY TRACKING
	Kp	Kd	Kpr	Ki	log(N)	J	B	K
20	1.650	0.000	0.018	0.031	10.259	0.053	0.552	14.694
20	1.482	0.001	0.313	0.352	10.303	0.047	1.355	17.947
20	1.712	0.000	0.410	0.679	8.914	0.071	0.898	16.414
24	2.896	0.006	0.222	0.932	8.685	0.106	0.579	14.032
24	3.848	0.007	0.323	2.569	9.011	0.070	0.376	13.840
25	2.065	0.004	0.157	4.758	9.166	0.046	0.997	16.074
25	3.299	0.001	0.038	0.513	9.443	0.053	0.803	6.656
26	1.969	0.004	0.129	2.680	8.679	0.061	0.826	9.340
27	11.882	0.005	0.172	2.301	9.498	0.061	0.565	5.712
27	2.094	0.006	0.501	2.114	9.325	0.080	0.827	11.679
29	3.120	0.005	0.184	1.153	9.451	0.096	0.995	5.148
32	3.212	0.005	0.126	0.770	9.354	0.096	0.517	5.623
40	2.345	0.002	0.124	1.406	8.872	0.063	1.242	13.573
40	3.753	0.007	0.330	0.338	9.119	0.038	0.890	14.840
41	1.874	0.001	0.170	3.435	9.489	0.108	0.826	11.495
50	1.074	0.000	0.082	0.607	10.669	0.050	0.910	18.335
55	0.741	0.011	0.097	3.431	11.045	0.058	0.839	11.893
59	0.757	0.004	0.092	0.360	11.025	0.062	0.748	13.317
60	1.621	0.004	0.106	0.568	9.661	0.075	0.916	5.423
61	0.314	0.005	0.035	0.026	12.523	0.064	0.847	19.650
63	1.883	0.003	0.136	1.171	9.425	0.060	0.908	12.216
66	1.392	0.009	0.220	5.988	9.845	0.067	1.120	13.736
70	0.273	0.008	0.273	6.234	11.435	0.085	1.144	21.468
76	1.172	0.003	0.093	0.052	11.978	0.063	1.781	42.263

Table B-5. Delays, motor noise, and movement outcomes during aging.

Age	DELAYS		MOTOR NOISE	MOVEMENT OUTCOMES	
	Tv (ms)	Tp (ms)	α	MSE (deg^2)	AT (s)
20	435.0	142.3	0.061	0.004	0.958
20	473.7	141.8	0.109	0.004	0.880
20	408.1	165.6	0.084	0.004	0.736
24	434.5	239.6	--	0.007	0.779
24	393.3	192.0	0.088	0.007	0.729
25	341.5	252.7	0.108	0.004	0.913
25	410.5	414.8	0.080	0.008	0.584
26	381.6	176.6	0.048	0.007	0.658
27	410.3	276.8	0.086	0.006	0.650
27	432.0	284.0	0.035	0.006	0.603
29	504.0	271.5	0.058	0.003	0.939
32	405.0	261.0	0.099	--	--
40	458.2	117.3	0.014	0.005	0.741
40	578.0	238.8	--	0.007	0.840
41	421.3	104.7	0.057	0.007	0.497
50	437.0	198.0	0.104	0.005	0.794
55	472.2	323.0	0.053	0.010	0.830
59	472.1	261.5	0.048	0.007	0.790
60	456.4	344.3	0.054	0.004	1.160
61	438.4	434.6	0.063	0.007	1.035
63	508.4	166.0	0.085	0.004	0.899
66	512.6	189.8	0.066	0.005	0.898
70	599.2	138.3	0.034	0.004	1.124
76	384.4	159.5	0.054	0.016	1.151

APPENDIX C

Table C-1. Model parameters for visual compensatory tracking in subjects with MS.

Subject	Kv	Kd	Kpr	Ki	J	B	K	J*	B*	K*
1	0.194	0.008	0.724	12.04	0.068	1.947	17.62	0.046	2.077	15.11
2	0.403	0.007	0.141	4.563	0.043	0.499	5.092	0.043	0.703	8.011
3	0.224	0.012	0.257	8.531	0.043	0.767	4.247	0.070	0.867	6.563
4	0.375	0.000	0.290	3.379	0.066	1.196	9.829	0.050	1.042	9.507
5	0.872	0.012	0.086	4.265	0.072	0.754	6.955	0.142	0.553	14.45
6	0.524	0.011	0.108	1.241	0.053	0.983	1.516	0.075	3.197	0.037
7	0.864	0.007	0.147	5.698	0.053	0.352	2.954	0.082	0.840	5.567
8	0.234	0.010	0.231	15.134	0.015	0.250	2.463	0.030	0.244	5.852

Table C-2. Model parameters for visual compensatory tracking in control subjects.

Subject	Kv	Kd	Kpr	Ki	J	B	K	J*	B*	K*
1	0.511	0.002	0.053	1.694	0.025	0.225	1.978	0.022	0.260	2.370
2	0.230	0.007	0.151	7.890	0.031	0.916	5.324	0.023	0.455	2.487
3	0.528	0.002	0.076	0.857	0.020	0.269	1.676	0.023	0.261	2.258
4	0.809	0.003	0.165	0.486	0.068	0.898	3.905	0.071	0.852	5.159
5	0.365	0.004	0.095	1.671	0.015	0.574	1.643	0.020	0.524	2.394
6	0.420	0.002	0.069	2.571	0.021	0.171	2.421	0.017	0.228	2.329
7	0.997	0.002	0.097	1.035	0.048	0.443	2.981	0.052	0.562	4.006
8	0.336	0.004	0.096	1.258	0.036	0.554	3.080	0.051	0.491	3.069